



Ceramic coaxial resonator filter in a CubeSat system

by

Odette Sandrine Bakam Nguenouho

**Thesis submitted in fulfillment of the requirements for the degree
Master of Engineering: Electrical Engineering**

**in the Faculty of Engineering
at the Cape Peninsula University of Technology**

Supervisor: Ms. Susan Maas

Co-Supervisor: Prof Robert Van Zyl

Bellville

December 2017

CPUT copyright information

The thesis may not be published either in part (in scholarly, scientific or technical journals) or as a whole (as a monograph) unless permission has been obtained from the University.

DECLARATION

I, Odette Sandrine Bakam Nguenouho, declare that the contents of this thesis represent my own unaided work and that the thesis has not previously been submitted for academic examination towards any qualification. Furthermore, it represents my own opinions and not necessarily those of the Cape Peninsula University of Technology.

.....

.....

OS Bakam Nguenouho

Bellville

December 2017

ACKNOWLEDGEMENTS

I would like to thank the following who contributed to the success of this thesis, and without whose support its completion would not have been possible:

The Lord, for preparing the way ahead of me all these years, who gave me the physical power and strength to complete this work.

Prophet TB Joshua and the Emmanuel TV team for their prayers and spiritual nourishment.

My supervisor, Ms. Susan Maas, for her invaluable support and guidance throughout the research project, and for being a sister, mother, friend and role model. My grateful thanks to your family also.

My co-supervisor, Prof. Robert van Zyl, for his continued guidance and support and for all the encouragement throughout the project.

My family and friends for their love, support, and prayers. Special thanks go to my lovely husband for always being there when things mattered the most, for taking care of our lovely babies from time to time, thereby allowing me to progress with my work. Thank you also to my babies, Wilfried and Laetitia, for reminding me why I must remain strong each day.

TRANS-TECH for providing the required sample used in this research.

RF design, especially Mr. Shane Starita, for engaging with TRANS-TECH regarding the samples and also for providing a sample of the SMA connectors.

The French–South African Institute of Technology (F’SATI) for their generous support through NRF financial assistance.

Mr. Gualbert Maas, for assisting with the PCB Gerber file.

Robert Robertson, for his time and assistance with the PCB manufacturing machining operation.

Ms. Anneke Bester at Stellenbosch University, for her assistance in the test setup.

ABSTRACT

RF and microwave filters can be implemented using ceramic coaxial resonators. This technology has been widely employed in nanosatellite communications systems recently, owing to its large quality factor (Q), permitting them to have low loss and narrow bandwidth. Features such as high selectivity, high power handling, excellent rejection, and low passband insertion loss are just a few of the key performance areas offered by ceramic coaxial resonators. This feature makes them suitable for use in bandpass filters.

Applications with demanding specifications requiring low volume and mass make use of this technology. Fulfilling the required performance goals can be challenging, given the size and weight restriction. Difficulties such as finding the correct length of resonators and the coupling capacitors' structure to meet the size restriction, limit the type of ceramic coaxial resonators to use.

This thesis presents the design of a bandpass filter using ceramic coaxial resonators, which provides evidence of the concept for F'SATI's future needs. This design will be used in an imminent space mission and the intention is to mount the bandpass filter in the receiver communications system. An intensive investigation was conducted into the use of filters for nanosatellite communication systems. The Chebyshev LC ladder low pass prototype was used to derive the conventional bandpass filter. Thereafter, the coupled resonator bandpass filter was derived using the conventional bandpass filter topology combined with the admittance inverter. Following this, using the ceramic coaxial resonators datasheet and information provided by the manufacturers, the coupled resonator bandpass filter was converted into a 3D model for further simulations, using CST Microwave Studio®. The ceramic coaxial resonator filter fabricated using Rogers's material provided satisfactory results at its operating frequency between 2.2 GHz and 2.3 GHz. A radiation level test was performed on the filter to justify the use of the metallic enclosure. The test presented a low level of radiation measured at the filter operating frequency (2.25 GHz). The filter was also subjected to temperature cycling.

CONTENTS

DECLARATION	ii
ACKNOWLEDGEMENTS	iii
ABSTRACT	iv
CONTENTS.....	v
LIST OF FIGURES	vii
LIST OF TABLES	x
ABBREVIATIONS AND ACRONYMS	xi
CHAPTER 1	1
INTRODUCTION	1
1.1 Application of microwave filters	1
1.2 Rationale.....	3
1.3 Objectives	4
1.4 Investigative questions	5
1.5 Overview of the thesis	5
1.6 Organisation of the thesis.....	5
CHAPTER 2	7
CERAMIC COAXIAL RESONATOR	7
2.1 Microwave resonators	7
2.2 Transmission line resonators.....	15
2.3 Ceramic coaxial resonator.....	19
CHAPTER 3	27
COUPLED RESONATOR.....	27
3.1 Filter transfer function.....	27
3.2 Filter implementations	31
3.2.2 Coupled resonator filter	33
CHAPTER 4	39
S-BAND BANDPASS FILTER DESIGN.....	39
4.1 Skywork CCR equivalent circuit	39
4.2 Filter specification	40
4.3 Capacitively coupled resonator bandpass filter	40
4.3.1 Lumped element capacitively coupled resonator bandpass filter	41
4.3.2 Coupled resonator bandpass filter symmetry characteristic.....	42
4.4 Parallel LC element conversion to CCR	47
4.5 Ceramic coaxial resonator bandpass filter design using CST Microwave Studio®	48
4.6 Coupling effects of CCR.....	51
4.6.1 Electromagnetic study on a single CCR	52

4.7	Coupling capacitor structure design	54
4.8	E-field and H-field distribution around the overall system	64
4.8.1	E-field and H-field distribution with no enclosure	65
4.9	Summary.....	68
CHAPTER 5		69
FABRICATION, TESTING AND DISCUSSION OF RESULTS.....		69
5.1	Bandpass filter manufacturing	69
5.3	Testing	72
5.3.2	Ceramic bandpass filter testing	73
5.3.3	Temperature cycling.....	73
5.4	Discussion of results	75
5.5	Summary.....	76
CHAPTER 6		77
CONCLUSION, RECOMMENDATION & FUTURE WORK.....		77
6.1	Final conclusion	77
6.1.1	Addressing the investigative question	78
6.1.2	Simulation and modelling results	79
6.1.3	Experimental results.....	79
6.2	Recommendations	80
6.3	Future work	80
REFERENCES		81
APPENDIX A		84
Coaxial Resonators and Inductors.....		84
APPENDIX B		96
CCR FREQUENCY TUNING.....		96

LIST OF FIGURES

Figure 1.1: ZACUBE 1 transceiver block diagram (F’SATI, 2013:10)	1
Figure 1. 2: Down converter section in a receiver system	2
Figure 1.3: Ceramic coaxial resonator bandpass filter with capacitive coupling structure.....	4
Figure 2.1: (a) Real world Capacitor, (b) Real world Inductor.....	7
Figure 2.2: (a) Real world inductor magnitude response,	8
Figure 2.3: RLC series resonant circuit (adapted from Pozar, 2008:267)	9
Figure 2.4: Series RLC response (adapted from Pozar, 2005:267)	11
Figure 2.5: Parallel RLC circuit (adapted from Pozar, 2005:269)	12
Figure 2.6: Parallel RLC circuit response (adapted from Pozar, 2005:269)	13
Figure 2.7: Short circuited transmission line (adapted from Pozar, 2005:273).....	15
Figure 2.8: Short circuited quarter wavelength and a parallel RLC equivalence (adapted from Matthaei et al., 1980:216)	18
Figure 2.9: Open circuit half wavelength line (adapted from Pozar, 2005:276).....	18
Figure 2.10: Coaxial cable schematic	20
Figure 2.11: Ceramic coaxial resonator structure.....	21
Figure 2.12: Parallel RLC with its equivalent coaxial resonator (Temex, 2015a:143)	21
Figure 2.13: Q factor versus frequency for different resonators’ profiles (Trans-Tech, 2013:2)	25
Figure 3.1: Transfer function block diagram.....	27
Figure 3.2: Example of a complex plane	28
Figure 3.3: Frequency response of Butterworth low pass filter for varying N (adapted from Pozar, 2005:402)	29
Figure 3.4: Chebyshev low pass response (adapted from Pozar, 2005:402; Verdellin, 2005:276-278)	30
Figure 3.5: Operation of impedance and admittance inverters	32
Figure 3.6: Impedance and admittance inverters. (a) Implementation as quarter- wave transformers. (b) Implementation using transmission line and reactive elements. (d) Implementation using capacitor network (adapted from Podzar, 2005:411-412)	33
Figure 3.7: Third order coupled resonator bandpass filter (adapted from Rhea, 1994:155) ..	34
Figure 4.1: Quarter wavelength ceramic coaxial resonator.....	39

Figure 4.2: Fifth order capacitively coupled resonator bandpass filter	41
Figure 4.3: Fifth order bandpass filter simulated response	42
Figure 4.4: Fourth order coupled resonator bandpass filter	42
Figure 4.5: Fourth order capacitively coupled resonator	44
Figure 4.6: Simulated result of the fourth order coupled resonator	45
Figure 4.7: Finite transmission zero topology placement.....	45
Figure 4.8: Fourth order Coupled resonator bandpass filter with TZ.....	46
Figure 4.9: Simulation result of a fourth order coupled resonator	47
Figure 4.10: LS profile dimension diagram (adapted from Trans-Tech, 2007a:1).....	48
Figure 4.11: Coupled bandpass filter equivalent 3D structure	49
Figure 4.12: Simulated results of the equivalent 3D structure bandpass filter	49
Figure 4.13: Optimised equivalent 3D structure bandpass filter response	51
Figure 4.14: Simulation setup on a tabless CCR 3D structure.....	52
Figure 4.15: Simulation setup on a CCR structure with tab	53
Figure 4.16: Single S-parameter response of a tabless CCR	54
Figure 4.17: Single S-parameter response of CCR with tab.....	54
Figure 4.18: Gap capacitor equivalent circuit (adapted from Mathhaei et al., 1980:442)	55
Figure 4.19: Configuration for electric coupling (adapted from Hano et al., 1986:973)	55
Figure 4.20: Equivalent circuit of the coupling between two CCRs with a coupling capacitor (adapted from Hano et al., 1986:973)	56
Figure 4.21: Equivalent circuit of a coupling between a CCR and an input or output resistance (adapted from Hano et al., 1986:974)	57
Figure 4.22: Equivalent circuit of the coupling between all 4 resonators and the external circuit (adapted from Hano et al., 1986:974)	58
Figure 4.23: Coupling capacitor structure equivalent circuitry (adapted from Lierena Castro, 2014:66)	58
Figure 4.24: Geometry of the parallel Plate Capacitor (Adapted from stuart, 2007:3).....	59
Figure 4.25: Parallel Plate capacitors overlapping area adapted from (Lierena Castro, 2014:66, Fei et al., 2009:43-46)	60
Figure 4.26: E-field distribution around the coupling capacitors	61

Figure 4.27: Ceramic coaxial resonator bandpass filter with 4 CCR in 3D form and the coupling capacitor structure	63
Figure 4.28: Ceramic coaxial resonator bandpass filter simulated result	63
Figure 4.29: Ceramic coaxial resonator bandpass filter optimised result	64
Figure 4.30: Colour map	64
Figure 4.31: E-field distribution at 1.98 GHz (0, 30, 60 degrees)	65
Figure 4.32: E-field distribution at 2.2 GHz.....	66
Figure 4.33: E-field Distribution at 2.25 GHz	66
Figure 4.34: E-field Distribution at 2.3 GHz	66
Figure 4.35: H-Field Distribution at different frequencies.....	67
Figure 4.36: Surface Current flow	68
Figure 5.1: PCB layout and printed board.....	69
Figure 5.2: Top and bottom plate capacitor structure	69
Figure 5.3: CNC milling machine and oven	70
Figure 5.4: Coupling capacitor structure dimension	71
Figure 5.5: Populated board dimension	71
Figure 5.6: Metallic enclosure	71
Figure 5.7: Ceramic coaxial resonator bandpass filter: back and front view	72
Figure 5.8: Test setup	72
Figure 5.9: Measured result	73
Figure 5.10: Temperature cycling test setup	74
Figure 5.11: Temperature cycling at different temperature levels	75
Figure 5.12: Comparison of results	75

LIST OF TABLES

Table 2.1: Ceramic coaxial resonator dimensions (adapted from Trans-Tech, 2013a:1-7) ...	24
Table 2.2: Frequency range for different materials and profiles (adapted from Trans-Tech, 2013a:1-7)	24
Table 4.1: Specification.....	40
Table 4.2: Fifth order bandpass filter parameter values	41
Table 4.3: Calculated values of the coupled resonator bandpass filter	44
Table 4.4: CCR lengths and frequency values	47
Table 4.5: Optimised CCR length and frequency values	50
Table 4.6: Differences in frequencies.....	53
Table 4.7: Coupling structure values.....	62
Table 5.1: Comparison table.....	76

ABBREVIATIONS AND ACRONYMS

ADS:	Agilent Technology Software
CCR:	Ceramic Coaxial Resonator
COTS:	Commercial off-the-shelf
CPUT:	Cape Peninsula University of Technology
CST:	Computer Simulation Technology
E-field:	Electric Field
EM:	Electromagnetic
F'SATI:	French–South African Institute of Technology
3D:	Three-dimensional
H-Field:	Magnetic Field
HP:	High Profile
I/O	Input/ Output
LC:	Inductor, Capacitor
LEO:	Low Earth Orbit
LS:	Standard Profile
n.d:	No date
PCB:	Printed Circuit Board
Q factor:	Quality Factor
RF:	Radio Frequency
RLC:	Resistor, Inductor, Capacitor.
S-band:	IEEE Microwave band from 2 GHz to 4 GHz
SRC:	Self-Resonant Frequency
TE:	Transversal Electric
TEM:	Transversal Electromagnetic
TZ:	Transmission Zero
VCO:	Voltage control Oscillator
VNA:	Vector Network Analyser

CHAPTER 1 INTRODUCTION

1.1 Application of microwave filters

A CubeSat is a small satellite in the shape of a cube, weighing less than 1 kilogram. Launched into a low earth orbit (LEO), a CubeSat has a mission life expectancy less than 2 years compared with robust satellites. A CubeSat consists of different subsystems, each performing a specific task (Chin & Clark, 2012:1). The CubeSat has a telemetry and command system respectively in charge of sending and receiving data to and from the CubeSat. This telemetry system comprises the transceiver system, which then uses microwave filters to ensure that the information send and received is in the respective frequency band by separating the signals coming from various sources, to improve selectivity (Cebrián Herrera, 2014:14-16, 35; Kalde, 2015:26-32). The CubeSat communication subsystem is the most power consuming of all subsystems. This is due to the linearity requirement of the high power amplifier in the final stage of the transmitter of the communication subsystem. Figure 1.1 illustrates the receiver system used on board F'SATI ZACUBE 1 (F'SATI, 2013:10).

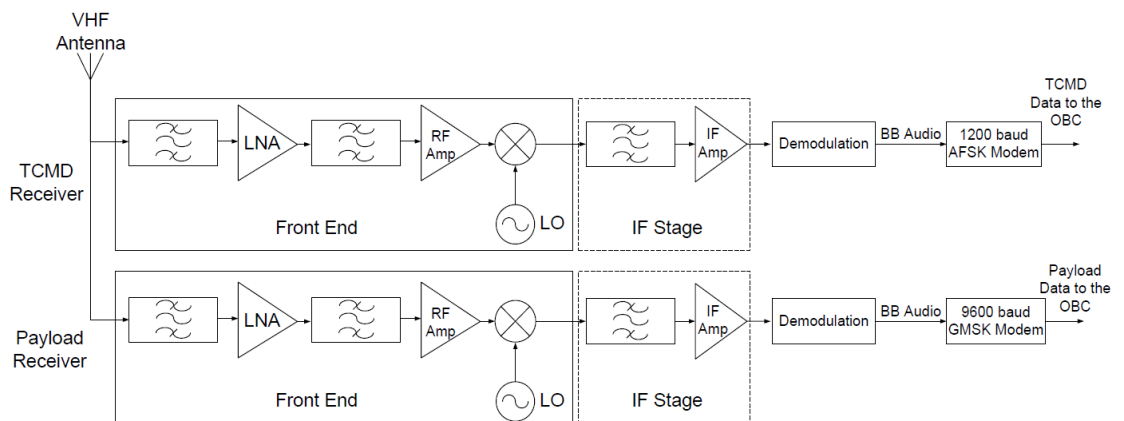


Figure 1.1: ZACUBE 1 transceiver block diagram (F'SATI, 2013:10)

Satellite missions are diverse, but their primary mission is the ability to exchange information with the ground station. Such exchange of information relies on many subsystems to communicate with each other. The realization of a high Q filter at microwave frequencies when using lumped elements may become impractical because the wavelength becomes comparable, or smaller, to the physical dimensions of the circuit elements (Goyal et al., 2014:333). Each filter type (lowpass, highpass, bandpass and bandstop) has diverse responses (Chebyshev, Butterworth, Gaussian,

etc.). Cohn, 1968: 218-227, showed how a high Q dielectric resonators microwave bandpass filter is implemented using a dielectric disc as resonator. The disc resonator was implemented using filter and dielectric design theory. The analysis of the specification correlates well the measured and simulated results. Similarly Hano *et al.*, 1986: 972-976, designed a directly-coupled quarter wavelength coaxial resonator bandpass filter for mobile application. The resonators were coupled to each other through apertures and were made from metalized high Q dielectric ceramic material. The filter was constructed by adjusting the resonant frequency and was beneficial for size-reduction due to coupling method used. Circuit complexity reduction can also be achieved by cascading two third-order parallel bandpass filters using common resonator sections as demonstrated by Chen *et al.*, 2006: 1945-1952. Another way of implementing filters are by using waveguides, as demonstrated by Hunter *et al.*, 2002: 794-803, who designed a waveguide and coaxial resonator filter with a Chebyshev response for military and satellite communication. Much work was done after this using others type of microwave filter implementation.

With the advancement of technology, the development of communications systems requires the implementation of microwave filters of high-performance, lower manufacturing cost and high quality. Microwave filter design concentrates on some of the aspects mentioned above. These aspects are important limiting factors on the size and weight of the overall system.

The goal of filter design and synthesis is to find a physical requirement that can satisfy the communication channel's predefined specification. With the improvement of the communications system, meeting the specifications has become more challenging.

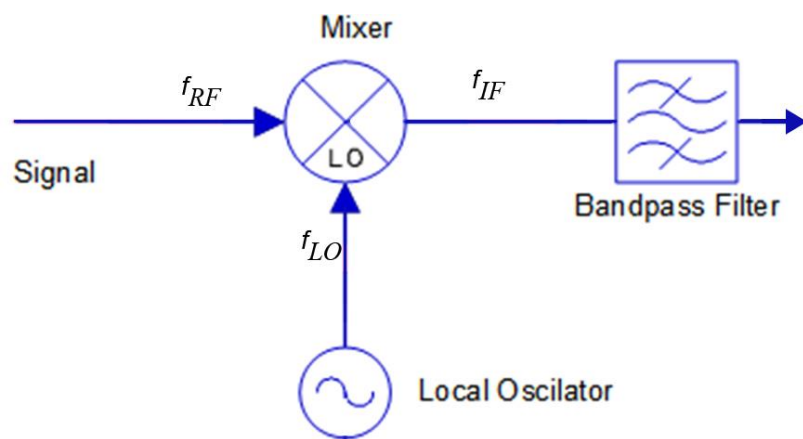


Figure 1. 2: Down converter section in a receiver system

Figure 1.2 demonstrates the down converting path of a receiver communication system. In the system the received radio frequency (f_{RF}) is mixed with the local oscillator frequency (f_{LO}) to create an intermediate frequency (f_{IF}). The intermediate frequency is the difference between the receive signal and the local oscillator signal. Frequencies such as the undesired image frequency and local Oscillator (LO) frequency should be rejected to an adequate degree to avoid performance degradation of the intermediate frequency signal.

A common problem for bandpass filters are that the image frequency can be very close to the intermediate frequency, which could also pass through the bandpass filter, and therefore cause the reception of unwanted frequencies. The reception of unwanted frequencies will produce inter-symbol-interference which will result in the degradation of the signal of interest (Blake, 1997:156-165). The receiver system presented in Figure 1.1 requires a low passband insertion loss with high rejection at the passband edge, which prevents the degradation of the wanted signal.

There are many ways of achieving good rejection, including the increase of the filter's order and the use of transmission zeros. The increase of the filter's order, leads to a degradation of the passband insertion loss as well as the addition of more components to the design, which thus results in an increase in the size, weight and cost of the generated system. The usage of transmission zeros is a more effective approach since it does not require additional components on the circuit and are generated by means of cross-coupling (Musonda *et al.*, 2015: 8-10, Devlin,nd:1-12).

Ceramic coaxial resonators (CCRs) are suitable for use on bandpass filters, as they can be easily arranged into the desired configuration because of their electrical properties. Aspects such as low cost, size reduction and good performance are some of the features achievable using CCR.

1.2 Rationale

The idea for this topic was initiated by the French–South African Institute of Technology (F'SATI). The nanosatellite programme at the Cape Peninsula University of Technology is run at the research centre F'SATI. A study involving the design of a bandpass filter was required by F'SATI for their CubeSat transceiver system, based on CCR technology and operating at S-band. The realisation of the design using off-the-shelf CCR is cost-effective as they are commercially available. Ceramic filters also offer small-size, low-loss, and reliable systems, owing to their high quality. The

process used to design the bandpass filter with CCR starts with the use of coupled resonator bandpass filter design techniques combined with some filter theory to implement the coupled resonators bandpass filter presented in Figure 1.3. To avoid the perturbation of the response, the structure of the coupling capacitor and the four CCRs are covered with a metallic enclosure.

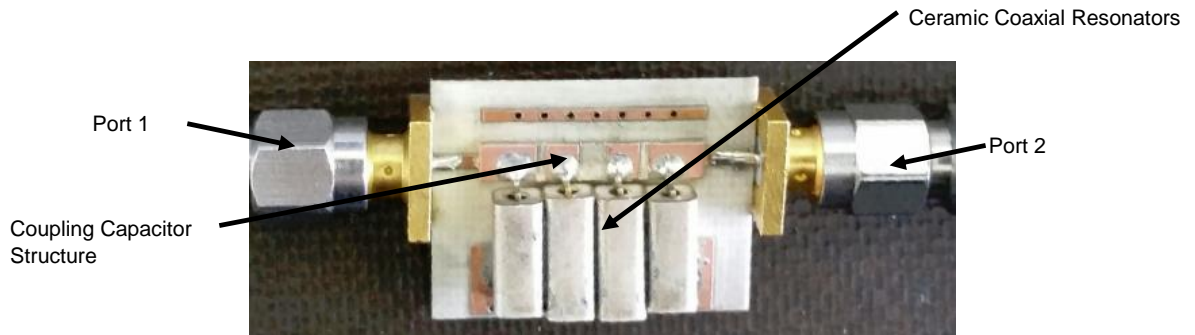


Figure 1.3: Ceramic coaxial resonator bandpass filter with capacitive coupling structure

1.3 Objectives

The ultimate aim of the project was to design a bandpass filter that would operate at commercial S-band used for downlink communication (2.2 GHz to 2.3 GHz), using CCR technology. The filter size should not be greater than 30 mm × 30 mm. A transmission zero should be designed between 1.9 GHz and 2.0 GHz to allow high attenuation at the defined rejection frequency.

Certain outcomes were set to be achieved at the end of this study. The outcomes envisaged were:

1. Design a lumped element bandpass filter circuit, at the desired frequency, with transmission zeros using ADS and CST Microwave Studio®.
2. Transform the lumped element filter circuit to the capacitively coupled resonator circuit using couple resonator bandpass filter techniques.
3. Convert it to a 3D field model in CST Microwave Studio® to optimise and evaluate the filter response and identify possible unwanted coupling.
4. Manufacture the PCB and assemble the filter.
5. Test the filter response and conduct environmental testing.
6. Observe the radiation and coupling results with and without the filter enclosure.
7. Redesign the filter if it does not meet the design specifications.

1.4 Investigative questions

The investigation questions to guide the research were:

1. How to assemble the ceramic resonators on the PCB without altering too much the inductance and capacitance between each ceramic resonator, which in turn will alter the filter response.
2. How to minimise electromagnetic coupling at the end points of the resonator owing to the length of the resonator tab.
3. How to implement an enclosure to prevent unwanted magnetic coupling from escaping into the surrounding environment.
4. How to implement transmission zeros.
5. How to implement the coupling capacitor structure.

1.5 Overview of the thesis

The purpose of the work presented in this thesis was to design a bandpass filter using COTS CCR technology. CST Microwave Studio[®] was used to perform 3D simulations of the bandpass filter circuitual model, the capacitor coupling structure and the CCR structure. EM modelling simulation was done to visualise the effect of radiation around each CCR. Finally, the designed bandpass filter needed to meet not only the specification requirement, but also space environmental and physical requirements (size and weight).

1.6 Organisation of the thesis

The thesis is arranged in six chapters, with Chapter 1 providing the introduction.

Chapter 2 provides background information on ceramic coaxial resonators and their electrical characteristics. Some background on microwave resonators as presented by their series and parallel equivalents is given.

Chapter 3 presents an overview of the fundamental theory of RF and microwave filters. It first addresses the filter transfer function and the types of response. This is followed by the types of transformation design formulae and their implementation, using the Coupled resonator bandpass formulae.

Chapter 4 presents the design. Here the detailed solution process to achieve the target is described. It first addresses the design formula to build the lumped element Coupled resonator bandpass filter. This chapter also discusses the bandpass filter implementation stage of the CCR 3D model construct using CST

Microwave Studio® and the electromagnetic simulation of the filter and the CCR 3D model.

Chapter 5 presents the fabrication, testing, and discussion of results. Each building stage of the ceramic coaxial resonator bandpass filter is addressed here. The measurement procedure is also addressed in this chapter, and finally, a comparison between the simulated and measured results is presented.

Chapter 6 provides conclusions and recommendations. It also provides recommendations for future work on the topic.

CHAPTER 2 CERAMIC COAXIAL RESONATOR

In this chapter, an overview of the basic properties of the ceramic coaxial resonator (CCR) is presented and the lumped element equivalent of the CCR is derived. In Section 2.1, microwave resonator RLC (resistor, inductor, and capacitor) lumped element basic properties are introduced. Section 2.2 describes the use of the transmission line as a resonator, and finally, Section 2.3 discusses the literature survey on ceramic coaxial resonators.

2.1 Microwave resonators

A resonator is a device that exhibit resonance at its resonant frequency. Applications such as filters, oscillators, tuned amplifiers and frequency meters make use of resonators which are key to their performance. At a frequency close to resonance, microwave resonators can be represented by either a series or a parallel RLC circuit. Circuits containing RLC elements have special characteristics useful in many applications (Pozar, 2005:266).

At microwave frequencies, lumped element components, particularly capacitor and inductors, can no longer be treated as ideal. A real world capacitor and inductor is describes in Figure 2.1 (a) and (b) respectively.

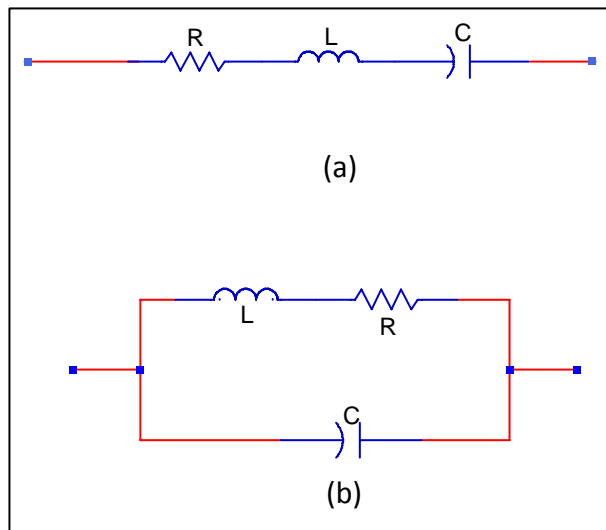
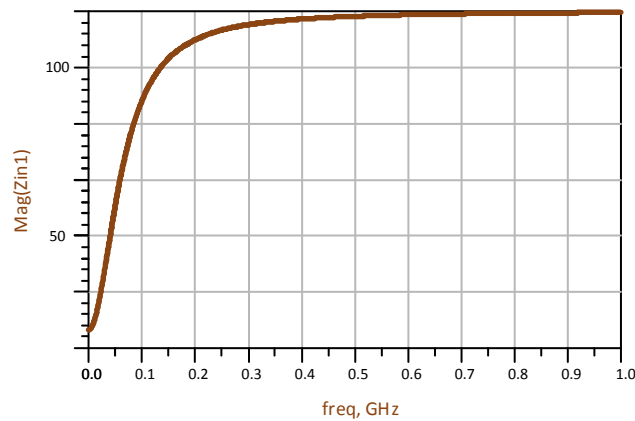


Figure 2.1: (a) Real word Capacitor, (b) Real world Inductor

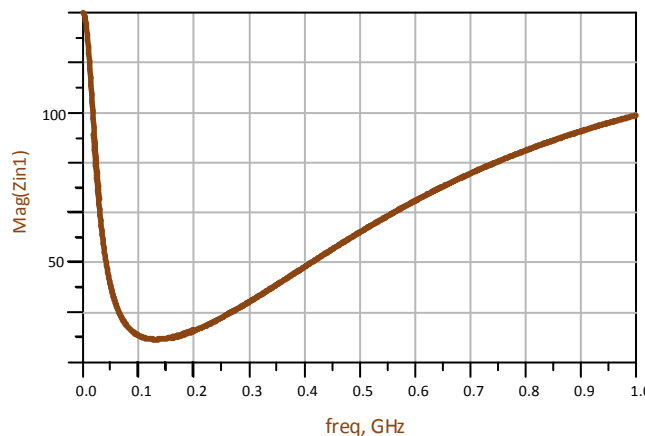
As presented by figure 2.1 (a) a real world capacitor is made of a series resistance (R) which represent the dielectric loss tangent as demonstrate by equation (2.1), and of series inductor (L) which is parasitic inductance introduced by the leads, which should be kept as short as possible.

$$R = \frac{1}{\omega C \tan \delta} \quad (2.1)$$

Similarly, a real word inductor in figure 2.1 (b) comprise of a parasitic resistance (R) in series with the inductor (L) which is the ohmic losses in the wire. This loss increase with frequency, due to skin effect, and due to the parasitic capacitance (C) as electric fields are formed between the winding (Wentworth, 2007:506-515).



(a)



(b)

Figure 2.2: (a) Real world inductor magnitude response, (b) Real world capacitor magnitude response (Adapter from Wentworth, 2007:506-515).

Figure 2.2 (a) and (b) represents respectively the response of a real world inductor (a) and capacitor (b) (Verdelin, 2005:38-43).

2.1.1 Series resonant circuit

A series resonant circuit is an electrical resonance accomplished with a resistor, an inductor and capacitor disposed in series so that the total impedance falls to a minimum at the resonant frequency. Figure 2.3 presents a lumped RLC connected in series across a voltage supply.

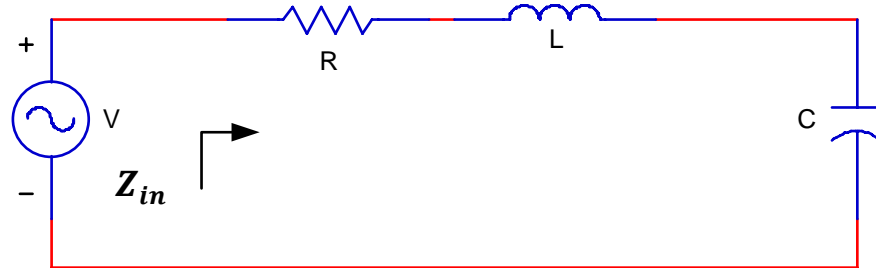


Figure 2.3: RLC series resonant circuit (adapted from Pozar, 2008:267)

The series RLC circuit has a property of resonating at a specific frequency called resonant frequency (f_r).

The RLC connected in series configuration has an input impedance (Z_{in}) defined by equation (2.2) (Pozar, 2005:266-267; Collin, 2001:481-485),

$$Z_{in} = R + j\omega L - j\frac{1}{\omega C} \quad (2.2)$$

The complex power delivered to the resonator is

$$P_{in} = \frac{1}{2}|I|^2 \left(R + j\omega L - j\frac{1}{\omega C} \right) \quad (2.3)$$

and the power dissipated by the resistor (R) is

$$P_{loss} = \frac{1}{2}|I|^2 R \quad (2.4)$$

Energy is stored in two ways in the series RLC presented in Figure 2.3.

- a. As a magnetic field when the current (I) passes through an inductor (L)

The total energy stored in the magnetic field (E_m) is defined using equation (2.5) to (2.7). Equation (2.5) describes the total energy stored per unit time when current (I) flows down the wire. Taking the integral of this energy stored per unit time, with (L) as a constant it can be demonstrated in equation (2.6), that the energy stored in the magnetic field can be described by equation (2.7) (Griffiths, 2008:317).

$$\frac{dE_m}{dt} = -WI = LI \frac{dI}{dt} \quad (2.5)$$

$$\int \frac{dE_m}{dt} dt = L \int I \frac{dI}{dt} dt \quad (2.6)$$

$$E_m = \frac{1}{4} |I|^2 L \quad (2.7)$$

b. As a static electric field when the capacitor (C) is charged

The total energy stored in the electric field (E_e) is defined using equations (2.8) to (2.10). Equation 2.8 describes the rate of change of the energy stores in the electric field.

$$dE_e = \left(\frac{q}{C} \right) dq \quad (2.8)$$

Where:

q : is the charge

Taking the integral of equation (2.8) to find the necessities energy stored when $q=0$ and $q=Q$ lead to equation (2.9)

$$E_e = \int_0^Q \left(\frac{q}{C} \right) dq = \frac{1}{2} \frac{Q^2}{C} \quad (2.9)$$

Where:

Q : is the total charge when current flow from the positive plate to negative plate.

Then knowing that $Q = CV$, substituting in equation (2.9), equation (2.10) which is the total energy is derived (David, 2008:103-106).

$$E_e = \frac{1}{4} |I|^2 \frac{1}{\omega^2 C} \quad (2.10)$$

Resonance occurs in a series RLC circuit when the average stored magnetic and electric energy are equal.

At resonance:

- The input impedance $Z_{in} = R$ which shows that the input impedance is purely real
- The resonant frequency is derived using equation (2.11)

$$\omega_0 = \frac{1}{\sqrt{LC}} \quad (2.11)$$

At frequency close to resonance $\omega = \omega_0 + \Delta\omega$, the input impedance of Equation (2.2) can be transformed as follows:

$$Z_{in} \approx R + j2L\Delta\omega \quad (2.12)$$

Figure 2.4 represents a series RLC magnitude response which is the variation of impedance versus frequency.

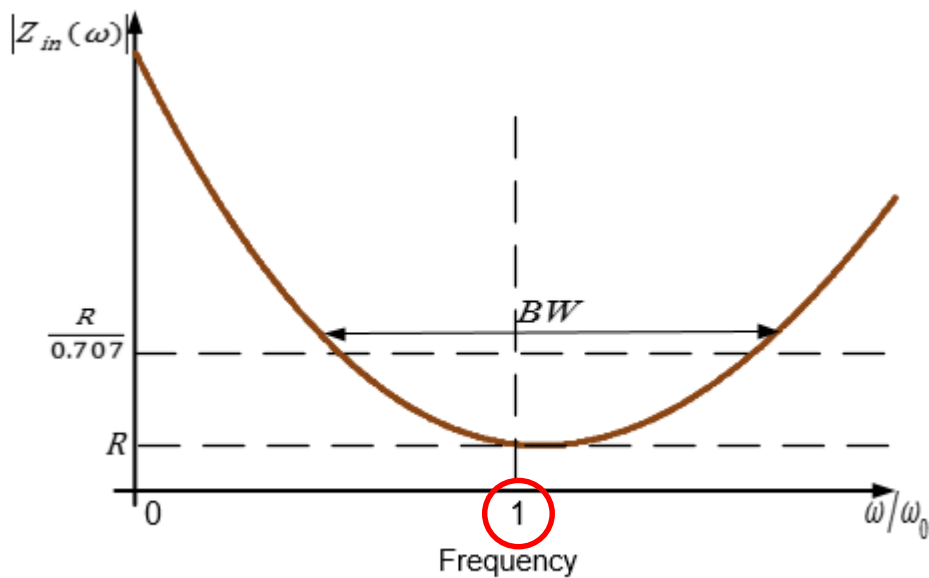


Figure 2.4: Series RLC response (adapted from Pozar, 2005:267)

The response presented in figure 2.4 behaves both as a real world capacitor with magnitude response below resonance as well as a real world inductor above resonance as shown in Figure 2.2. Resonance occur at the frequency point 1 in Figure 2.4, therefore the inductive and capacitive reactance are equal in magnitude, but cancel each other because they are 180° apart in phase (Pozar, 2005:266-268; Behagi, 2015:4-7).

2.1.2 Parallel resonant circuit

A parallel resonant circuit is an electrical resonance accomplished with a resistor (R), an inductor (L) and capacitor (C) arranged in parallel so that the total impedance rises to a maximum at the resonant frequency. Figure 2.5 below is a lumped element RLC connected in parallel across a voltage supply.

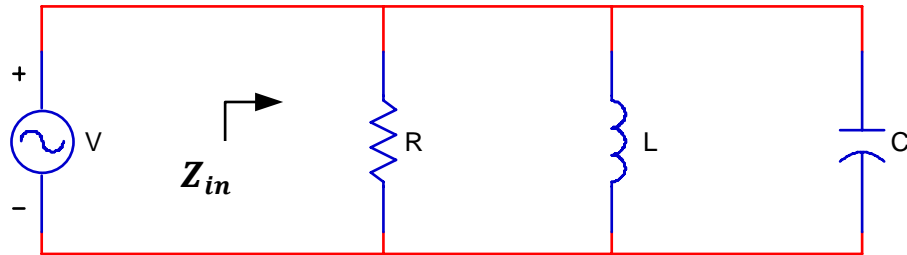


Figure 2.5: Parallel RLC circuit (adapted from Pozar, 2005:269)

The parallel RLC circuit is said to have a dual relationship with a series RLC circuit (Pozar, 2005:269-271). The RLC connected in parallel configuration has an input impedance defined by equations (2.13).

$$Z_{in} = \left(\frac{1}{R} + \frac{1}{j\omega L} + j\omega C \right)^{-1} \quad (2.13)$$

The complex power delivered to the resonator is

$$P_{in} = \frac{1}{2} |V|^2 \left(\frac{1}{R} + \frac{j}{\omega L} - j\omega C \right) \quad (2.14)$$

and the power dissipated by the resistor (R) is

$$P_{loss} = \frac{1}{2} \frac{|V|^2}{R} \quad (2.15)$$

Energy is stored in two ways in the parallel RLC presented in Figure 2.5.

- a. As a magnetic field when the current passes through an inductor

$$E_m = \frac{1}{4} |V|^2 \frac{1}{\omega^2 L} \quad (2.16)$$

b. As a static electric field when the capacitor is charged

$$E_e = \frac{1}{4} |V|^2 C \quad (2.17)$$

Resonance occurs in a parallel RLC circuit when the average stored magnetic and electric energy are equal $E_m = E_e$

- The input impedance $Z_{in} = R$
- The resonant frequency is derived using Equation (2.18)

$$\omega_0 = \frac{1}{\sqrt{LC}} \quad (2.18)$$

At frequency close to resonance $\omega = \omega_0 + \Delta\omega$, the input impedance of Equation (2.13) can be transformed as follows

$$Z_{in} \approx \frac{R}{1 + 2j\Delta\omega C} \quad (2.19)$$

This form of equation will be useful to derive the parameter of the distributed element resonator. Figure 2.6 represents a parallel RLC response which is the variation of impedance versus frequency (Pozar, 2005:269-271; Behagi, 2015:7-9).

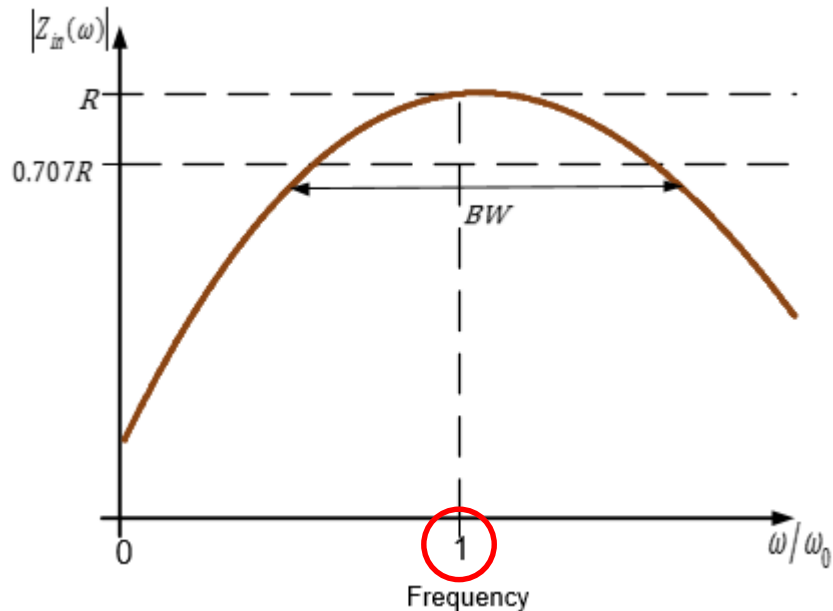


Figure 2.6: Parallel RLC circuit response (adapted from Pozar, 2005:269)

The response presented in figure 2.6 behaves as both a real world inductor below resonance as well as a real world capacitor above resonance as demonstrated in Figure 2.2. Resonance occur at 1 as shown in Figure 2.6, therefore the inductive and capacitive reactance are equal in magnitude, but cancel each other because they are

180° apart in phase. The parallel resonance circuit is resistive at resonance, inductive below resonance, and capacitive above resonance.

2.1.3 Quality (Q) factor

The Q factor of a resonant circuit is a measure of the selectivity of a resonant circuit. It is the ratio of the energy stored in the reactive element (inductor, capacitor) to the power dissipated (P_{loss}) in the circuit resistance (R), multiplied by the angular frequency (ω). The resistor (R) in Figure 2.3 and 2.5 represents the loss in the resonator. It includes losses in the capacitor as well as in the inductor.

a. Q factor in a series RLC resonant circuit

The Q factor in a series resonant circuit is represented by Equation (2.20).

$$Q = \omega \frac{E_m + E_e}{P_{loss}} \quad (2.20)$$

at resonance where $E_m = E_e$ the Q factor transforms to equation (2.21).

$$Q = \frac{1}{\omega_0 RC} \quad (2.21)$$

The Q factor in a series RLC circuit increases as the resistor (R) value decreases (Pozar, 2005:268). However, the Q factor will decrease if the resistor value increases, causing losses in the circuit.

b. Q factor in a parallel RLC resonant circuit

The Q in a parallel resonant circuit is represented by Equation (2.22).

$$Q = \omega \frac{E_m + E_e}{P_{loss}} \quad (2.22)$$

at resonance where $E_m = E_e$ the Q factor transforms to equation (2.23)

$$Q = \omega_0 RC \quad (2.23)$$

The Q factor in a parallel RLC circuit increases as the resistor (R) value increases.

The selectivity of a circuit is dependent upon the amount of resistance (losses) in the circuit. The lower the loss, the higher the Q and narrower the bandwidth. The higher the loss, the lower the Q, and wider the bandwidth (Pozar, 2005:270; Behagi, 2015:9; (Levy, 2002:784)).

2.2 Transmission line resonators

At microwave frequency, the conventional RLC lumped elements tends to be very difficult to achieve, as the small values of inductance and capacitance are physically unrealisable. Resonators can be implemented as short circuited half wavelength ($\lambda/2$) and quarter wavelength ($\lambda/4$) lines or open circuited half wavelength ($\lambda/2$) (Pozar, 2005:272).

2.2.1 Short circuited half wavelength and quarter wavelength line

Figure 2.7 represents a short-circuited line of length (ℓ) with a characteristic impedance (Z_0), propagation constant (β) and attenuation constant (α) (Pozar, 2005:272-275).

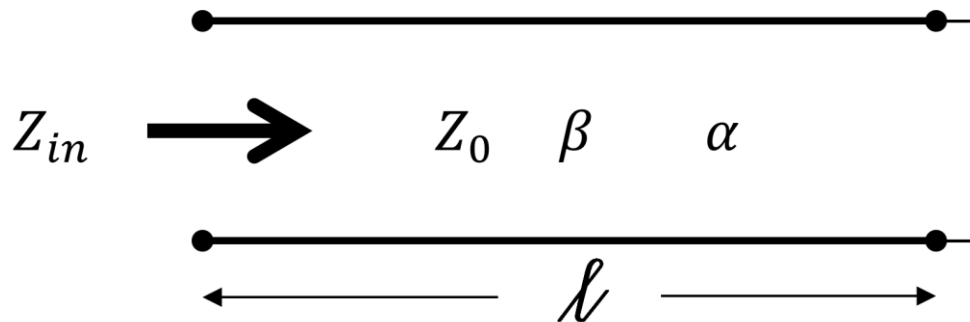


Figure 2.7: Short circuited transmission line (adapted from Pozar, 2005:273)

a. Short circuited half wavelength ($\lambda/2$) line

The input impedance (Z_{in}) of a line of $\ell = \lambda/2$ where $\lambda = \frac{2\pi}{\beta}$ at frequency $\omega = \omega_0$ is defined by

$$Z_{in} = Z_0 \tanh(\alpha + j\beta)\ell \quad (2.24)$$

Using an identity of hyperbolic tangent equation (2.25) of the input impedance is derive

$$Z_{in} = Z_0 \frac{\tanh \alpha \ell + j \tan \beta \ell}{1 + j \tan \beta \ell \tanh \alpha \ell} \quad (2.25)$$

At frequency near resonance, $\omega = \omega_0 + \Delta\omega$, assuming a transversal electrical magnetic line (TEM) with $\Delta\omega$ small the following is derived:

$$\beta \ell = \frac{\omega \ell}{v_p} = \frac{\omega_0 \ell}{v_p} + \frac{\Delta\omega \ell}{v_p} \quad (2.26)$$

Where:

v_p : phase velocity

With the length $\ell = \lambda/2$, for $\omega = \omega_0$, equation (2.26) transform to:

$$\beta \ell = \pi + \frac{\Delta\omega \pi}{\omega_0} \quad (2.27)$$

Substituting $\beta \ell$ in the input impedance in equation (2.25) the input impedance then transforms to

$$Z_{in} = Z_0 \left(\alpha \ell + j \frac{\Delta\omega \pi}{\omega_0} \right) \quad (2.28)$$

for $\Delta\omega \alpha \ell / \omega_0 \ll 1$ the input impedance becomes

$$Z_{in} = R + 2jL\Delta\omega \quad (2.29)$$

Equation (2.29) shows that the short circuited half wavelength line and the series RLC circuit input impedances are similar. By equating Equation (2.12), (2.29) and (2.11), the resistance, inductance and capacitance equivalents are derived:

$$R = Z_0 \alpha \ell \quad (2.30)$$

$$L = \frac{Z_0 \pi}{2\omega_0} \quad (2.31)$$

$$C = \frac{1}{\omega_0 L} \quad (2.32)$$

b. Short circuited quarter wavelength ($\lambda/4$) line

The input impedance Z_{in} of a short circuited transmission line of $\ell = \lambda/4$ is defined by

$$Z_{in} = Z_0 \tanh(\alpha + j\beta)\ell \quad (2.33)$$

$$Z_{in} = Z_0 \frac{\tanh \alpha \ell + j \tan \beta \ell}{1 + j \tan \beta \ell \tanh \alpha \ell} \quad (2.34)$$

Equation 2.35 is then obtained by multiplying the numerator and the denominator of equation (2.34) by $-j \cot \beta \ell$ then using the hyperbolic identity.

$$Z_{in} = Z_0 \frac{1 - j \tanh \alpha \ell \cot \beta \ell}{\tanh \alpha \ell - j \cot \beta \ell} \quad (2.35)$$

for $\ell = \lambda/4$ at $\omega = \omega_0$, and letting $\omega = \omega_0 + \Delta\omega$ considering a TEM line the following are derived.

$$\beta \ell = \frac{\pi}{2} + \frac{\Delta\omega\pi}{\omega_0} \quad (2.36)$$

And taking the cotangent (cot), equation (2.36) becomes:

$$\cot \beta \ell = \cot\left(\frac{\pi}{2}\right) + \frac{\pi\Delta\omega}{2\omega_0} \quad (2.37)$$

Which transform to:

$$\cot \beta \ell = -\tan \frac{\pi\Delta\omega}{2\omega_0} = -\frac{\pi\Delta\omega}{2\omega_0} \quad (2.38)$$

Substituting equation (2.38) in equation (2.35) give the new input impedance defined by equation (2.39).

$$Z_{in} = \frac{Z_0}{\alpha \ell + j\pi\Delta\omega/2\omega_0} \quad (2.39)$$

For $\Delta\omega\alpha\ell\pi/2\omega_0$ the input impedance becomes

$$Z_{in} = \frac{1}{1/R + 2j\Delta\omega C} \quad (2.40)$$

Equation (2.40) shows that the short circuited quarter wavelength line and the parallel RLC circuit input impedances are similar. By equating Equation (2.19), (2.40) and (2.18), the resistance, inductance and capacitance equivalents are derived:

$$R = \frac{Z_0}{\alpha \ell} \quad (2.41)$$

$$C = \frac{\pi}{4\omega_0 Z_0} \quad (2.42)$$

$$L = \frac{1}{\omega_0^2 C} \quad (2.43)$$

Figure 2.6 shows the parallel resonant circuit and its corresponding $\lambda/4$ short circuited.

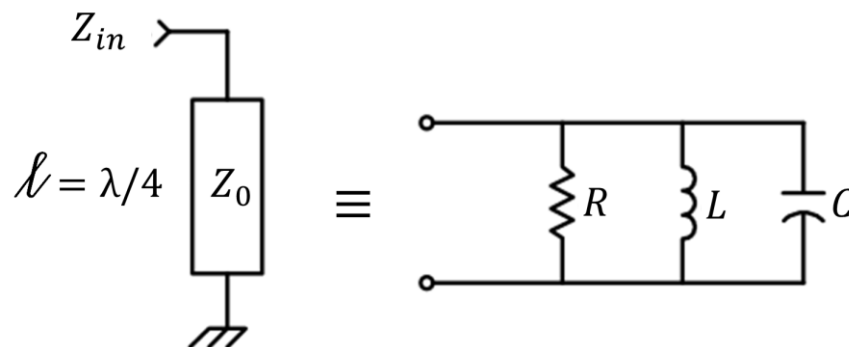


Figure 2.8: Short circuited quarter wavelength and a parallel RLC equivalence (adapted from Matthaei et al., 1980:216)

2.2.2 Open circuited $\lambda/2$ line

Figure 2.7 is a representation of an open circuited line which consists of an open circuited length of transmission line. This type of line is a practical resonator often used in microstrip circuits (Pozar, 2005:276-277). Such a resonator will behave as a parallel resonant circuit when the length is $l = \lambda/2$ or the multiple of $\lambda/2$.

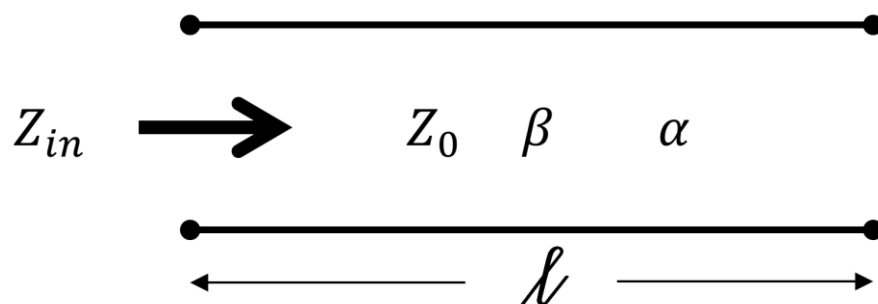


Figure 2.9: Open circuit half wavelength line (adapted from Pozar, 2005:276)

The input impedance of an open circuit of length (ℓ) is given by

$$Z_{in} = Z_0 \coth(\alpha + j\beta)\ell \quad (2.45)$$

At frequency near resonance, $\omega = \omega_0 + \Delta\omega$ the input impedance then transforms to

$$Z_{in} = \frac{Z_0}{\alpha\ell + j(\pi\Delta\omega/\omega_0)} \quad (2.46)$$

Comparing the parallel RLC circuit input impedance with that of the open circuited half wavelength by equating equation (2.18),(2.19) and (2.46), it shows

$$R = \frac{Z_0}{\alpha\ell} \quad (2.47)$$

$$C = \frac{\pi}{4\omega_0 Z_0} \quad (2.48)$$

$$L = \frac{1}{\omega_0^2 C} \quad (2.49)$$

2.3 Ceramic coaxial resonator

Coaxial resonators have become common components in applications such as filters, oscillators, etc. A typical resonator consists of a shortened quarter wavelength line section, although an open circuit half wavelength may be used for some applications. It exists in two different types of coaxial resonators (forms); a quarter wavelength resonator with one end metallised to short circuit the centre conductor to the outer conductor, and a half wavelength resonator with both ends open (non-metallised). One form of a short circuit quarter wavelength transmission line is a coaxial cable as displayed in Figure 2.10 (Lierena Castro, 2014:8-9; Nalwa, 1999:524-530) and can be demonstrated by means of an outer and center conductor running along same longitudinal axis. The shielding prevents coupling to the adjacent line.

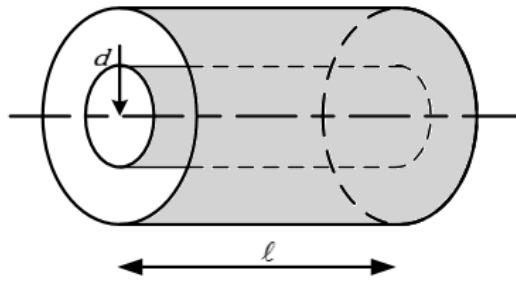


Figure 2.10: Coaxial cable schematic

The characteristic impedance of a coaxial cable with a square outer conductor is defined by equation (2.50) as reported by Cohn, 1969:22.

$$Z_0 = \frac{60}{\sqrt{\epsilon_r}} \ln \frac{1.0787W}{d} \quad (2.50)$$

Where:

ϵ_r : is the material dielectric constant

W : is the outer conductor width

d : is the center conductor diameter

Owing to their high dielectric constant (materials) value, coaxial resonators use the size-reducing effect to make the smallest possible components (filter, VCOs, etc.) at microwave frequency. Coaxial resonators with ceramic insert offer advantages such as high Q, size reduction, better shielding and temperature performance that are superior to those obtained from a conventional LC circuit or microstrip construction. Figure 2.11 below shows a typical structure of a commercially available ceramic coaxial resonator, with an approximately square-shaped cross-section outer conductor and a cylindrical inner conductor (Nalwa, 1999:495; Token, 2017:17-28; Trans-Tech, 2013a:1-12).

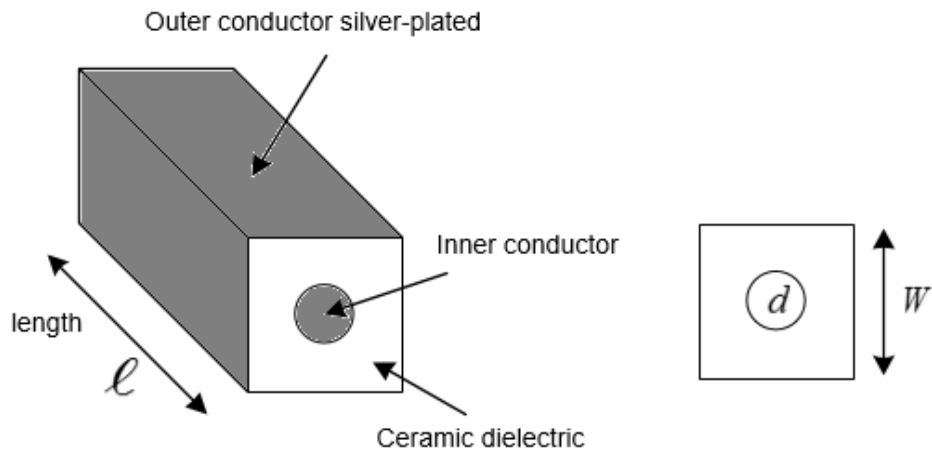


Figure 2.11: Ceramic coaxial resonator structure

Figure 2.12 represents the equivalent circuit of a quarter wavelength ceramic coaxial resonator given by a common RLC circuit in parallel configuration. It shares similarity in term of shielding performance and characteristic impedance with a coaxial cable. This type of resonator also shows similarity in the computation of its lumped element components (RLC) to that of a $(\lambda/4)$ short circuited transmission line. The coaxial resonator lumped RLC presented by equation (2.55), (2.56) and (2.57) is similar to equation (2.41), (2.42) and (2.43).

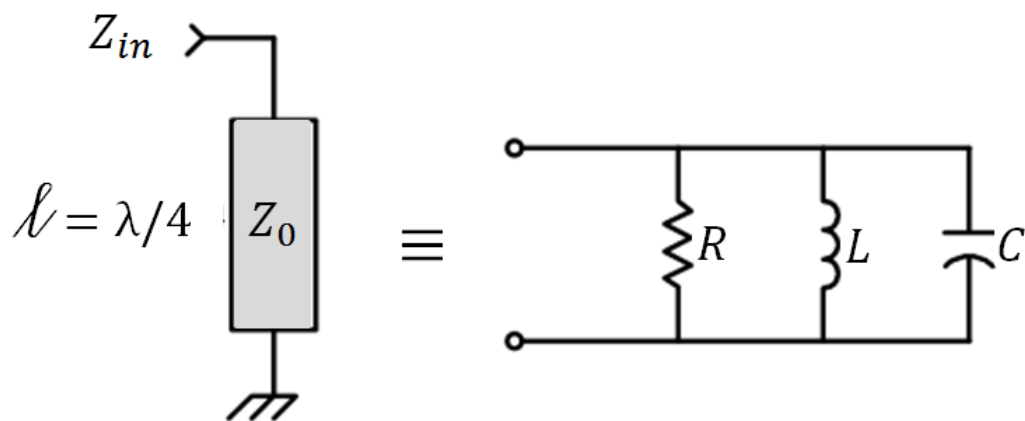


Figure 2.12: Parallel RLC with its equivalent coaxial resonator (Temex, 2015a:143)

The characteristic impedance of a coaxial resonator is directly linked to the physical dimensions of the coaxial element which are width (W), diameter (d) and length (l), together with the dielectric constant of the ceramic material. The ceramic coaxial resonator frequency is a function of the resonator length (l_{res}). This length is usually close to a half wavelength or a quarter wavelength of the required frequency.

The CCR length at its resonant frequency (f_r) for a quarter-wavelength configuration is

$$\ell = \lambda_g / 4 \quad (2.51)$$

where λ_g is the wavelength of the guided TEM mode excited in the resonator defined by Equation (2.52) below

$$\lambda_g = \frac{c}{f_{res} \sqrt{\epsilon_r}} \quad (2.52)$$

where c is the speed of the light equal to 3×10^8 m/s. Substituting Equation (2.52) into Equation (2.51), the length of the quarter-wavelength CCR is defined by

$$\ell_{res} = \frac{c}{4 f_{res} \sqrt{\epsilon_r}} \quad (2.53)$$

The frequency of a quarter wavelength length CCR is then derived as

$$f_{res} = \frac{c}{4 \ell_{res} \sqrt{\epsilon_r}} \quad (2.54)$$

The lumped elements of a quarter wavelength length CCR is then given by (TEMEX 2015a:142-146)

$$L = \frac{1}{\omega_0^2} C \quad (2.55)$$

$$C = \frac{\pi}{4 \omega_0 Z_0} \quad (2.56)$$

$$R = \frac{Q}{\omega_0 C} \quad (2.57)$$

$$Q = \frac{f_0}{BW} \quad (2.58)$$

with

$$Z_0 = \frac{60}{\sqrt{\epsilon_r}} \cdot \ln \left(1.079 \cdot \frac{W}{d} \right) \quad (2.59)$$

$$Q = 60 \frac{W \sqrt{f_{res}}}{25.4} \quad (2.60)$$

Where:

W : width of the resonator profile

d : inner conductor diameter

ε_r : material dielectric constant

Equation (2.59) helps to determine the characteristic impedance of the TEM coaxial component knowing the physical dimension of the profile (HP, LP, LS, SP, etc) and the dielectric constant (ε_r) of the material (1000, 2000, 8800 and 9000) (trans-tech, 2013:10). A CCR with high Q is suitable for filters; the higher the Q the lower the loss and the narrower the bandwidth as demonstrated by equation (2.57) and equation (2.58). Equation (2.53) shows that the resonator length decreases as the dielectric constant (11.5, 39.5 and 90) of each material increases. The higher the dielectric constant of each material, the higher the quality factor as per trans-tech datasheet provided in Appendix A. Figure 2.13 shows that from one material (D1000) to another (D2000) there is an increase in the quality factor value. The datasheet provided by the manufacturer shows limitation over the CCR length depending on each profile and operating frequency. This limitation in CCR length is to avoid the deterioration of the resonator performance in the operating frequency range. This deterioration in performance is caused by the removal of the silver coating of the CCR which then exposes the ceramic material (Vendelin et al., 2005:306).

2.3.1 Coaxial resonators mode propagation

A wave propagates in a medium using various modes. Those modes are the transversal electric mode (TE), the transversal magnetic mode (TM) and the transversal electromagnetic mode (TEM). TE and TM are often found in a medium consisting of a single conductor such as waveguides and they are dispersive and frequency dependent (Stuart, 2007:377-396). A Transmission line, consisting out of two or more conductors such as a coaxial cable, can propagate a wave using the transversal electromagnetic wave mode (TEM). This mode is characterised by having the electric and magnetic fields perpendicular to each other and the direction of the conductor. In the TEM mode, the velocity of propagation is equal to the velocity of light in the dielectric material. Parameters such as voltage, characteristic impedance and current are exclusively defined in the TEM wave. The mode used in the CCR provided by trans-tech is the TEM mode. TEM mode in the CCR has no electric and magnetic field in the direction of propagation because they are shielded with the silver

enclosure as presented by Figure 2.11(Stuart, 2007:306, 388, 394; Pozar 2015:106-117; Collin, 2001:96).

2.3.2 CCR size and materials

Ceramic coaxial resonators are offered by numerous manufacturers, such as Trans-Tech, Integrated Microwave Corp, Tusonix, Temex Ceramics, etc. Depending on each manufacturer, ceramic resonators are offered in different sizes and materials (dielectric constant). CCRs from each manufacturer are made for specific applications and can operate at microwave frequency ranges depending on their applications.

Coaxial resonators offered by Trans-Tech are available in seven sizes and four materials (dielectric constant) value. These resonators are for applications that span from ultra-high frequency (UHF) to 6 GHz. Table 2.1 below shows the different sizes of ceramic resonators provided by Trans-Tech with their nominal length.

Table 2.1: Ceramic coaxial resonator dimensions (adapted from Trans-Tech, 2013a:1-7)

Sizes (Profile)	Width (inches)	Diameter (inches)
HP	0.476 ± 0.005	0.131 ± 0.004
EP	0.316 ± 0.005	0.101 ± 0.004
SP	0.237 ± 0.004	0.095 ± 0.004
LS	0.155 ± 0.004	0.062 ± 0.004
LP	0.155 ± 0.004	0.038 ± 0.003
MP	0.119 ± 0.004	0.032 ± 0.003
SM	0.080 ± 0.003	0.032 ± 0.003

Table 2.2 presents the different materials and their operating frequency ranges for a quarter wavelength resonator.

Table 2.2: Frequency range for different materials and profiles (adapted from Trans-Tech, 2013a:1-7)

Profile	HP	EP	SP	LS	LP	MP	SM
1000 Er=11.5±0.5	1100-1720	1100-2390	1100-2960	1100-4400	1100-3920	1100-4860	1100-4860
2000 Er=21.5±1	800-1200	800-1700	800-2200	800-3200	800-2900	800-3600	800-3600
8800 Er=39.5±1	600-900	600-1200	600-1600	600-2300	600-2100	600-2600	600-2600
9000 Er=93±2	400-600	400-800	400-1000	400-1500	400-1400	400-1700	400-1700

Figure 2.13 overleaf shows the chart describing the resonator Q factor versus frequency for different materials and sizes. This is available on the manufacturer datasheet (Trans-Tech, 2013a:1-7). Appendix A contains the complete datasheet from Skyworks.

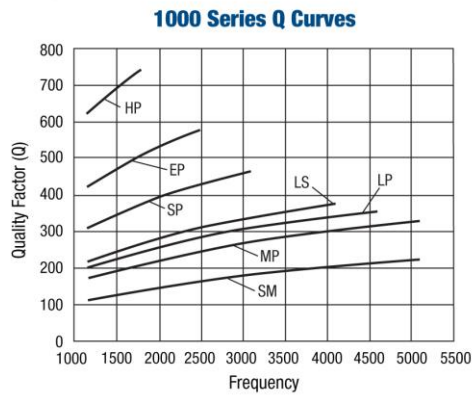


Figure 2. D1000 Quarter-Wave Q Curves

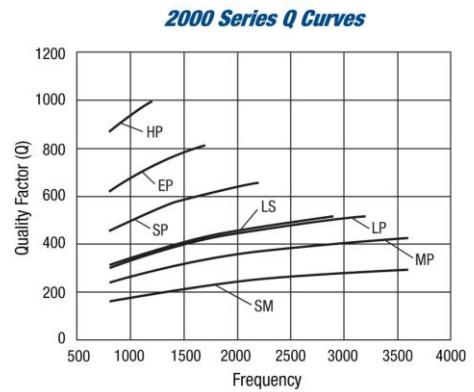


Figure 4. D2000 Quarter-Wave Q Curves

Figure 2.13: Q factor versus frequency for different resonators' profiles (Trans-Tech, 2013:2)

The graph of Figure 2.13 indicates that each size (HP, EP, SP, LS, MP, SM) only operate in a specific range of frequency. Larger sizes (HP, EP and SP) have the highest Q in all the materials, while lowest sizes (LS, LP, MP and SM) have moderated Q factor and a larger operating frequency band. Figure 2.13 also presents deciding criteria, frequency of operation and quality factor, to consider when selecting the size and material to use. These criteria are important factors that would affect the weight and size of the overall design. In this design, the selected CCR size is based on these factors and the design specification. This criterion would play a big role at the design stage in Chapter 4. The designer would have to carefully choose the size of the resonator, having different sizes is not recommended as it can comprise the overall weight and size of your design. Also, to avoid degradation of the frequency response the designer should ensure that the selected size remains in the defined range.

2.4 Summary

This chapter discussed the theory of ceramic resonators. Initially, a review of microwave resonators and transmission line resonators was presented. Next, a presentation on ceramic resonators in terms of their applications and features was done. Transmission line resonators such as quarter wavelength short circuited and half wavelength open circuited resonators result in a parallel resonant circuit. Close to resonance, the series and parallel RLC network input impedances reduce to equation (2.12) and (2.19). Similarly, the Q factors of the series and parallel resonant circuit reduce to Equation (2.21) and (2.23), which show the variation of the Q factors in function of the resistance (R) which represents the loss. Therefore a high Q corresponds to a low loss and a lower Q corresponds to a higher loss as per equation

(2.57). It is usually desirable to achieved high Q factors in resonators, as they will lead to lower losses in filter applications.

At higher RF frequencies, resonators are seldom realised with discrete lumped element RLC components. This is due primarily to their small values, which are physically unrealisable. To avoid the disadvantage of lumped elements RLC, microwave resonators can be realised as ceramic resonators which have a high-quality factor, low loss, better shielding, are small in size, etc. Ceramic resonators are available in various types and materials. The quarter wavelength short circuited and the half wavelength open circuited resonators behave similarly to the parallel resonant circuit.

CHAPTER 3 COUPLED RESONATOR

This chapter provides a literature review on the concept and theory of microwave filter basics. The chapter also discuss transmission zeros and filter implementation for various types of filters. Finally, the rationale for a particular choice of filter in nanosatellites is presented.

3.1 Filter transfer function

The transfer function of a two-port network can be described in terms of a block diagram and equations as follows:

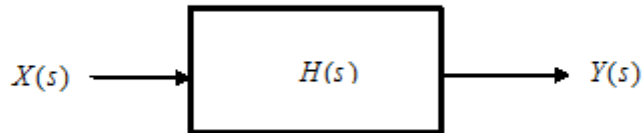


Figure 3.1: Transfer function block diagram

The filter transfer function is defined as

$$\frac{\text{output}}{\text{input}} = H(s) = \frac{Y(s)}{X(s)} \quad (3.1)$$

$$|S_{21}(j\omega)|^2 = \frac{1}{1 + \varepsilon^2 F_n^2(\omega)} \quad (3.2)$$

where ε is the Chebyshev ripple constant, $F_n(\omega)$ represents a filtering or characteristic function and ω is a frequency variable of a low pass prototype filter. The transfer function of a linear time-invariant network can be defined as a rational function:

$$S_{21}(\rho) = \frac{N(\rho)}{D(\rho)} \quad (3.3)$$

where $N(\rho)$ and $D(\rho)$ are polynomials in a complex frequency variable $\rho = \sigma + j\Omega$

The insertion loss response of the filter is then given by:

$$L_A(\omega) = 10 \log \frac{1}{|S_{21}(j\omega)|^2} \text{ dB} \quad (3.4)$$

and the return loss for a lossless passive two-port network is derived by:

$$L_R(\omega) = 10 \log(1 - |S_{21}(j\omega)|^2) \text{ dB} \quad (3.5)$$

3.1.1 Poles and zeros on the complex plane

Considering the complex plane (σ, Ω) in Figure 3.2, having $S_{21}(\rho) = \frac{N(\rho)}{D(\rho)}$ as transfer function.

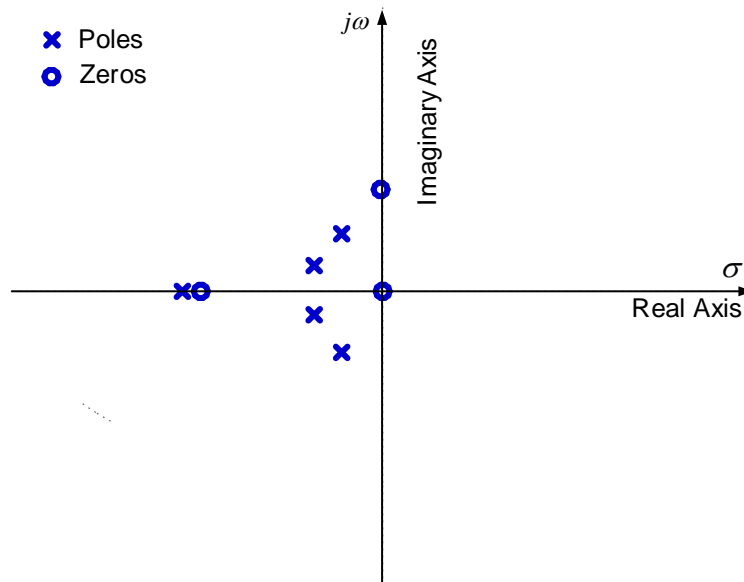


Figure 3.2: Example of a complex plane

The zeros of $S_{21}(\rho)$ or transmission zeros are the roots of the numerator $N(\rho)$ and the poles of $S_{21}(\rho)$ or natural modes are the roots of the denominator $D(\rho)$. Each zero or pole can be either a real or complex number. In the filter stopband, the transmission is required to be zero or small, and the filter transmission zeros are usually placed on the $j\omega$ axis at the stopband frequencies. For the filter to be stable, all the poles must lie in the left half of the ρ plane or on the imaginary axis (Hong & Lancaster, 2001:29-30).

3.1.2 Butterworth response

The Butterworth response is the simplest approximation to an ideal low pass filter. The response is flat at DC and rolls off to 3 dB at $\omega = 1$ before flattening out again at infinity as shown in Figure 3.3.

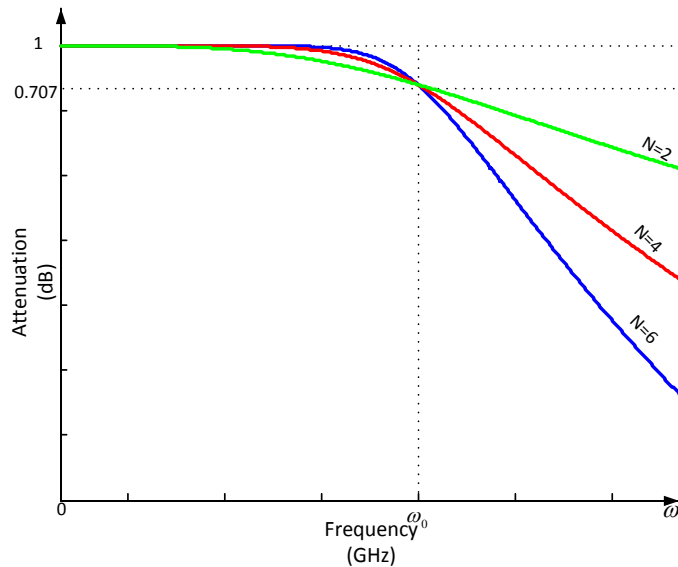


Figure 3.3: Frequency response of Butterworth low pass filter for varying N (adapted from Pozar, 2005:402)

The transfer function describing this response is given by

$$|S_{21}(j\omega)|^2 = \frac{1}{1 + \omega^{2N}} \quad (3.6)$$

and the insertion loss is

$$L_A(\omega) = 10 \log(1 + \omega^{2N}) \text{ dB} \quad (3.7)$$

where N is the degree or order of the network, which corresponds to the number of reactive elements required in the low pass prototype filter (Hong & Lancaster, 2001: 31; Verdellin, 2005:274-275).

3.1.3 Chebyshev response

The Chebyshev response contains ripples in the pass-band region and is maximally flat in the stop-band region as shown in Figure 3.4.

The transfer function that describes this type of function is defined by

$$|S_{21}(j\omega)|^2 = \frac{1}{1 + \varepsilon^2 T_N^2(\omega)} \quad (3.8)$$

The insertion loss of this response is defined by

$$L_A(\omega) = 10 \log(1 + \varepsilon^2 T_N^2(\omega)) \text{ dB} \quad (3.9)$$

where the ripple constant ε , controls the ripple in the passband and is defined as

$$\varepsilon = \sqrt{10^{\frac{L_A}{10}} - 1} \quad (3.10)$$

where T_N is the N^{th} order Chebyshev polynomial and $\varepsilon < 1$ is a real constant (Hong & Lancaster, 2001:32; Awang, 2014:244).

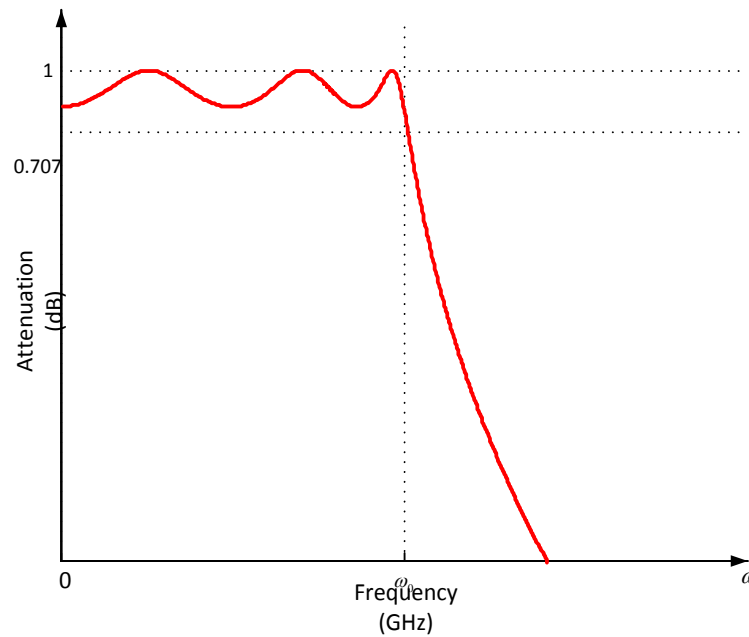


Figure 3.4: Chebyshev low pass response (adapted from Pozar, 2005:402; Verdellin, 2005:276-278)

3.1.4 Transmission Zeros

Transmission zeros (TZ's) are critical frequencies where signal transmission between the input and output of a linear two port network has zero transmission. Transmission zeros can occur at DC, finity and infinity. The transmission zero at DC produces a series capacitor or a shunt inductor. If the number of transmission zeros at DC is increased, it would result in the increase of the filters selectivity in the lower stopband.

The transmission zero at DC would add one degree to the filter transfer function and it is used in the highpass and bandpass filters.

Transmission zeros at infinity on the other hand is needed in lowpass and bandpass filters. An increase in the number of infinity transmission zeros would result in an increase of filter selectivity in the upper stopband. This type of transmission zero also adds one degree to the filter transfer function. Finally, a transmission zero at a finite frequency add two degrees to the filter transfer function. They are realized either as a parallel resonator in series or series resonator to ground. The parallel resonator in series stops signal flow by being an open circuit at the resonant frequency while the series resonator to ground becomes a short circuit at the resonant frequency (R.W Rhea, 2014:1-3, 13). In Chapter 4 the finite transmission zero (1.98 GHz) is implemented at the 3D model design stage. This transmission zero will be created by cross-coupling between two CCRs (Tung, 2015:1-3).

3.2 Filter implementations

Filters can be designed using the image parameter method or the insertion loss method. The image parameter method does not offer a distinctive way to improve the response of the design compared to the insertion loss method. This conventional lumped element filter is available for a limited microwave frequency range, as it is awkward to implement at higher frequency. In addition, at microwave frequency, the electrical distance between filter components is not negligible. For this reason, distributed components are used as reactive elements (Pozar, 2005:405).

3.2.1 Transmission line resonators

A. Impedance and admittance inverters

This technique is used in order to implement bandpass and bandstop LC series and parallel resonators into the transmission line. Series and parallel LC resonators are very difficult to implement using transmission line section. For this reason it is preferred to have either all shunt or all series elements. Kuroda's identities are useful for transforming a capacitor or an inductor to either series or shunt transmission line stubs, but not useful for transforming a LC resonator. Impedance and admittance inverters are used to transform series and parallel resonators to transmission line stubs. These techniques are especially useful for bandpass and bandstop filter having narrow bandwidths.

An impedance inverter converts load impedance (Z_L) to its inverse, while an admittance inverter converts load admittance (Y_L) to its inverse:

$$Z_{in} = \frac{K^2}{Z_L} \quad (3.11)$$

$$Y_{in} = \frac{j^2}{Y_L} \quad (3.12)$$

They can be used to transform between series connected and shunt connected elements. A series LC resonator can be transformed to a parallel LC resonator or vice versa.

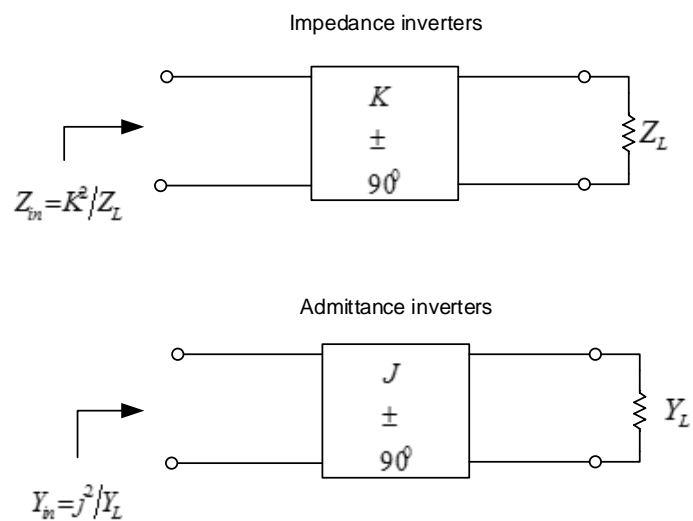


Figure 3.5: Operation of impedance and admittance inverters

Impedance and admittance inverters can be constructed using a quarter wave transformer as shown in Figure 3.6 (a), or as T network and pi network of capacitors as shown in Figure 3.6 (c) and finally as a transmission line with reactive elements as presented on Figure 3.6 (b).

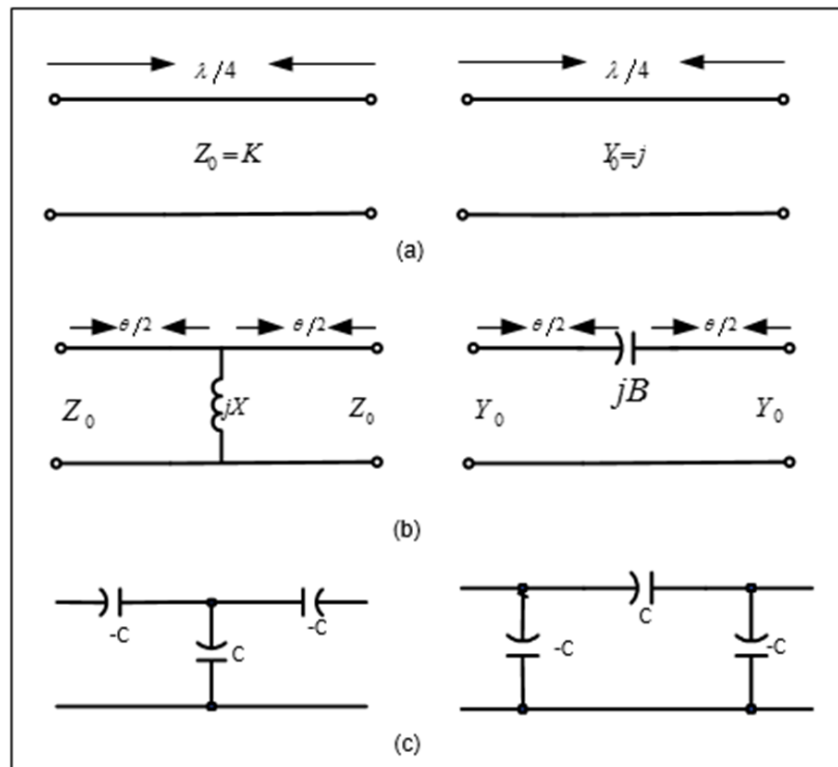


Figure 3.6: Impedance and admittance inverters. (a) Implementation as quarter-wave transformers. (b) Implementation using transmission line and reactive elements. (d) Implementation using capacitor network (adapted from Pozar, 2005:411-412)

B. Quarter-wave resonators filter

Quarter-wave short circuit transmission line stubs look like a parallel resonant circuit. They can be used as the shunt parallel LC resonator for bandpass filter. Quarter wavelength connecting lines between the stubs will act as admittance inverter, effectively converting alternate shunt stubs to series resonators. The response of this type of filter using N stubs is essentially the same as that of the lumped element band-pass filter of order N for a narrow bandwidth passband. The circuit topology of such filter is convenient in that only shunt stubs are used, but a disadvantage in practice is that the required characteristic impedance of the stubs lines is often unrealistically low (Pozar, 2005:427).

3.2.2 Coupled resonator filter

Another way of implementing bandpass filters is by using the top C coupled parallel resonators as shown in Figure 3.7, where parallel LC resonators to ground are capacitively coupled internally and externally with series capacitors. One can decide to either equalise all inductors or all parallel capacitors. The parallel LC resonator shorted to ground can be made from a section of coaxial line using ceramic materials

having a very high dielectric constant and low loss, resulting in a very compact design. Such filters are often referred to as ceramic resonator filters, and they are currently the most common type of RF bandpass filter used in portable wireless systems (Sagawa et al., 1985:152-157). This design method is shown in Chapter 4, for an S-band bandpass filter.

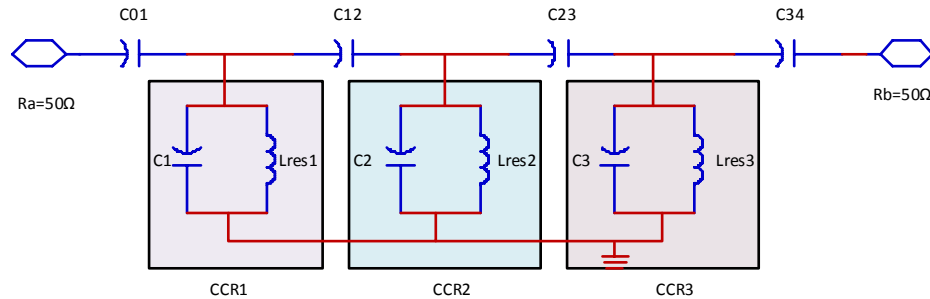


Figure 3.7: Third order coupled resonator bandpass filter (adapted from Rhea, 1994:155)

The transformation of a conventional bandpass filter into a coupled coaxial bandpass filter with capacitive coupling is possible using the J-inverter method (Matthaei et al., 1980:429-433, 482-483). The method is used in circuit having a shunt type resonance. It should be noted that the K-inverter method is used in circuit having series type resonance but it is be discussed in this design (Verdelin, 2005:286-288).

The method of implementing coupled resonator using J-inverter is as follows,

1. Choose the values for the parallel capacitors $C_{res\ 1}$, $C_{res\ 2}$, and $C_{res\ n}$.
2. From the parallel capacitors calculate the resonator Inductance values.

Let first determine the equation of the slope (b_j) of the j resonator. This equation is key in finding the resonator inductance (L_{res}) values. The susceptance slope (b_j) is define by (Levy, 2002:785):

$$b_j = \left. \frac{\Delta dB_j}{2 d\omega} \right|_{\Delta=\omega_0} \quad (3.13)$$

Where:

b_j : is the susceptance of the resonator for all values of j

Equation 3.13 is then transformed to equation 3.14 for a shunt LC resonator, which shows the resonance condition presented in Chapter 2.

$$b_j = \omega_0 C = \frac{1}{\omega_0} L \quad (3.14)$$

Depending on the value chosen to be fixed or to varied Let make L_{res} the subjects of the formula equation (3.15) is derive:

$$L_{res\ j} = \frac{1}{C_{res\ j} \cdot \omega_0^2}, \text{ for } j=1 \text{ to } n \quad (3.15)$$

Note that the inductance can be chosen and the node capacitances calculated if desired.

3. Calculate the admittance inverters:

$$J_{01} = \sqrt{\frac{\omega_0 G_A b_1}{g_0 g_1 \omega_1}} \quad (3.16)$$

Substituting equation (3.14) in equation (3.16) equation (3.17) is derived with

$$G_A = \frac{1}{R_A}$$

$$J_{01} = \sqrt{\frac{\omega_0 C_{res1} \Delta}{R_A g_0 g_1 \omega_1}} \quad (3.17)$$

The j admittance for the rest of j elements are found using the below equations:

$$J_{j, j+1} = \frac{\Delta}{\omega_1} \sqrt{\frac{b_j b_{j+1}}{g_j g_{j+1}}}, \text{ for } j=1 \text{ to } n-1 \quad (3.18)$$

Substituting equation (3.14) in equation (3.18) it leads to equation (3.19)

$$J_{j, j+1} = \frac{\Delta \omega_0}{\omega_1} \sqrt{\frac{C_{res\ j} C_{res\ j+1}}{g_j g_{j+1}}}, \text{ for } j=1 \text{ to } n-1 \quad (3.19)$$

Similarly equation 3.20 is derived and transform to equation 3.21

$$J_{n, n+1} = \sqrt{\frac{G_B b_n \Delta}{g_n g_{n+1} \omega_1'}} \quad (3.20)$$

$$J_{n, n+1} = \sqrt{\frac{G_B \omega_0 C_{resn} \Delta}{g_n g_{n+1} \omega_1'}} \quad (3.21)$$

4. Calculate the coupling capacitance using the admittance inverters.

This is possible by first deriving the external Q factors at the input and output port. Equations below define the external Q.

At input port

$$(Q_e)_A = \frac{b_1}{(J_{01}^2 / G_A)} \quad (3.22)$$

Let substitute equation (3.16) in equation (3.22) the external Q reduce to equation

$$(Q_e)_A = \frac{g_0 g_1 \omega_1'}{\Delta} \quad (3.23)$$

At output port

$$(Q_e)_B = \frac{b_n}{(J_{n, n+1}^2 / G_B)} \quad (3.24)$$

Let substitute equation (3.20) in equation (3.24) the external Q reduce to equation (3.25)

$$(Q_e)_B = \frac{g_n g_{n+1} \omega_1'}{\Delta} \quad (3.25)$$

The coupling coefficient are then derived by equation (3.26)

$$k_{j,j+1} = \frac{J_{j,j+1}}{\sqrt{b_j b_{j+1}}} \quad \text{fo } j=1 \text{ to } n-1 \quad (3.26)$$

By substituting equation (3.18) into equation (3.26), the coupling coefficient is reduce to equation (3.27)

$$k_{j,j+1} = \frac{\Delta}{\omega_1 \sqrt{g_j g_{j+1}}} \quad \text{fo } j=1 \text{ to } n-1 \quad (3.27)$$

With the k-inverter values define by:

$$k_{j,j+1} = \frac{M_{j,j+1}}{\sqrt{L_j L_{j+1}}} \quad \text{fo } j=1 \text{ to } n-1 \quad (3.28)$$

Substituting equation (3.28) with equation (3.27) after manipulation, the coupling capacitances are defined by:

$$C_{01} = \frac{J_{01}}{\omega_0 \sqrt{1 - (J_{01} R_A)^2}}, \quad (3.29)$$

$$C_{j,j+1} = \frac{J_{j,j+1}}{\omega_0}, \quad \text{for } j=1 \text{ to } n-1 \quad (3.30)$$

$$C_{n,n+1} = \frac{J_{n,n+1}}{\omega_0 \sqrt{1 - (J_{n,n+1} R_B)^2}} \quad (3.31)$$

5. Calculate the net shunt capacitance using the coupling capacitance and the preselected nodal capacitance.

$$C_1 = C_{res1} - C_{01}^e - C_{1,2} \quad (3.32)$$

$$C_j = C_{resj} = C_{j-1,j} - C_{j,j+1}, \quad \text{for } j=2 \text{ to } n-1 \quad (3.33)$$

$$C_n = C_{resn} = C_{n-1,n} - C_{n,n+1}^e \quad (3.34)$$

where

$$C_{01}^e = \frac{C_{01}}{1 + (\omega_0 C_{01} R_A)^2} \quad (3.35)$$

Summary

A filter is a very important block in a transceiver system. Its role is to separate signals coming from various sources and to improve selectivity. Depending on its primary role, various types of passband exist. Different ways to design and implement RF and microwave filters exist. Filters can be implemented using lumped element methods such as the image parameter and insertion loss method, transmission line stub and transmission line resonator.

The form of filter chosen for any given application will depend on many factors, such as:

- Filter performance
- Cost
- Emplacement in the system
- Operating frequency
- Weight
- Size

It is evident that traditional lumped element and waveguide filters at microwave frequency are no longer suitable, adequate and efficient for today's technology that requires small-sized, compact and low-cost solutions. Microwave filters for use in CubeSat systems use critical components, thus the need to be lightweight and small. Filters with good performance parameters and of small size are required to improve the overall performance of the system while reducing the cost of the manufacture. Transmission line resonator filters are extremely useful when designing bandpass and bandstop filters. Recent innovations in ceramic materials have made it possible to achieve good performance while reducing the size, space, and cost of the system.

CHAPTER 4

S-BAND BANDPASS FILTER DESIGN

This chapter deals with the design and implementation process using the design specifications in Table 4.1 defined by F'SATI. Sections of this chapter comprise the presentation of the CCR large profile (LS) from Trans-Tech, the lumped element and 3D implementation of the bandpass filter, the E-field distribution characterisation of the ceramic resonator and finally the design of the capacitor coupling structure.

4.1 Skywork CCR equivalent circuit

In Section 2.3 of Chapter 2, the equivalent circuitry of the CCR was introduced. Skyworks coaxial resonators are available in seven sizes (HP, EP, SP, LS, LP, MP, SM) and four dielectric constants (11.5, 21.5, 39.5, and 93) with application frequency ranging from 300 MHz to 6 GHz. Provided in Appendix A is a Skyworks datasheet with valuable information on the CCR. There are two forms of CCR: the quarter wavelength and the half wavelength. The quarter wavelength has a silver coating applied to one end and the half wavelength has both ends open. Figure 4.1 presents the quarter wavelength CCR structure. The silver coating around the CCR makes for very low conductor losses. The losses of the dielectric material are very low due to their very low loss tangents (0.0005) (Trans-Tech. n.d: 2.34-2.40).

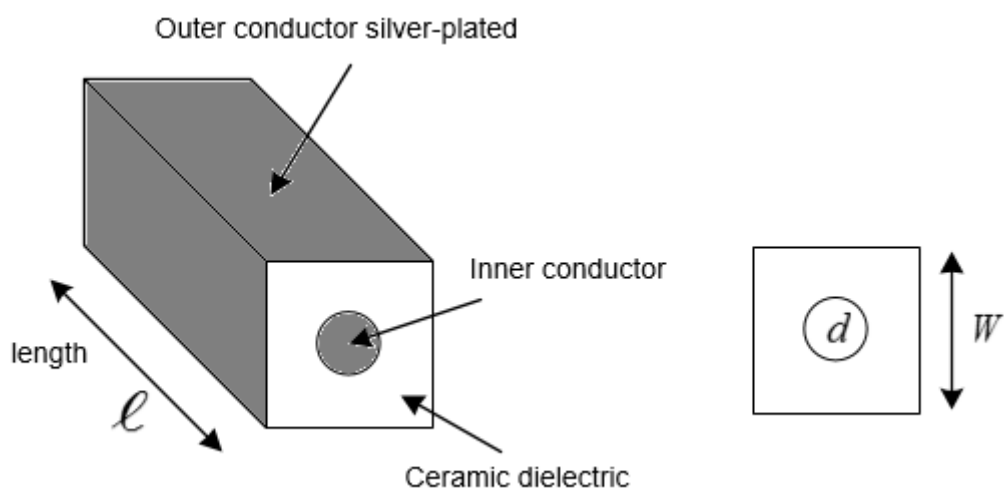


Figure 4.1: Quarter wavelength ceramic coaxial resonator

4.2 Filter specification

The specification presented in Table 4.1 was provided by F'SATI to meet the requirement of the forthcoming ZACUBE 2 communications system. A 4th order coupled resonator bandpass filter was designed using the equations defined in Chapter 3.

Table 4.1: Specification

Bandwidth	From 2.2 GHz to 2.3 GHz
Centre frequency	2.25 GHz
Insertion loss	< 2 dB
In-band Insertion loss flatness	Δ Insertion loss must be ≤ 0.5 dB
Return loss	≤ -14 dB
Transmission zero	Between 1.9 GHz and 2 GHz
Power handling	5 W – 10 W
PCB dimensions	Max height: 20 mm Thickness x width x length : 1.6 mm x 30 mm x 30 mm

4.3 Capacitively coupled resonator bandpass filter

The basic bandpass filter made of alternating series and parallel resonators is used to derive the coupled resonator bandpass filter. A practical microwave network is difficult to achieve by using this alternating resonator due to the unrealistic values of reactance. One way to deal with narrow band bandpass filters, is to think of the filter in terms of coupled resonators of identical topology as shown in Figure 3.7, which are based on the design formula of the lumped element capacitively coupled resonator bandpass filter. The resonator in Figure 3.7 is connected with coupling capacitors (Matthaei et al., 1980:481). It is important to know that inductive coupling is possible; however, it is not addressed in the current study.

4.3.1 Lumped element capacitively coupled resonator bandpass filter

To demonstrate the design method, a coupled resonator bandpass filter with a passband covering 2.2 to 2.3 GHz is required. This is used in the CubeSat transceiver module where a trade-off between performance and size is extremely important. The circuit topology adopted for the filter is identical to the 5th order coupled LC bandpass filter shown in Figure 4.2.

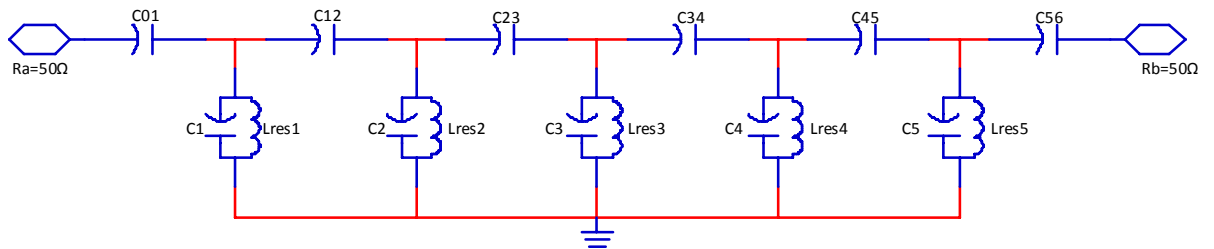


Figure 4.2: Fifth order capacitively coupled resonator bandpass filter

Presented in Table 4.2 are the lumped element values of a 5th order coupled resonator bandpass filter with 0.01 dB ripple. The values in Table 4.2 are computed using equation (3.13) to (3.38). Table 4.2 shows a consistency in the capacitor and inductor values. These values are kept constant in an attempt to use only one profile during the 3D model simulation and the implementation stage. The values are kept constant so that all the calculated frequencies would belong to one profile (LS, SP, SM, etc.). Making use of the selected profile gives the designer control over the cost and size of the filter. Figure 4.3 shows the simulated response with a passband insertion loss less than -0.5 dB and a return loss smaller than -20 dB.

Table 4.2: Fifth order bandpass filter parameter values

j	C_{resj} [pF]	L_{resj} [nH]	J_{jj+1}	C_{jj+1} [pF]	C_j [pF]
0	-	-	7.687	0.588	-
1	3.56	1.405	2.252	0.159	2.9
2	3.57	1.401	1.564	0.11	3.3
3	3.58	1.397	1.568	0.111	3.36
4	3.59	1.394	2.271	0.16	3.32
5	3.6	1.389	7.73	0.593	2.936

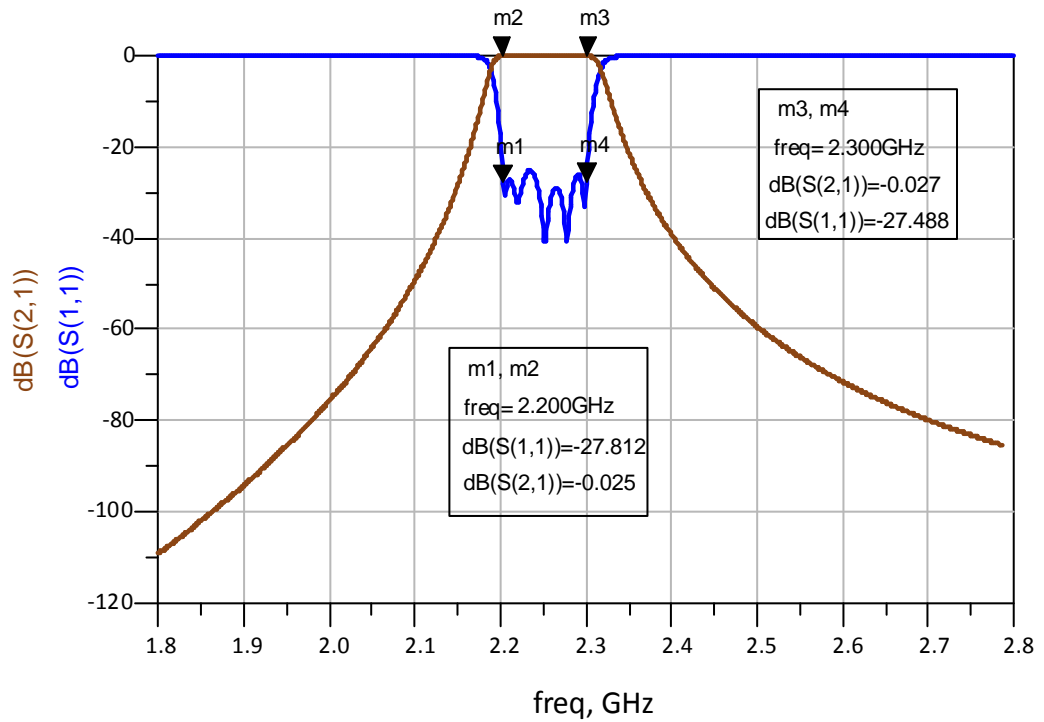


Figure 4.3: Fifth order bandpass filter simulated response

4.3.2 Coupled resonator bandpass filter symmetry characteristic

Important manifestations of symmetry in an electrical filter are the physical and the response symmetry. The physical symmetry is the reflection of the element type and value with regard to the input and output, while the response symmetry shows identical selective above and below the passband. Physical symmetry has the advantage of reducing the number of elements to be modelled, tested and ordered, as well as the required simulation time to devote during electromagnetic simulation by only simulating part of the design due to the fact that all the component in the left are mirror in the right (Rhea, 2014:115). Displayed in Figure 4.4 is a 4th order coupled resonator bandpass filter with physical symmetry.

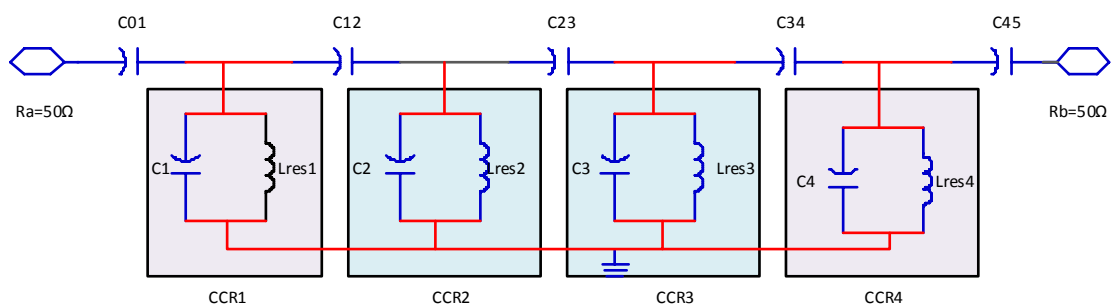


Figure 4.4: Fourth order coupled resonator bandpass filter

The element types and values in Figure 4.4 are mirrored around the coupling capacitor C_{23} . The physical symmetry is expressed by the following equivalences:

- $CCR\ 1 = CCR\ 4$
- $CCR\ 2 = CCR\ 3$
- $C_{0,1} = C_{4,5}$
- $C_{1,2} = C_{3,4}$

Following the design and procedure described in Section 3.2.2, and considering the physical symmetry, the following are derived:

- The values for $C_{res\ 1}$ and $C_{res\ 2}$ are selected to be $3.57\ pF$ and $3.56\ pF$ respectively. These values are selected in such a way to have the inductor values as close as possible to each other. Owing to the physical symmetry around C_{23} only $C_{res\ 1}$ and $C_{res\ 2}$ are chosen. The two selected CCR Lumped element (LC) values are purposely designed not to be equal, which can cause the entire resonator to resonate at the same frequency. This will cause the filter to have a flat return loss.
- The lumped elements values of the resonator inductance are found using Equation (3.15). The following values are obtained:
 - $L_{res\ 1} = L_{res\ 4} = 1.401\ nH$
 - $L_{res\ 2} = L_{res\ 3} = 1.405\ nH$
- The admittance inverter values are computed using Equation (3.17), (3.19) and (3.21):
 - $J_{0,1} = 7.929 \times 10^{-3}$,
 - $J_{1,2} = 2.419 \times 10^{-3}$
 - $J_{2,3} = 1.77 \times 10^{-3}$
- The coupling capacitor values are computed using Equation (3.29), (3.30) and (3.31):
 - $C_{0,1} = C_{4,5} = 0.61\ pF$
 - $C_{1,2} = C_{3,4} = 0.171\ pF$
 - $C_{23} = 0.125\ pF$

- The net shunt capacitances are computed using Equation (3.32), (3.33) and (3.34):

- $C_{01}^e = 0.514 pF$
- $C_1 = C_4 = 2.86 pF$
- $C_2 = C_3 = 3.264 pF$

Table 4.3 represents the admittance inverter calculated values. Figure 4.5 is the schematic of the 4th order coupled resonator bandpass filter. Similarly as in the demonstration example in Section 4.3.1, the capacitor and the inductor values are kept constant in order to have only one profile (LS, SP or SM).

Table 4.3: Calculated values of the coupled resonator bandpass filter

j	$C_{resj} [pF]$	$L_{resj} [nH]$	J_{jj+1}	$C_{jj+1} [pF]$	$C_j [pF]$
0	-	-	7.929×10^{-3}	0.61	-
1	3.56	1.405	2.419×10^{-3}	0.171	2.86
2	3.57	1.401	1.77×10^{-3}	0.125	3.264

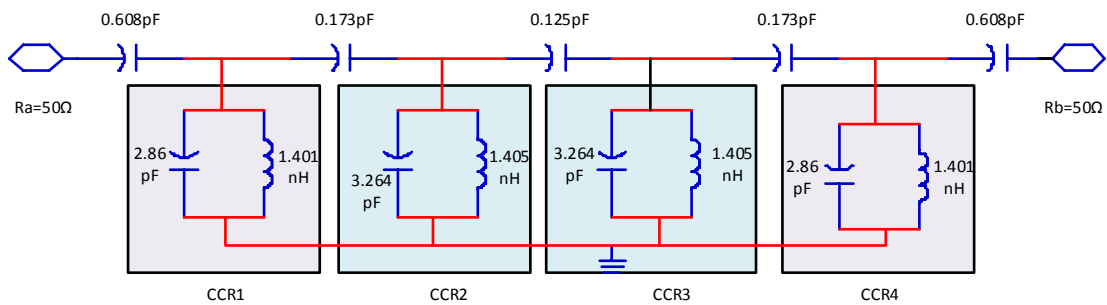


Figure 4.5: Fourth order capacitively coupled resonator bandpass filter

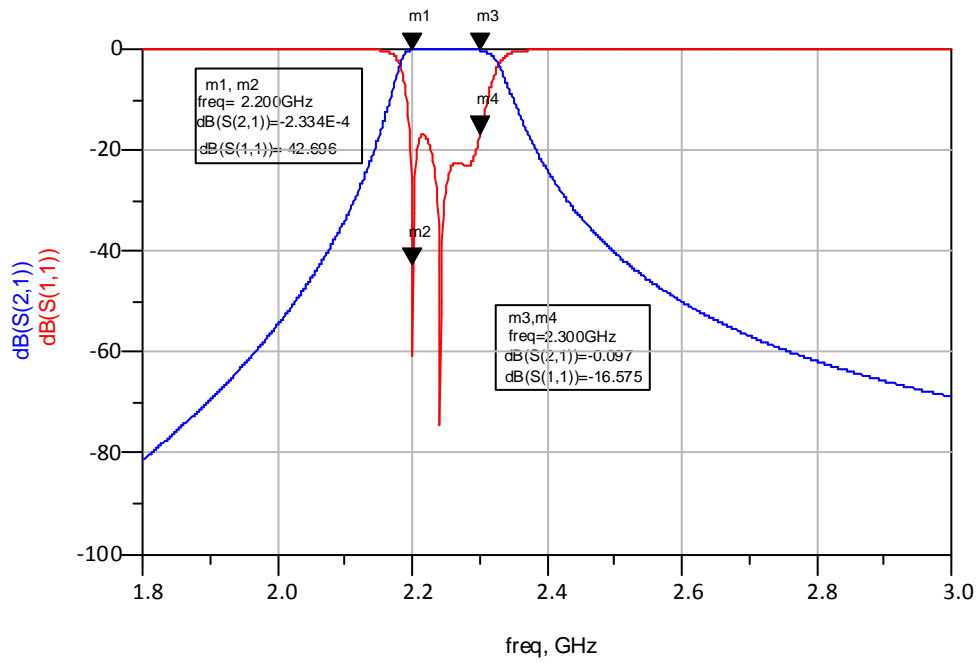


Figure 4.6: Simulated result of the fourth order coupled resonator bandpass filter

The response presented in figure 4.6 displayed two lobes instead of 4 lobes in the return loss response. Notice that the response is not even in the entire band because calculated values are used at this stage. The components will undergo tuning and optimisation for a more stable response in Section 4.3.3. It should be noted that when dealing with the 3D model simulation the transmission zero would result from the cross-coupling between two resonators.

4.3.3 Coupled resonator bandpass filter with finite transmission zero

There are different ways of implementing a finite transmission zero on a filter response. A finite transmission zero is implemented into the design by either adding a parallel resonator in the series arm of the network or a series resonator to the ground as presented in Figure 4.7.

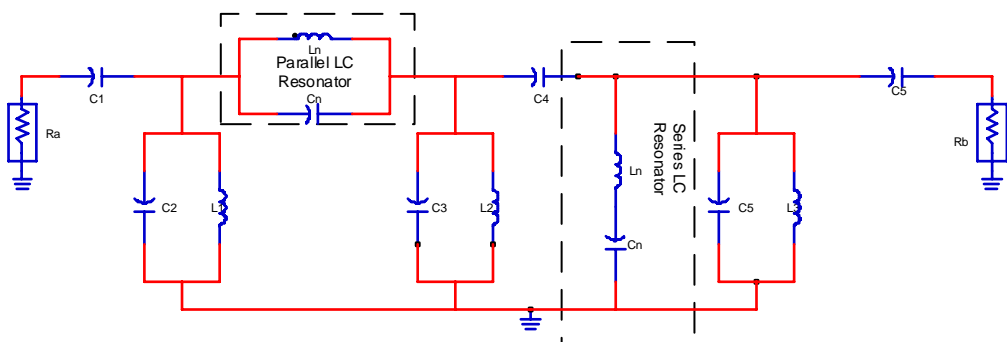


Figure 4.7: Finite transmission zero topology placement

Figure 4.8 below is the 4th order coupled resonator bandpass filter with one rejection. The rejection was implemented by adding a series resonator to ground in the network. The rejection notch is added to this design to avoid performance degradation or specification failure at the required frequency (1.98 GHz to 2 GHz).

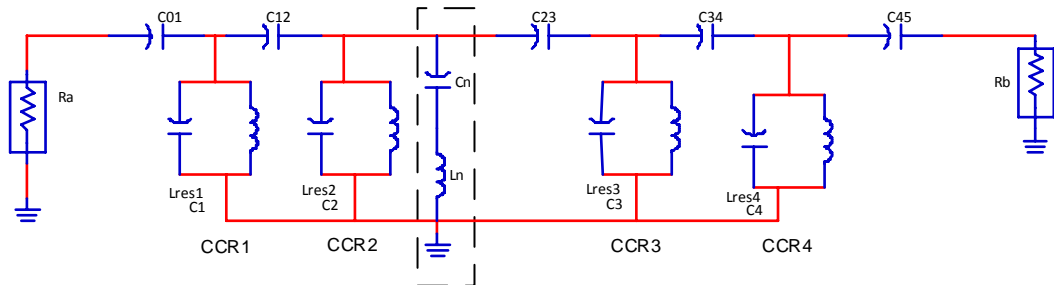


Figure 4.8: Fourth order Coupled resonator bandpass filter with TZ

In addition to finding the correct values of the capacitor, tuning and optimisation of the design components are also required to maintain an adequate response. The simulation result after adding the rejection notch is presented in Figure 4.9. The simulation shows clearly that there is a slight change in the insertion loss and return loss values, but the rejection at 1.98 GHz has improved. The transmission zero implementation may be more effective during the design using the CCR 3D model in CST Microwave Studio[®], as the coupling between CCR creates inductive and capacitive coupling. Thus at that stage, the lumped LC place to ground will be produced by the cross coupling between the resonators (Tung,2015:1-3).

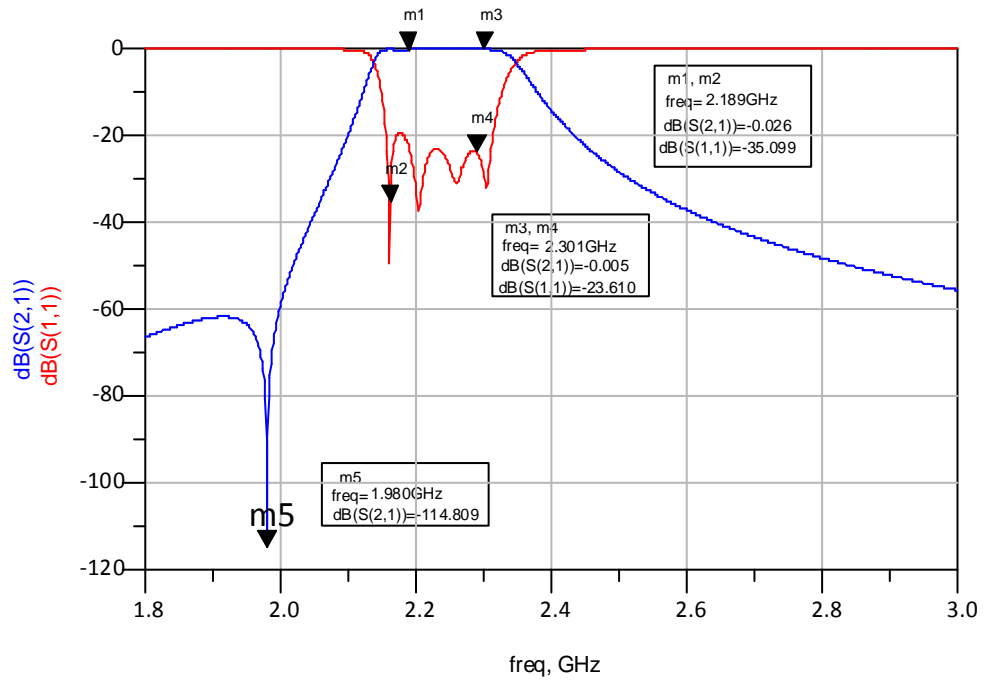


Figure 4.9: Simulation result of a fourth order coupled resonator bandpass filter with 1 TZ

4.4 Parallel LC element conversion to CCR

The parallel LC shunt elements in Figure 4.5 are converted into CCR using Equations (2.18), (2.53) and (2.56). The resonant frequency of each CCR is computed using Equation (2.18), its length using Equation (2.53) and the characteristic impedances are computed using Equation (2.55) or Equation (2.56).

Table 4.4 shows the calculated values for each resonator. Only resonator 1 and 2 are computed here because of the physical symmetry around C_{23} explained above.

Table 4.4: CCR lengths and frequency values

	Length (mm)	Frequency (GHz)	Characteristic impedance (Ω)
CCR1	8.796	2.514	17.382
CCR2	9.411	2.350	16.295

Based on the calculated values of each CCR, the resonators are selected using the available datasheet from the manufacturer. Skyworks LS profile with operating frequency from 1100 to 4400 MHz was selected. Although the selected profile characteristic impedance does not match that of the datasheet, the impedance value of the resonator at the practical stage can be increased by removing the silver coating

from the open side of the CCR, see Appendix B for more detail. At simulation stage using CCR 3D models, increasing the resonant frequency would cause a decrease in the resonator length, thus a physical reduction of the CCR length in the simulation software is required. Also the calculated resonant frequency of each CCR fall in the range of frequency allocate to the LS profile, therefore the component is ordered using the chart provided in the datasheet taking in consideration the calculated CCR frequency. Figure 4.10 is the representation of the physical dimensions of the LS CCR. This physical dimension is used in CST microwave studio to create the 3D models of the CCR (Trans-Tech, 2007a:1-2). The complete dimensions of all profiles may be found in Appendix A.

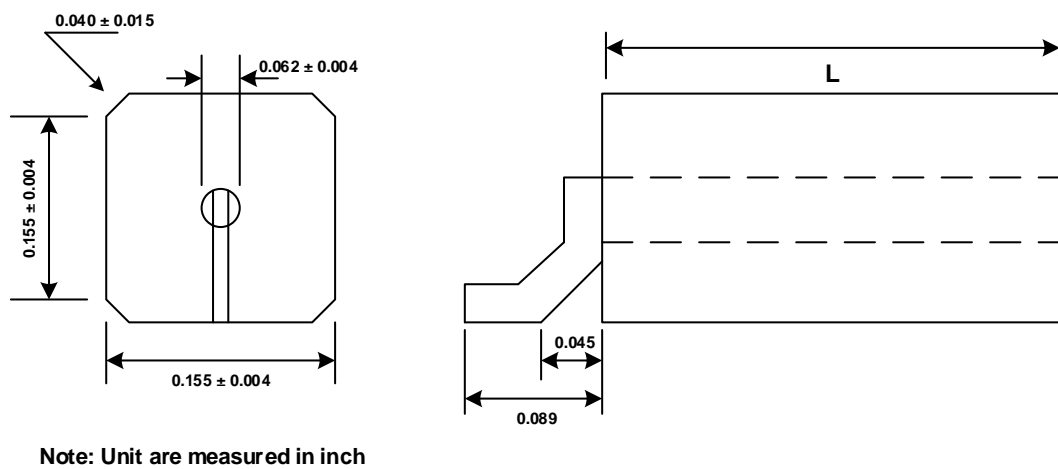


Figure 4.10: LS profile dimension diagram (adapted from Trans-Tech, 2007a:1)

4.5 Ceramic coaxial resonator bandpass filter design using CST Microwave Studio®

Using CST Microwave Studio®, the 3D structure of the resonator is built using the physical dimensions presented in Figure 4.10 with a dielectric constant (ϵ_r) of 11.5. Figure 4.11 is the 3D representation of the ceramic coaxial resonator with lumped element coupling capacitors and lumped element ports.

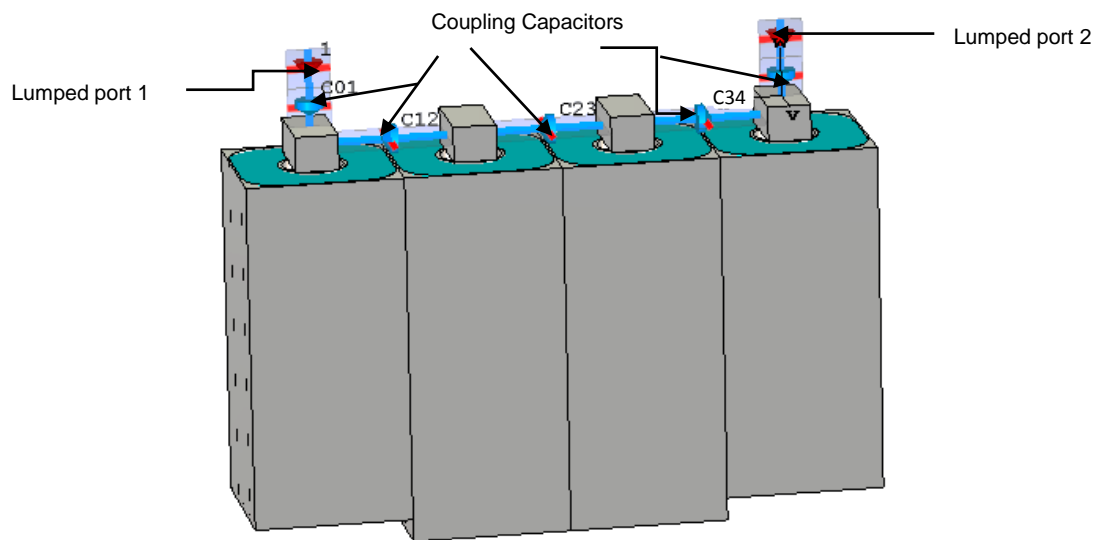


Figure 4.11: Coupled bandpass filter equivalent 3D structure

The simulated result is presented in Figure 4.12. This result clearly shows that the response is not sitting in the required band of frequency, causing a shifting of the frequency response to the left. This is due to the resonator tabs, which cause the increase in the resonator length and consequently the increase of inductance (L) of the equivalent circuit. Another parameter that contributes to this left shifting is the lumped coupling capacitor used in the design. This increase of inductance at circuit level causes a reduction of almost 70 MHz and 50 MHz in frequency at each node of the circuitual model, thus the left shifting. The reduction of frequency at each node causes a 2% increase in resonator length.

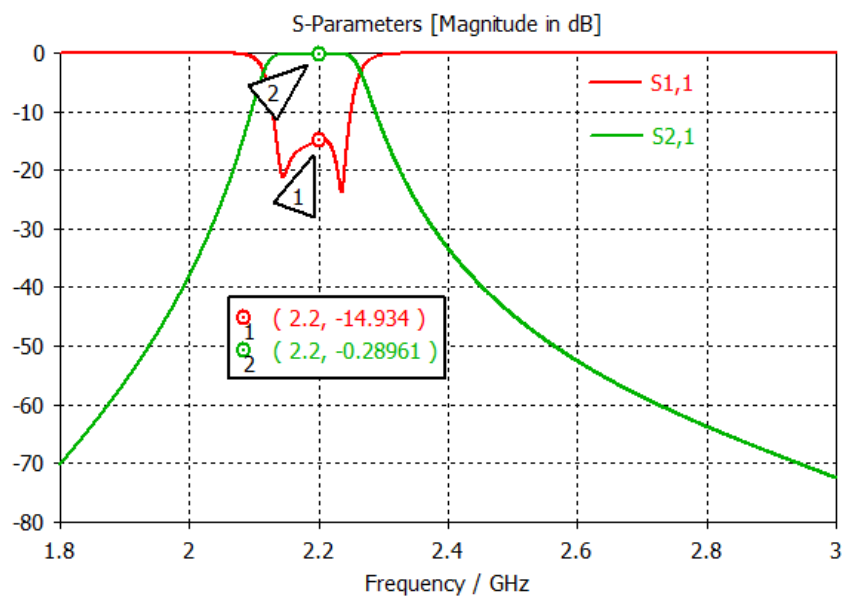


Figure 4.12: Simulated results of the equivalent 3D structure bandpass filter

Optimisation is performed on each CCR lengths and coupled capacitor to bring the response back to the initial position. Displayed in Table 4.5 are the values of each optimised parameter. Care should be taken during the optimisation of the CCR length to avoid having unrealistic value for the selected profile (LS) length. Obtaining the length of the CCR outside the set range by the manufacturer can lead to degradation of the response. The designer should always make sure to fall within the range of frequency set by the manufacturer for a specific profile (LS). Figure 4.13 is the optimised response of the ceramic coaxial resonator bandpass filter obtained by physically decreasing the four CCRs calculated lengths and by turning the coupling capacitors. At the construction stage, the CCR self-resonant frequency is increased by the removal of silver coating in the open side of the resonator which would affect the Q factor value as describes by equation (2.57). Decreasing the self-resonant frequency is also possible, this time by the removal of silver coating at the shortened end of the resonator. It should be noted that the removal of silver coating at the shorted side of the CCR would cause the degradation of the Q factor as describes by equation (2.57). Appendix B demonstrates the frequency turning of the coaxial resonators.

Table 4.5: Optimised CCR length and frequency values

	<i>Length 1 (mm)</i>	<i>Length 2 (mm)</i>	C₀₁ (pF)	C₁₂ (pF)	C₂₃ (pF)
Initial values	8.796	9.411	0.608	0.173	0.125
Optimised values	8.471	7.891	0.545	0.141	0.099

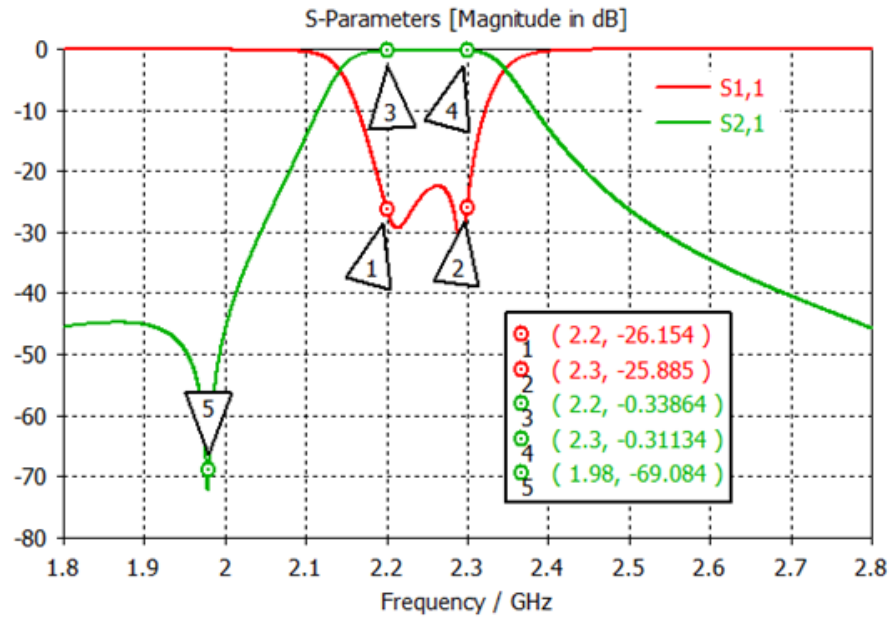


Figure 4.13: Optimised equivalent 3D structure bandpass filter response

4.6 Coupling effects of CCR

The equivalent RLC circuit of the CCR presented in Figure 2.12 and described in Section 2.3 illustrated that the resistor characterises the CCR losses. Practical filter has a component of finite resistance that causes degradation in performance of the signal response. The selected CCR provided by Skyworks is made of a dielectric material with high ϵ_r , as presented in the datasheet (Appendix A). The effect of the resistor in a parallel RLC circuit can be directly related to the Q as described by Equation (2.57). The higher the Q, the lower the energy dissipated through the CCR open sides and the lower the loss tangents (less than 0.0005), meaning the Q is a figure of merit of losses in the circuit (Trans-tech, 2013c:1-3; Temex, 2004: 1-2).

The CCR loss tangent is proportional to the Q factor and is defined by:

$$\tan \delta = \frac{\sigma}{\omega \epsilon_r \epsilon_0} \quad (4.1)$$

$$Q = \frac{1}{\tan \delta} \quad (4.2)$$

The coupling and ohmic loss of the CCR can be neglected as their loss tangent is very small (0.0005). One can assume that the resistor value in the RLC circuit presented in Figure 2.12 tends to infinity, thus an infinite parallel resistor would behave just like an open circuit. The resistor here is practically non-existent.

4.6.1 Electromagnetic study on a single CCR

An electromagnetic simulation is performed on a single ceramic resonator 3D structure construct using CST Microwave Studio®. The resonator structure is a large profile (LS) of the 1000 series from Skyworks. The structure is made of a ceramic material of dielectric constant of 11.5, and a single excitation waveguide port is connected at the open side of the resonator as presented in Figure 4.15.

The following setup is performed in CST Microwave Studio® in order to start the CCR simulation.

1. The background material is set to be normal for all walls
2. Boundary conditions are PEC for all walls
3. The excitation ports are the waveguide (CCR without tab) and lumped (CCR with solder tab) port respectively

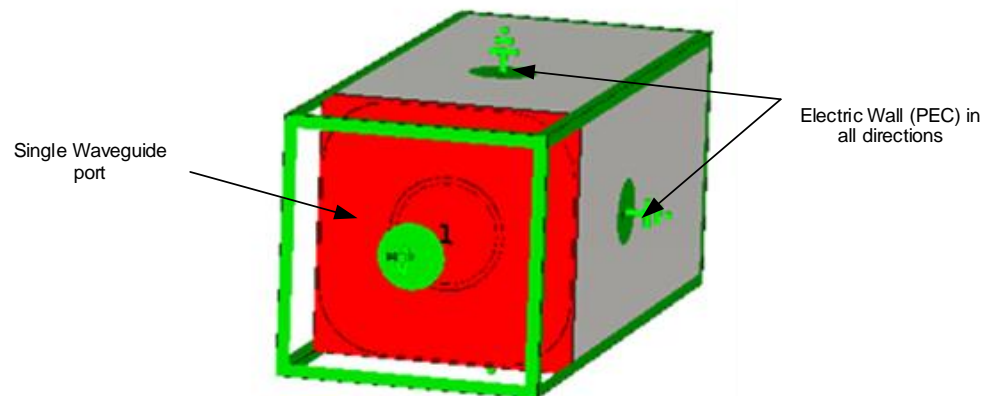


Figure 4.14: Simulation setup on a tableless CCR 3D structure

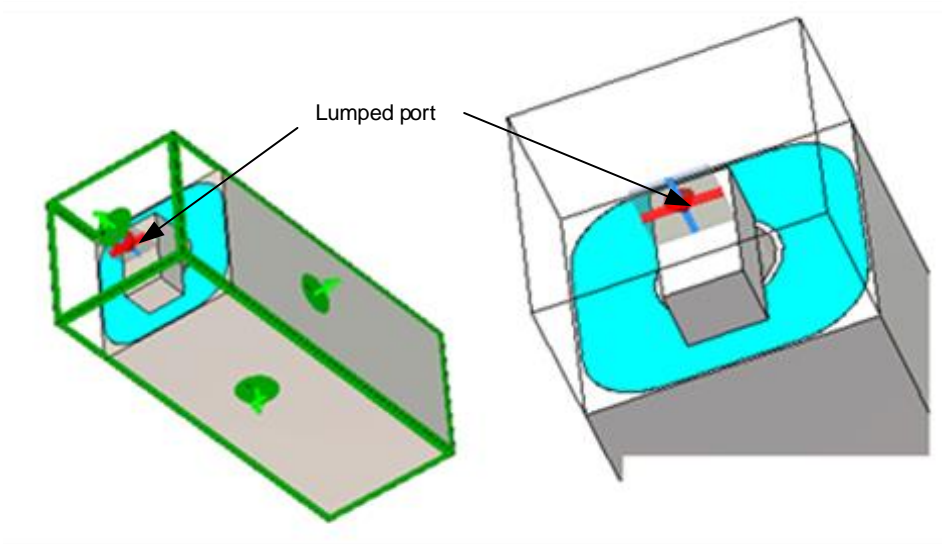


Figure 4.15: Simulation setup on a CCR structure with tab

The structure presented in Figure 4.16 is a single CCR with a tab and a lumped port on the open side of the CCR. This structure is made of ceramic material of dielectric constant 11.5. Figure 4.16 and Figure 4.17 show the response of the simulation performed on the tab and tabless CCR 3D structures. The purpose of this simulation is to check whether the CCR resonant frequency computed at circuitual level is close to the simulated frequency. The response is a single S-parameter (S_{11}) result, which shows the resonant frequency of a resonator with tab on the one hand, and on the other hand of the resonator without tab. This result shows the effect of the tab on the resonators. The tab causes the resonant frequency of the resonator to decrease. The solder tab also causes an increase of inductance of the CCR equivalent circuit. These changes around those parameters caused by the solder tab should be watched carefully when performing EMC simulation of all four CCRs. Table 4.6 shows the difference between the simulated and the calculated CCR frequency. Apart from the parasitic inductance introduced in the circuit by the tab, the lumped element port placed on the tab has created extra capacitance and inductance. The lumped port also plays a role in degrading the response thus causing the calculated frequency and the simulated frequency not to agree.

Table 4.6: Differences in frequencies

	Calculated	Simulated
CCR with tab	2.5142	2.4688
CCR without solder tab	2.5142	2.5019

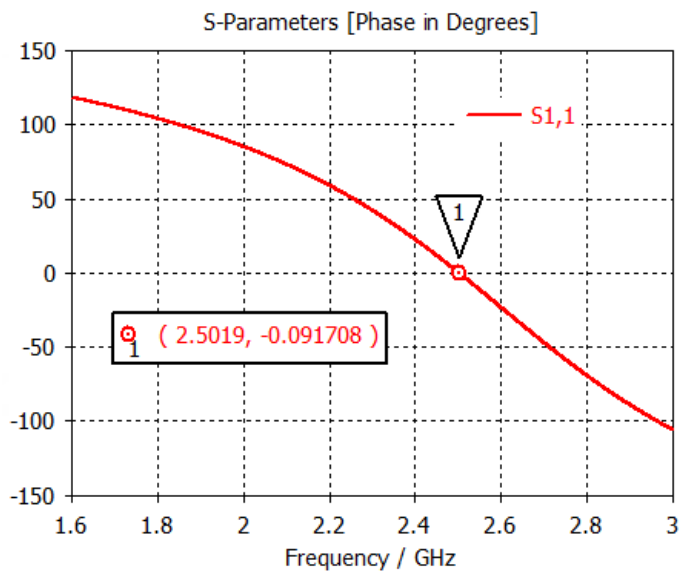


Figure 4.16: Single S-parameter response of a tableless CCR

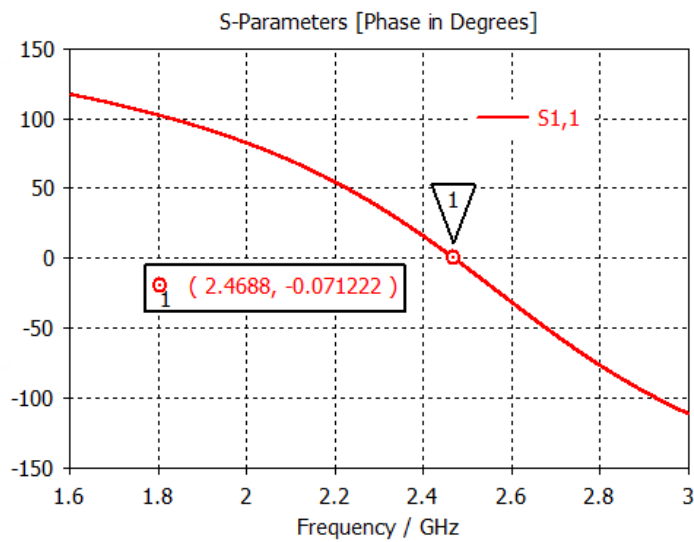


Figure 4.17: Single S-parameter response of CCR with tab

4.7 Coupling capacitor structure design

A capacitor is a lumped element that stores energy. Figure 2.1 (a) illustrates the representation of the real world capacitor. The series inductance in the circuit represents parasitic inductance due to infinite length of the component leads. The series resistance in the schematic represents a dielectric loss consequently, the resistance would increase with an increase of frequency (Verdelin, 2005:38-43). Capacitors used in a coupling circuit, operating at microwave frequency, require a dielectric with extremely low loss at the designed frequency. They can be arranged in several different configurations, one of these being the gap capacitor as presented by its equivalent circuit in Figure 4.18.

Each coupling capacitor of the lumped filter is converted into a gap capacitor. Figure 4.18 shows the equivalent circuit representation of a gap capacitor made of series capacitances ($C1$) and some negative shunt capacitances ($-Cp1$ and $-Cp2$) (Matthaei et al., 1980:442). Substituting the equivalent gap capacitor in the circuit would bring into play the creation of the parallel plate capacitor, which consists of two plates arranged in parallel and separated with a dielectric medium.

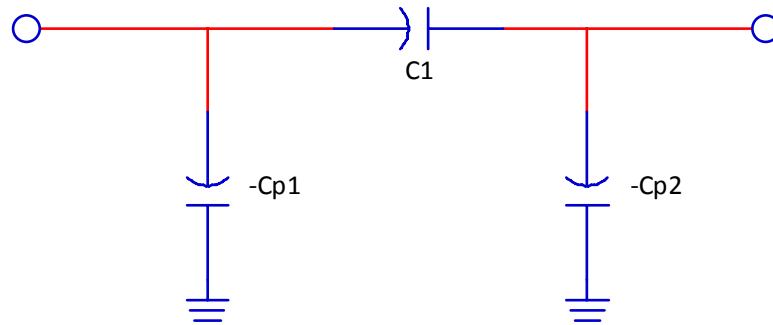


Figure 4.18: Gap capacitor equivalent circuit (adapted from Matthaei et al., 1980:442)

Figure 4.12 presented a left shifting of the response, due to extra component introduced by ideal world capacitor as well as the coupling created by two resonators placed close to each other. This extra component was not taken into consideration during circuit model design as presented in Figure 4.5. Figure 4.19 shows the coupling between the centre pins of two ceramic resonators. The two resonators are arranged in a way to have their surfaces touch. This improves coupling, hence leading to the narrowing of the filter bandwidth as shown in Figure 4.20. Also note a transmission zero can be introduced when the ceramic resonators are spaced apart from each other, this will be covered later in the chapter.

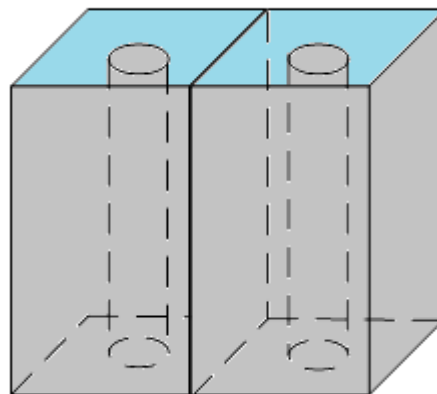


Figure 4.19: Configuration for electric coupling (adapted from Hano et al., 1986:973)

From the model presented in Figure 4.11, each resonator is separated by a coupling capacitor. Because of the coupling between two resonators and extra capacitor is introduced in the circuit represented by Figure 4.21 as C'_{12} . This extra capacitor is then placed in parallel with the negative capacitor generated by the gap capacitor equivalent circuit described in Figure 4.20.

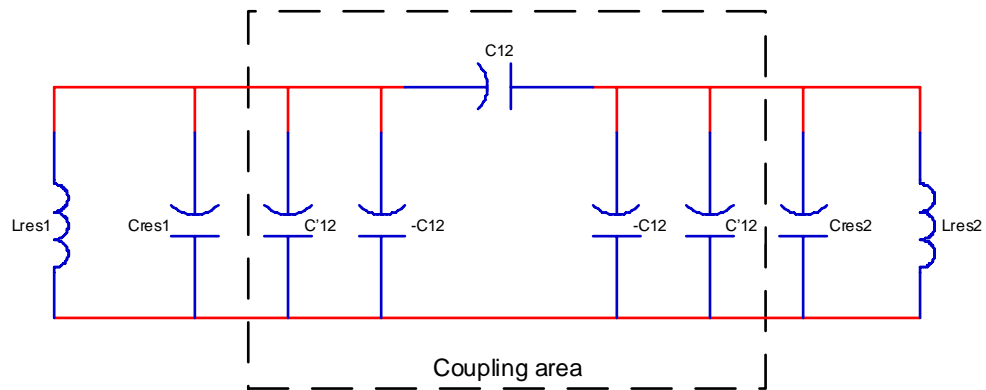
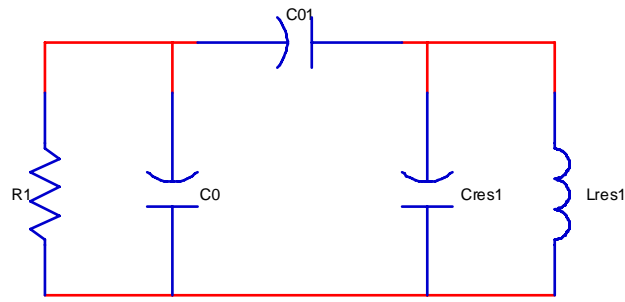
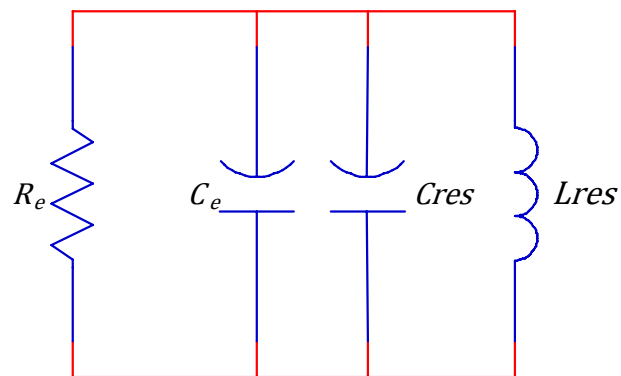


Figure 4.20: Equivalent circuit of the coupling between two CCRs with a coupling capacitor (adapted from Hano et al., 1986:973)

The equivalent circuit of Figure 4.20 unveils the negative capacitance from the gap capacitor equivalent in parallel with the capacitor created due to the coupling between two resonators. The dotted area is the coupling region between the resonators. Displayed in Figure 4.22 is the equivalent circuit of external coupling between the impedances respectively at the input and output, and the resonators ($Lres$ $Cres$). The source is represented by $R1$ and $C0$ which is the resistance and the capacitance. Similarly, the load can be represented using the same concept. Figure 4.21 (a) is converted to Figure 4.21 (b) where $C01$ represent the coupling capacitor, R_e and C_e are the equivalent resistive and capacitive elements of either the load or the source with the resonator elements ($Lres$ and $Cres$). The equivalent capacitance C_e result from cascading $C0$ and $C01$.



(a)



(b)

Figure 4.21: Equivalent circuit of a coupling between a CCR and an input or output resistance (adapted from Hano et al., 1986:974)

Figure 4.22 shows the equivalent circuit of the Bandpass filter with the resulting coupling between all the resonators, as well as with the external circuit. Figure 4.23 shows the derived equivalent circuit of the coupling capacitor's structure. It is noticeable that the structure formed by the gap capacitor and the parallel plate capacitor presented in Figure 4.24 is derived using the equivalent circuit of the coupling between two resonators presented in Figure 4.22 and the equivalent circuit of Figure 4.23 (Hano et al., 1986:972-976),

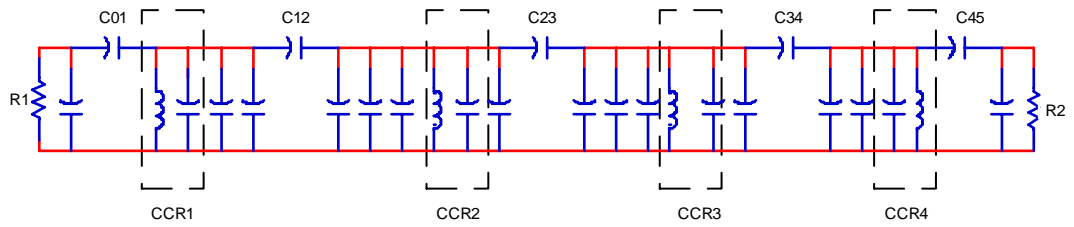


Figure 4.22: Equivalent circuit of the coupling between all 4 resonators and the external circuit (adapted from Hano et al., 1986:974)

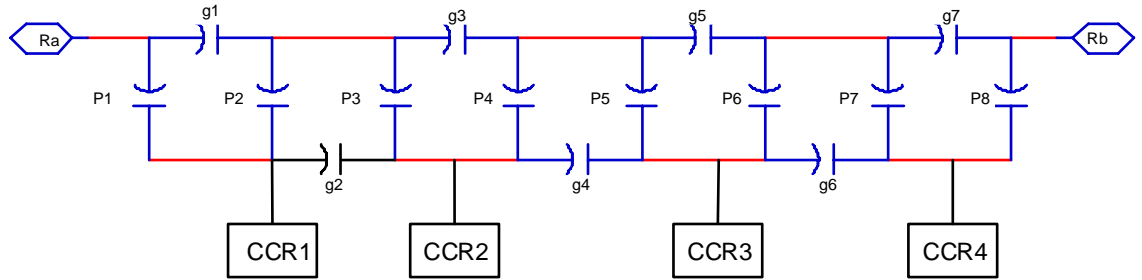


Figure 4.23: Coupling capacitor structure equivalent circuit (adapted from Lierena Castro, 2014:66)

where:

$g1$ to $g7$ are the gap capacitors

$p1$ represent the coupling capacitor C_{01}

$p2$ and $p3$ represent coupling capacitor C_{12}

$p4$ and $p5$ represent coupling capacitor C_{23}

$p6$ and $p7$ represent coupling capacitor C_{34}

$p8$ represent coupling capacitor C_{45}

From the coupling capacitor structure presented in figure 4.24 a physical symmetry is observe around coupling capacitor C_{23} the plate on the right matches the plate on the left. Therefore the following are observe:

$$C_{01} = C_{45} = p1 \text{ or } p8$$

$$C_{12} = C_{34} = p2 + p3 \text{ or } p6 + p7$$

$$C_{23} = p4 + p5$$

Figure 4.24 is the geometry of the parallel plates capacitor with some dielectric.

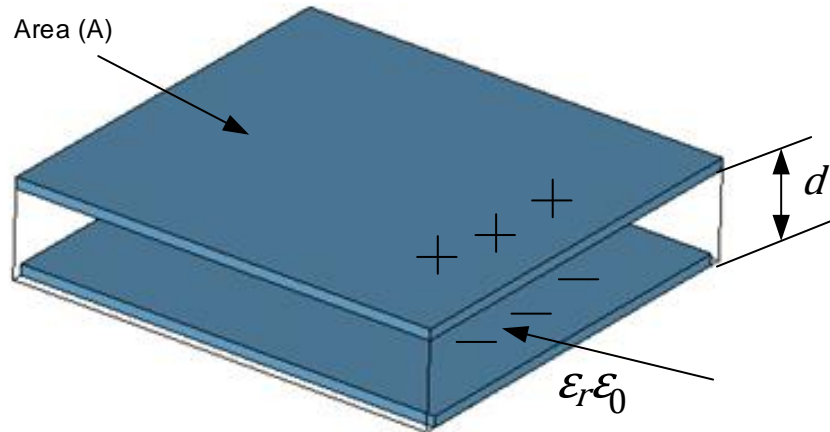


Figure 4.24: Geometry of the parallel Plate Capacitor (Adapted from Stuart, 2007:3)

The parallel plate capacitance values are found using the following equations (Maloratsky, 2004:56-57).

$$C = \frac{\epsilon_r \epsilon_0 A}{d} \quad (4.3)$$

where:

ϵ_r : Dielectric constant of the substrate material.

ϵ_0 : 8.85418 pF / m .

A : Parallel plate overlapped area.

d : Thickness of the dielectric substrate.

Figure 4.25 presents the parallel plate capacitor overlapping area. The focus would be on the first three plates (P1, P2, and P3) due to physical symmetry addressed in the circuit stage design. The overlapping area is defined by equation (4.4) to (4.6). The gap capacitor values were estimated base on the fact that the parallel plate capacitor contributes more to the structure performance. This was then justified during the E-field distribution study. The fields are denser below the plate than around the gap capacitor as illustrated in Figure 4.26. Also during simulation it was observed that changes made to the parallel plate capacitors value would affect the response of the filter compare to that of the gap capacitors.

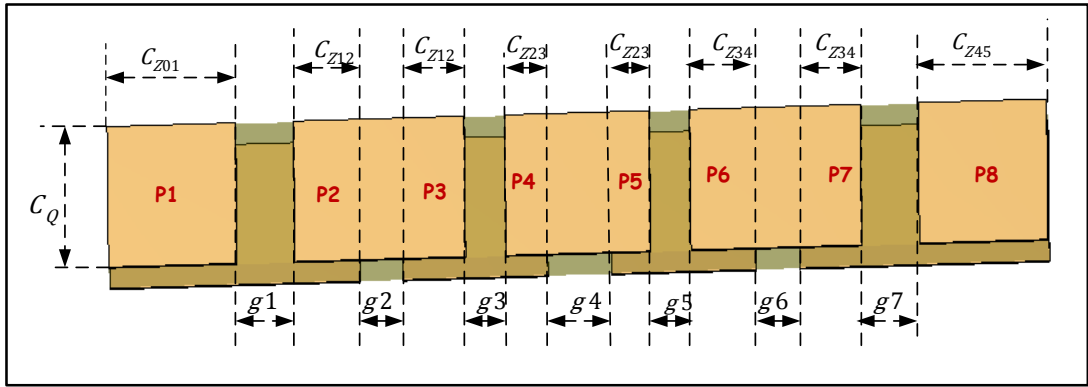


Figure 4.25: Parallel Plate capacitors overlapping area adapted from (Lierena Castro, 2014:66 and Fei et al., 2009:43-46)

Following the general formula of the parallel plate capacitor, each plate configuration is derived as follows:

$$C_{P1} = \frac{\epsilon_r \epsilon_0 A_{P1}}{d} \quad (4.4)$$

$$C_{P2} = \frac{\epsilon_r \epsilon_0 A_{P2}}{d} \quad (4.5)$$

$$C_{P4} = \frac{\epsilon_r \epsilon_0 A_{P4}}{d} \quad (4.6)$$

The area of each plate is defined as follows:

$$A_{P1} = C_Q \times C_{z01} \quad (4.7)$$

$$A_{P3} = C_Q \times C_{z12} \quad (4.8)$$

$$A_{P4} = C_Q \times C_{z23} \quad (4.9)$$

The coupling capacitor from the circuital model is related to parallel plate capacitors as follows:

$$C_{01} = C_{P1} \quad (4.10)$$

$$C_{12} = \frac{C_{P2}}{2} \quad (4.11)$$

$$C_{23} = \frac{C_{P4}}{2} \quad (4.12)$$

The length parameters of the overlapping area can then be computed using Equation (4.13) to (4.15). The following is then obtained, with the value of C_Q be chosen:

$$C_{Z01} = \frac{C_{01}d}{\epsilon_r \epsilon_0 C_Q} \quad (4.13)$$

$$C_{Z12} = \frac{2C_{12}d}{\epsilon_r \epsilon_0 C_Q} \quad (4.14)$$

$$C_{Z23} = \frac{2C_{23}d}{\epsilon_r \epsilon_0 C_Q} \quad (4.15)$$

These calculated length values will help start the design simulation. Therefore, as the simulation goes on, optimisation of those values will be done so that the design response is placed at desired frequencies. The reason why these calculated values will change is due to the fact that the actual value of each gap capacitor is not considered because the parallel plate capacitors are more dominant than the gap capacitors and also because of not considering in Equation (4.3) the fringe effect of capacitance. The observation of the E-field and H-field distribution around the overall structure of the ceramic bandpass filter presented in Figure 4.26 shows that the field is denser in the parallel plate capacitor region, thus the reason for not considering the contribution of the gap capacitor at beginning (Liang et al., 2009:43-46 and Lierena Castro, 2014:66, 68). The calculated value of each plate will decrease progressively as we perform optimisation.

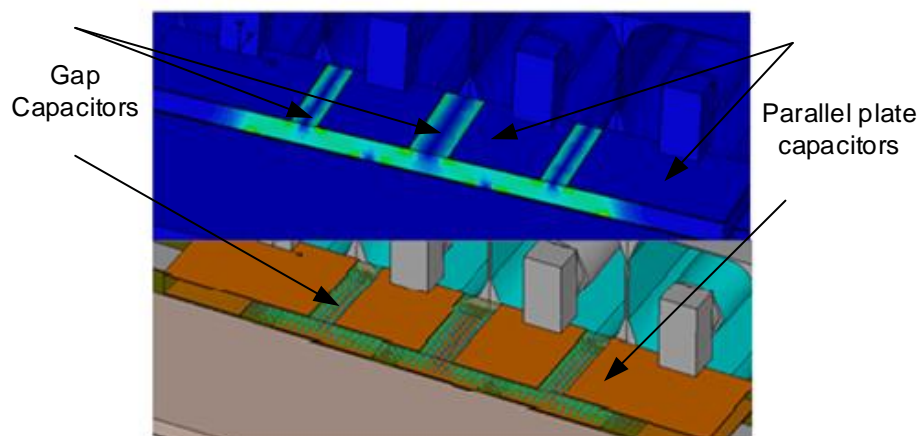


Figure 4.26: E-field distribution around the coupling capacitors

Table 4.7 shows the calculated values of each parameter needed for the coupling structure. The structure is constructed using Rogers 3210 material, that has a thickness of 0.64 mm and relative permittivity of 10. The board thickness and dielectric constant of the substrate plays a roll in the overlapping capacitors presented in equation (4.13), (4.14) and (4.15).

Table 4.7: Coupling structure values

C_{01} (pF)	0.614	C_{12} (pF)	0.18	C_{23} (pF)	0.135
A_{P1} (mm ²)	10.44	A_{P2} (mm ²)	3.1	A_{P3} (mm ²)	2.8
C_{Z01} (pF)	2.61	C_{Z12} (pF)	1.533	C_{Z23} (pF)	1.4

Figure 4.27, 4.28 and 4.29 respectively are the populated board with four 3D model CCRs cover with a metallic enclosure, the simulated results and optimised results. Figure 4.27 is the final design made of 4 CCRs, the coupling capacitor structure, and the 50 ohm lines where the SMA connectors are soldered on. The 4 CCRs have minimal space in between them which are not physically visible. The first two resonators are spaced 0.3 mm apart from each other, while the last two resonator are spaced of 0.1 mm apart. This resonator distance were calculated to creates a finite transmission zero at 1.98 GHz.

It was observe through-out the simulation that by altering the gap between resonators, the transmission zero would either go up or down. The insertion loss appears to be flat in the transmission band. This is due to the 0.01 Chebyshev ripple value used. Another important factor to take into account is the quality and the amount of solder used in order to realise the transmission zero, because any extra solder in between the resonators would cause the transmission zero and the response of the filter to shift. The amount of solder placed on the resonator tab is also problematic at certain point during the construction.

Figure 4.28 shows the simulated result with a finite TZ at 1.99 GHz and a good return loss and insertion loss can be observed. After some changes were made to the spacing between the first two resonators and the two inside parallel plate capacitors, an improvement on the TZ return loss and insertion loss could be seen as shown in Figure 4.29.

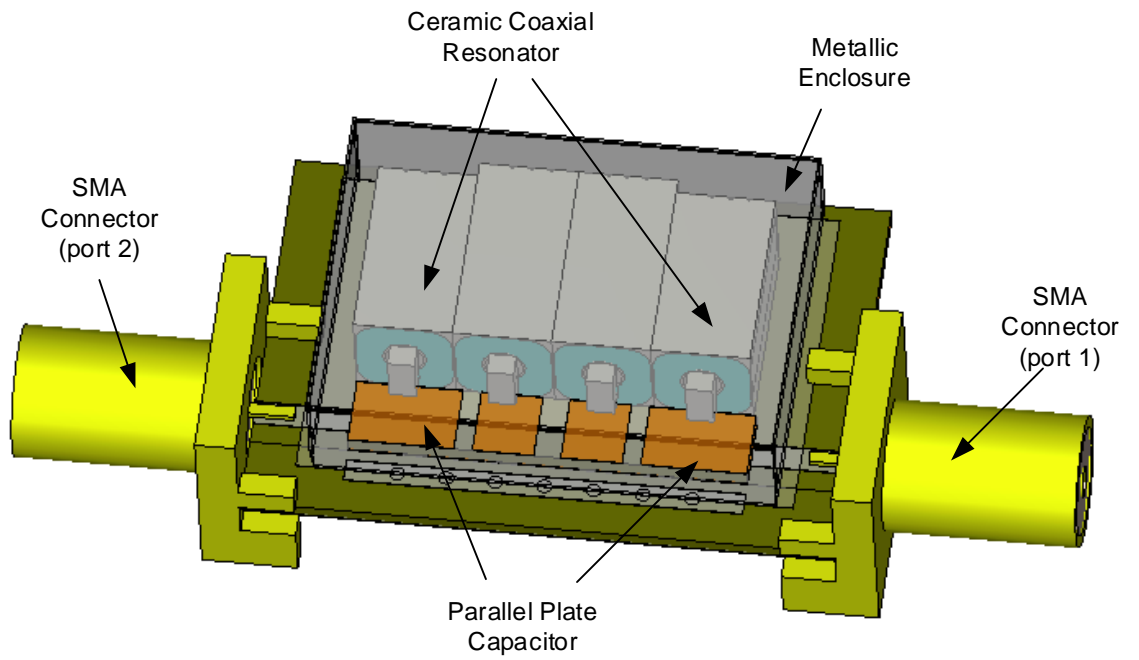


Figure 4.27: Ceramic coaxial resonator bandpass filter with 4 CCR in 3D form and the coupling capacitor structure

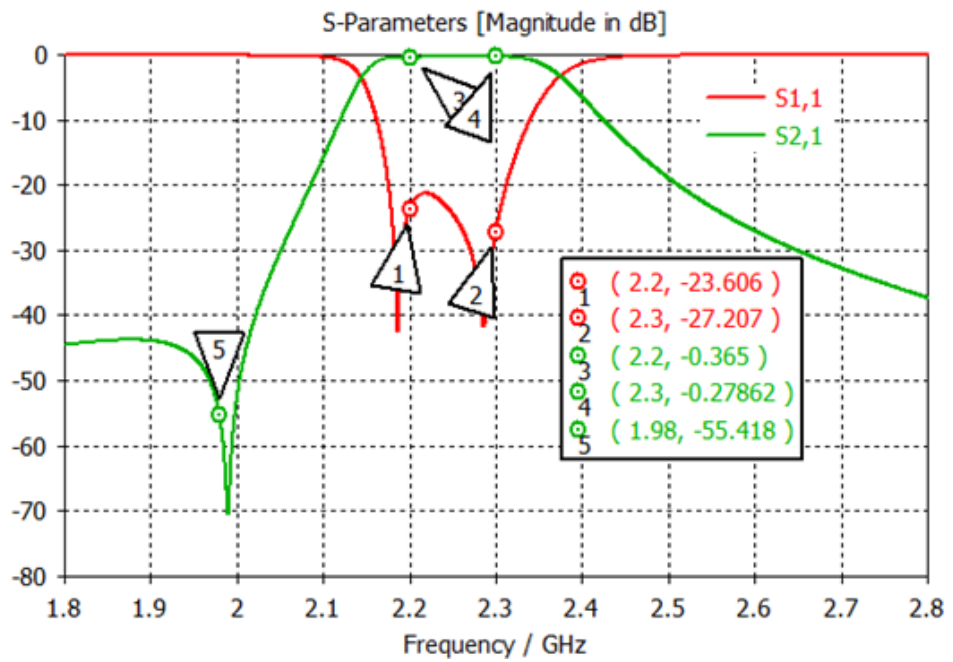


Figure 4.28: Ceramic coaxial resonator bandpass filter simulated result

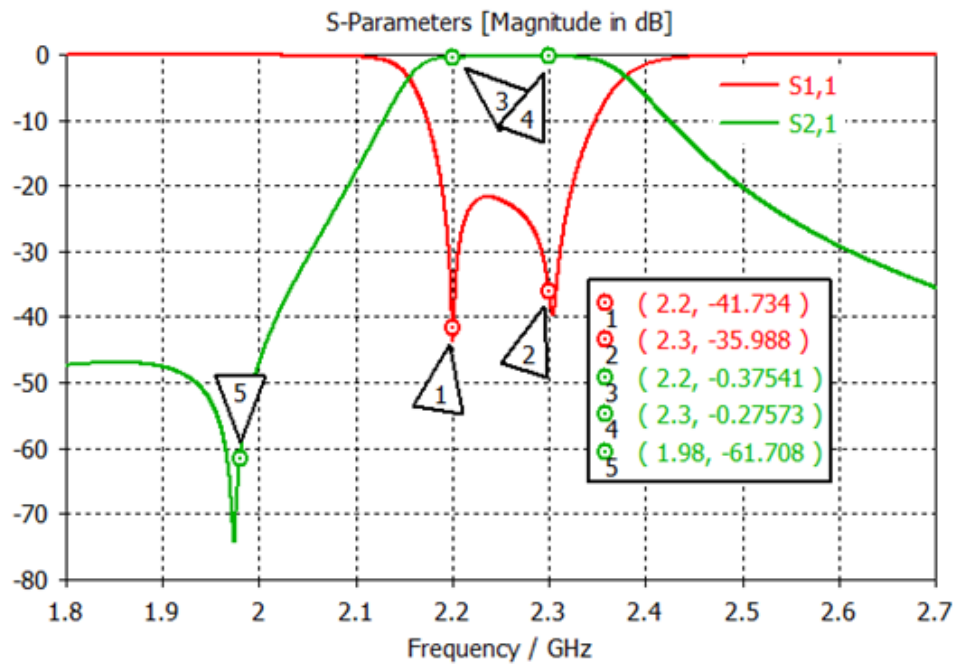


Figure 4.29: Ceramic coaxial resonator bandpass filter optimised result

4.8 E-field and H-field distribution around the overall system

The bandpass filter presented in Figure 4.27, is simulated using CST Microwave Studio® to visualise the distribution of electrical and magnetic fields. The study of E-field and H-field simulation will help characterise the use of the enclosure during the testing stage as well as presenting the effect of a transmission zero. Figure 4.30 is the colour map which represents the degree of coupling around CCR. The blue colour shows the lowest degree of coupling and the red colour the highest degree of coupling.

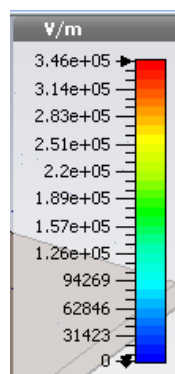


Figure 4.30: Colour map

4.8.1 E-field and H-field distribution with no enclosure

An E-field simulation is performed on the overall system at 0° , 30° and 60° phases, as well as at 1.98 GHz, 2.2 GHz, 2.25 GHz and 2.3 GHz frequencies.

Figure 4.31 represent the E-field distribution at 1.98 GHz with 30° and 60° phases. The distribution of E-field at these phases shows that the transmission has indeed stopped. The analysis of the field also shows that only the first resonator and parallel plate capacitor $P1$ is significant. After the first resonator, the transmission stopped. It should be noted that at phase zero, there was no transmission at all at 1.98 GHz.

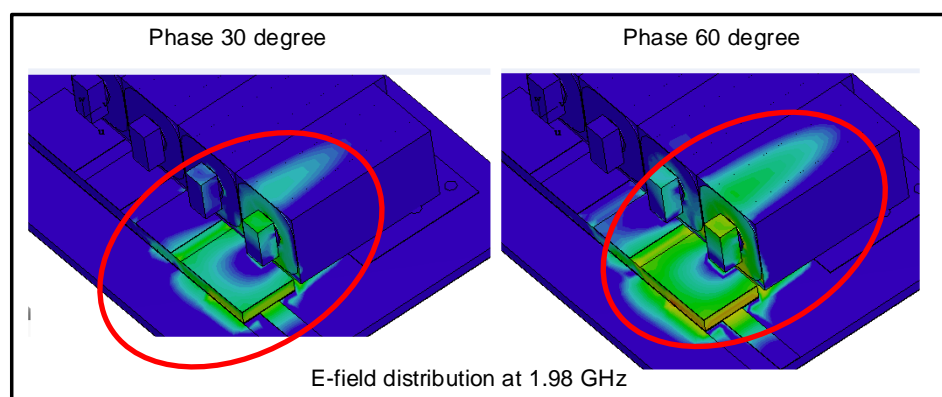


Figure 4.31: E-field distribution at 1.98 GHz (30° and 60° phases)

The study of the E-field at 2.2 GHz, 2.3 GHz and 2.25 GHz, and at all chosen phases, are presented in Figures 4.32, 4.33 and 4.34. There is a strong coupling at the open side of the resonator while at the short circuited side there is no coupling; this confirms the shielding properties of the resonator. As well below the parallel plate capacitor there is a dense coupling compared to in between the gap capacitor. The resultant E-field also presented the contribution of the coupling capacitor structure in the design.

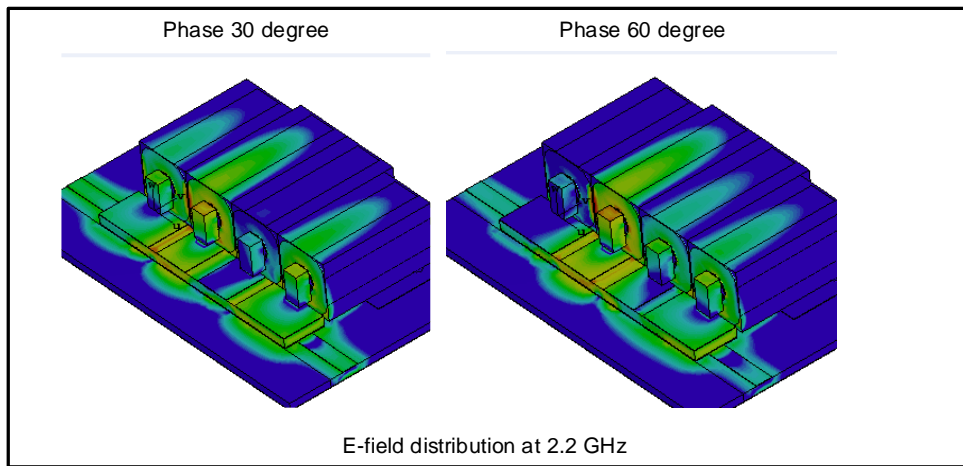


Figure 4.32: E-field distribution at 2.2 GHz

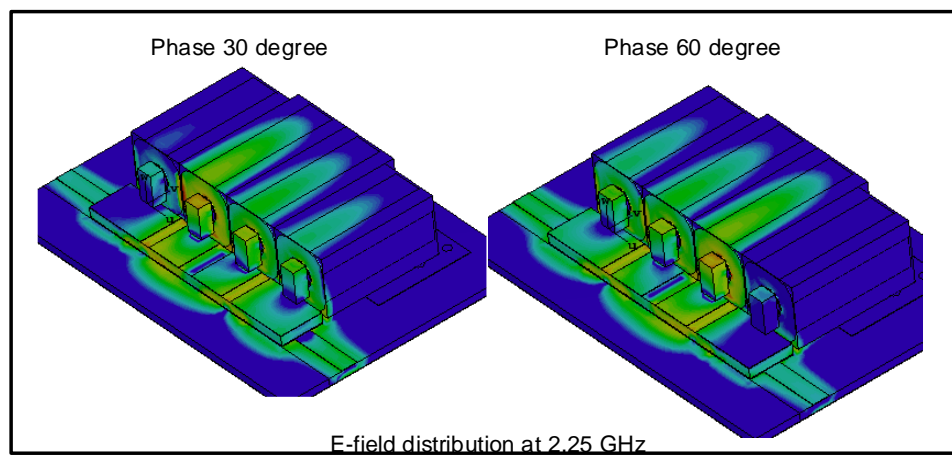


Figure 4.33: E-field Distribution at 2.25 GHz

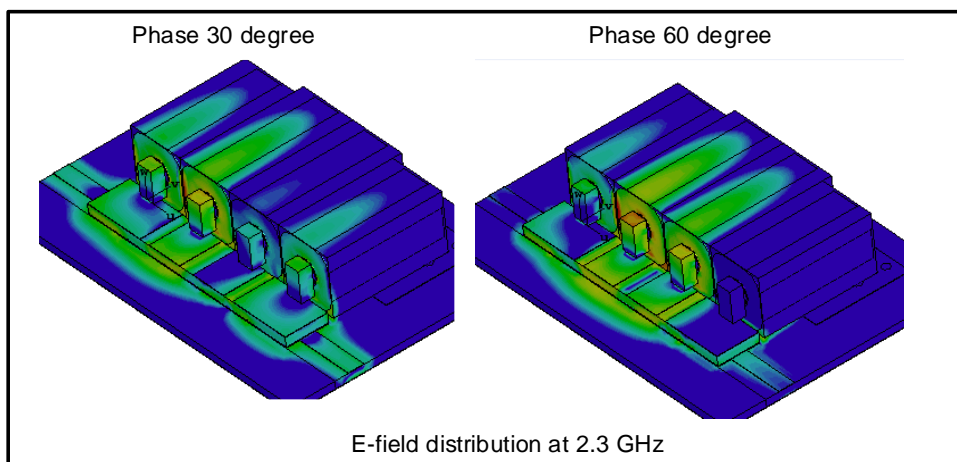


Figure 4.34: E-field Distribution at 2.3 GHz

On the other hand, the magnetic field study performed at 1.98 GHz, 2.2 GHz, 2.25 GHz and 2.3 GHz, with 0° , 30° and 60° phases, shows the following:

- At 1.98 GHz, with all phases, there is transmission only on the first resonator and the first parallel plate capacitor.
- At 2.2 GHz, with all phases, all 4 resonators coupled to each other's. The same observations are made at 2.25 GHz and 2.3 GHz.

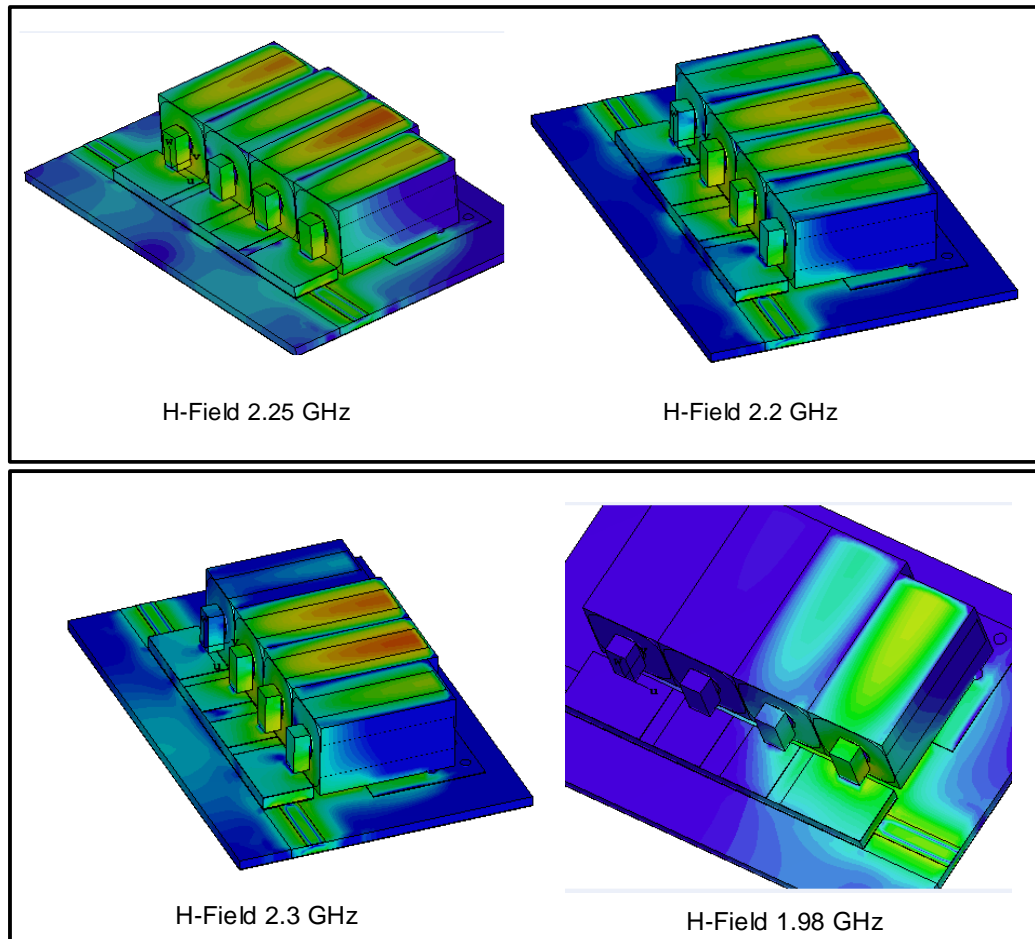


Figure 4.35: H-Field Distribution at different frequencies.

Figure 4.36 represent the surface current flow at all phases. The current flows from port 1 to port 2. This analysis shows the effect of the ground plane in the overall design. This ground plane also added capacitance into the circuit which was crucial for the TZ calculation. To conclude this analysis, there are strong coupling between the parallel plate capacitors. Please note that the 50 ohm lines at the bottom of parallel plate capacitor $P1$ and $P2$, also add extra capacitance in the circuit, all of which were not considered during the circuit design stage.

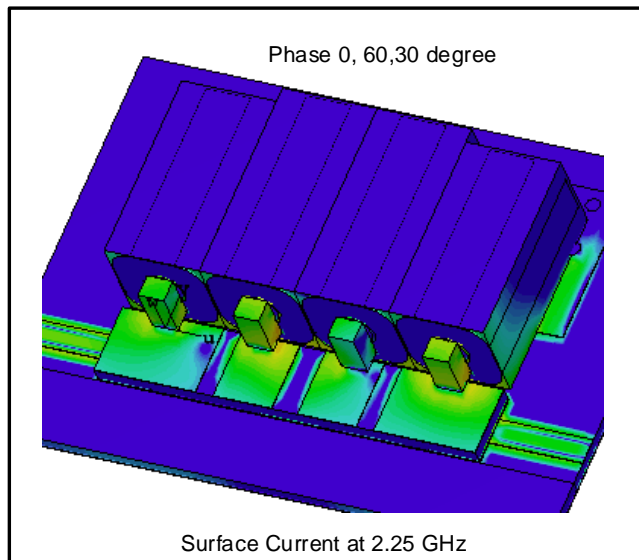


Figure 4.36: Surface Current flow

4.9 Summary

This chapter dealt with the implementation of the 4th order ceramic coaxial resonator bandpass filter using specifications displayed in Table 4.1. The large profile (LS) resonator from Trans-Tech was selected as component to construct the filter. The capacitive-coupled resonator method introduced in Chapter 3 and the filter symmetry was used to implement the lumped element filter presented in Figure 4.4. A finite transmission zero at 1.98 GHz was introduced into the circuit by placing a lumped LC series resonator to ground. This was done to increase the attenuation at that point which contributed to some performance degradation of the system. The 3D model of the overall filter was created using CST Microwave Studio[®] as shown in Figure 4.11, and the simulated result presented in Figure 4.12 showed a shift in the result due to the presence of the tab. This leads to the increase of the resonant frequency in each CCR. The coupling capacitor structure was then designed as demonstrated in Section 4.7. From the electromagnetic simulation done on the circuit, it showed that the contribution of the gap capacitor in the structure compared with that of the parallel capacitor was minimal. The E-field and the H-field distribution were performed on each CCR to observe the amount of coupling around the CCR open side. The effects of the simulation from the system with no enclosure as presented in Figures 4.31, 4.32, 4.33 and 4.35. The ground plane and the 50 ohm transmission lines, beneath the parallel plate capacitors, have added extra capacitance to the model.

CHAPTER 5

FABRICATION, TESTING AND DISCUSSION OF RESULTS

In this chapter, the fabrication of the bandpass filter presented in Figure 1.2 is discussed, followed by the testing stage and the comparison of results.

5.1 Bandpass filter manufacturing

Figure 5.1 is the PCB layout designed using Altium Designer and the actual Rogers 4003C PCB. The bandpass filter consists out of four CCRs presented in Figure 1.2 is constructed using Rogers material. The filter has a port at each end of the board connected to a 50 ohm line. The coupling structure board is also made using Rogers material of varying thicknesses and dielectric constants. Figure 5.2 represents the coupling structure board cutting using Rogers 3210.

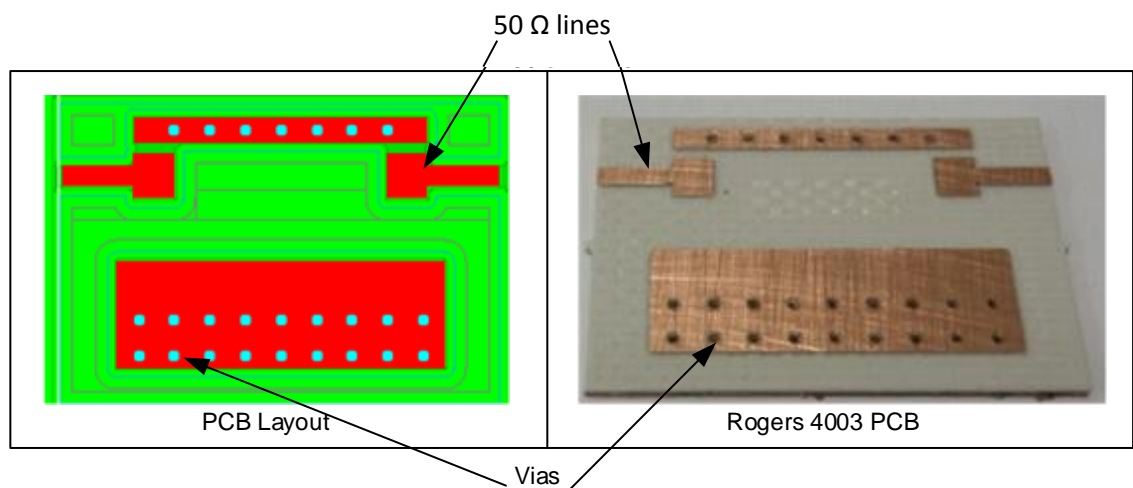


Figure 5.1: PCB layout and printed board

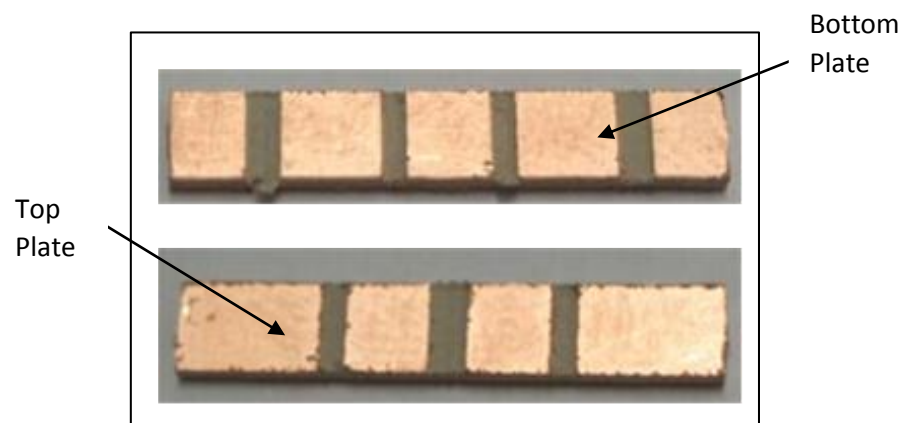


Figure 5.2: Top and bottom plate capacitor structure

Microwave filters can be manufactured using various machining techniques. The techniques used to manufacture the PCB prototype presented in Figure 5.1 and 5.2 are computer numerical controller (CNC) milling. This cost-effective technique uses a rotating bit to remove material. The process is as follows:

- Bottom PCB(Rogers 4003C) drilled and filled with solder paste
- Bottom PCB (Rogers 4003C) place in oven. The solder paste melts and makes a ground connection between the top and bottom side of the PCB
- Finalising the milling of the Bottom PCB (Rogers 4003C)
- Milling of the coupling structure PCB (Rogers 3210)

All the above-mentioned steps are done using the machinery presented in Figure 5.3.

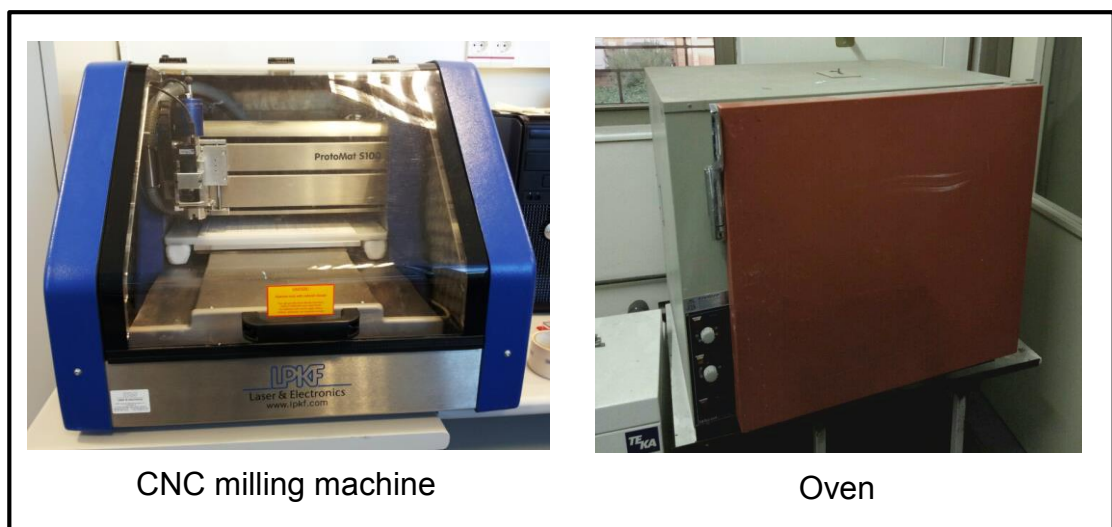


Figure 5.3: CNC milling machine and oven

5.2 Filter dimension

From the specification drawn by the engineering team of F'SATI, the prescribed dimension was to have a PCB of 1.6 mm thickness, 30 mm width and 30 mm length. The populated board had to have a total height of 20 mm. Figures 5.4 and 5.5 respectively show the coupling capacitor structure dimension and the populated microwave dielectric filter dimension. The conclusion drawn from this is that the designed filter dimension has met the described specification. Figure 5.6 and 5.7 respectively show the metallic enclosure with the 50 Ω lines for the I/O port's connection.

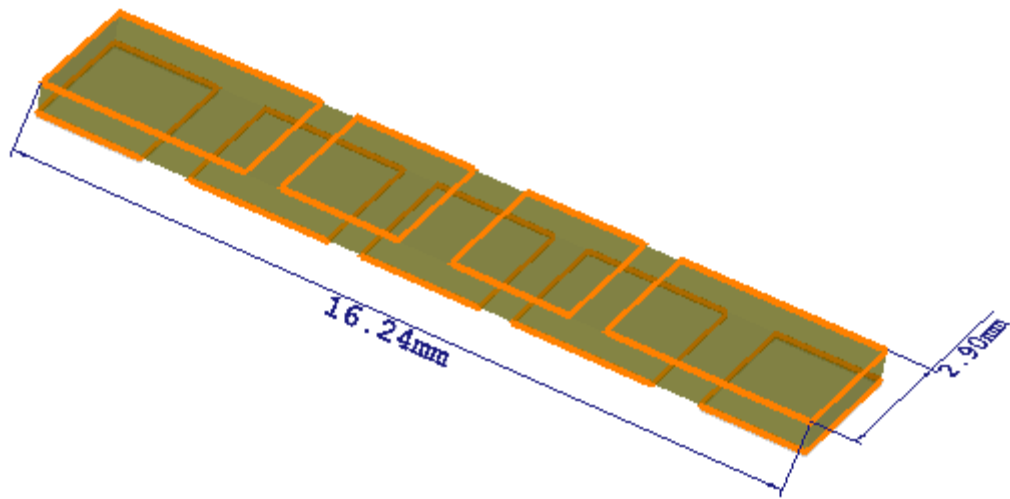


Figure 5.4: Coupling capacitor structure dimension

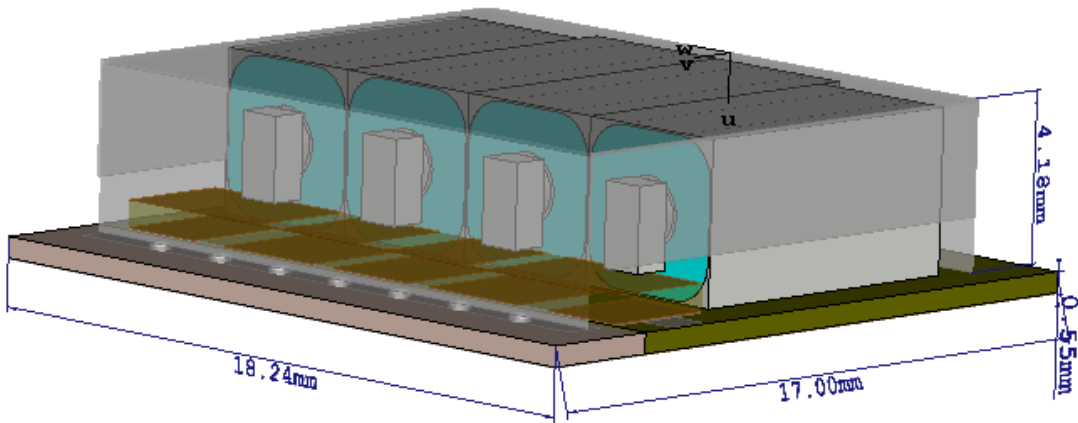


Figure 5.5: Populated board dimension

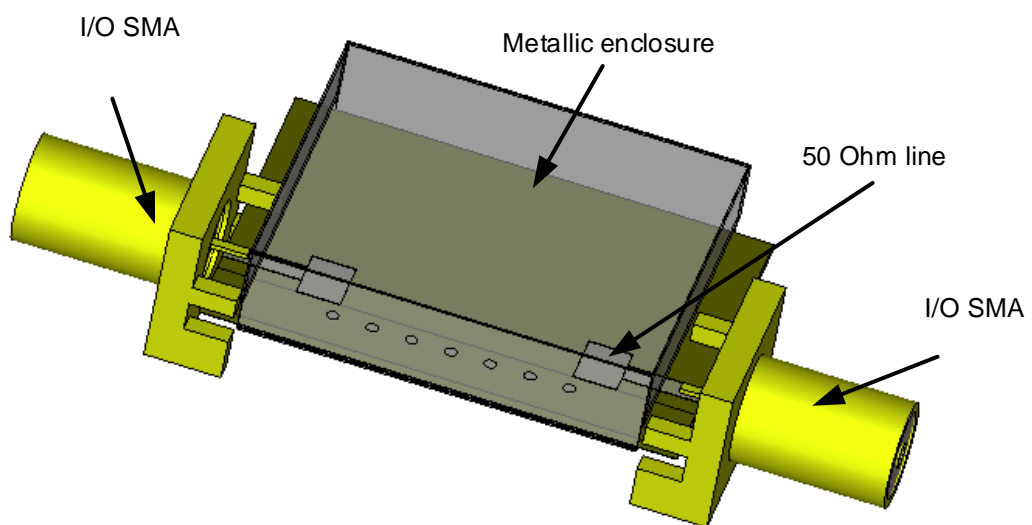


Figure 5.6: Metallic enclosure

5.3 Testing

The designed bandpass filter presented in Figure 5.7 was tested to validate the design procedure. This filter had a 1.22 mm x 18.24 mm x 17 mm dimension.

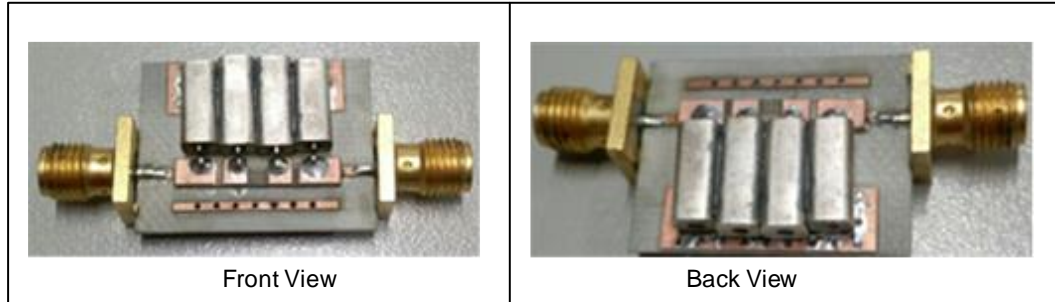


Figure 5.7: Ceramic coaxial resonator bandpass filter: back and front view

5.3.1 VNA preparation

The actual goal of this work was to develop a bandpass filter using ceramic coaxial resonator technology which can be used in the receiver system of a CubeSat. The Agilent 8753ES S-parameter network analyser was used to test the filter. Figure 5.8 refers the test setup. An electronic calibration kit was used to perform the two port calibration of the vector network analyser. The start and stop frequency were set from 1.7 GHz to 2.7 GHz.

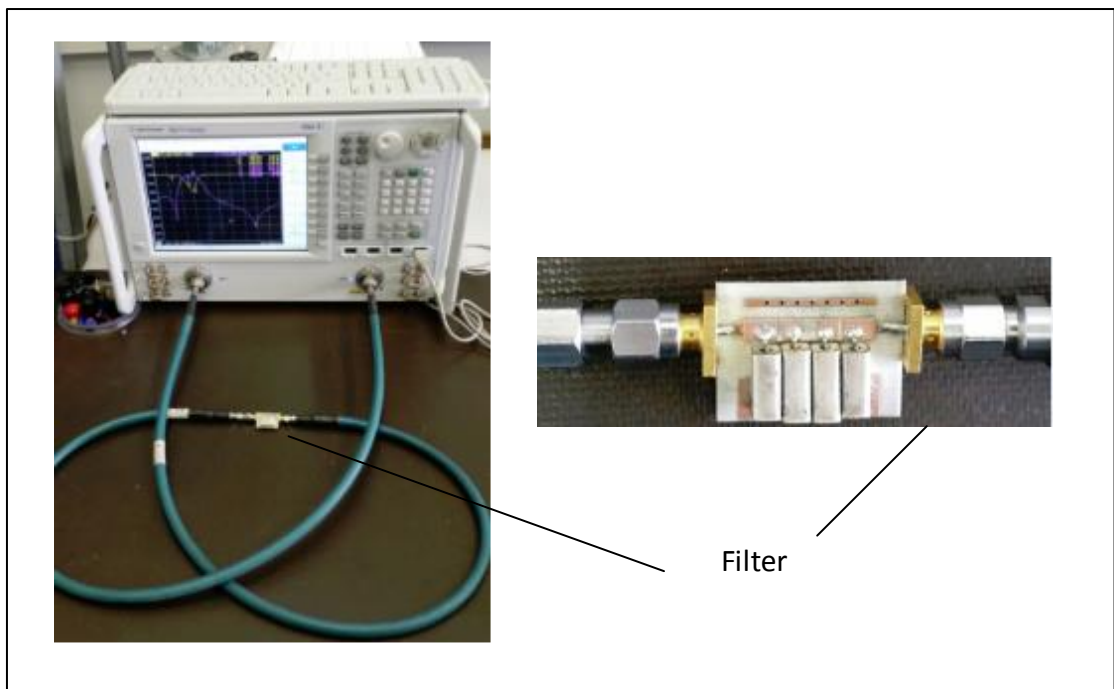


Figure 5.8: Test setup

5.3.2 Ceramic bandpass filter testing

The SMA connector at each port of the bandpass filter presented in Figure 5.7 was connected to the VNA ports as demonstrated in Figure 5.8. Data collected from the VNA representing the insertion loss and the return loss values were used to plot the magnitude response of the bandpass filter. Figure 5.9 is the logarithmic response of the bandpass plotted using MATLAB. The magnitude response showed that the filter has two lobes because of the physical symmetry addressed in Section 4.3.2. This physical symmetry showed that CCR1 would resonate at the same frequency as CCR3 and CCR2 would resonate at the same frequency as CCR3.

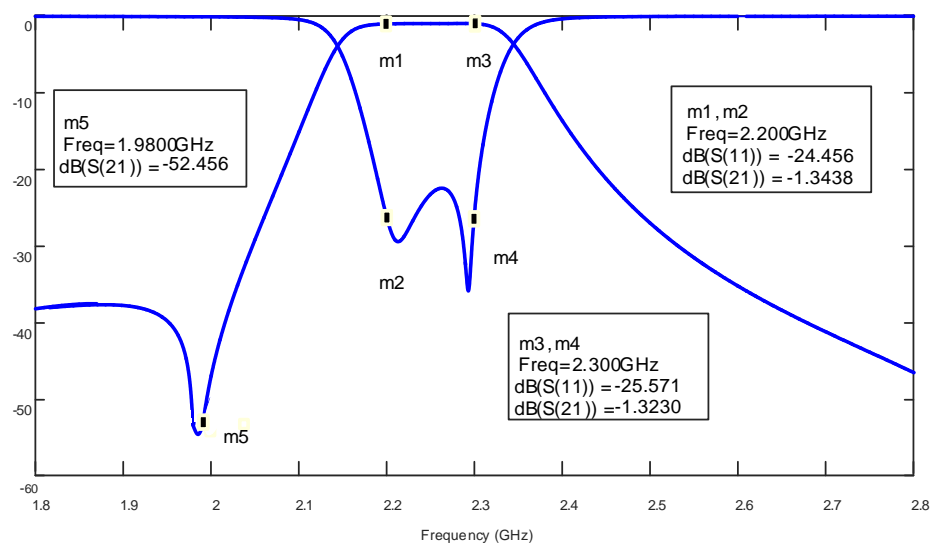


Figure 5.9: Measured result

5.3.3 Temperature cycling

Temperature cycling is a process of exposing a manufactured product to thermal cycling in order to observe defects on the manufactured product as well as to observe possible failure. The designed bandpass filter as part of the communications systems needs to survive the CubeSat launch and the harsh temperatures in the LEO.

The designed filter with passband frequency between 2.2 GHz to 2.3 GHz with a transmission zero between 1.98 GHz to 2 GHz, built on Rogers material, is suggested for thermal cycling from $-21\text{ }^{\circ}\text{C}$ to $61\text{ }^{\circ}\text{C}$ for the Acceptance Hot and Cold procedure. The diagram presented in Figure 5.10 represents the test procedure. The filter connected to the input and output port of the VNA is placed in a thermal chamber, a simulation at $-21\text{ }^{\circ}\text{C}$, room temperature, and $61\text{ }^{\circ}\text{C}$ are performed. The ceramic

coaxial resonator can still operate between $-40\text{ }^{\circ}\text{C}$ to $90\text{ }^{\circ}\text{C}$ (Trans-Tech, 2007b:1-3), but future work will test for temperature levels in LEO ($-170\text{ }^{\circ}\text{C}$ to $123\text{ }^{\circ}\text{C}$) and the Qualification Hot and Cold procedure will be conducted. Figure 5.11 below shows the result of simulation at $-21\text{ }^{\circ}\text{C}$, room temperature, and $61\text{ }^{\circ}\text{C}$. The following observations are made based on the simulation results.

- The response has shifted a bit to the left with the temperature at lower level ($-21\text{ }^{\circ}\text{C}$)
- The insertion loss of the filter has improved at lower level, comparable to that of the higher level ($61\text{ }^{\circ}\text{C}$)
- The minimal shifting of the response has not affected the target specification as much.

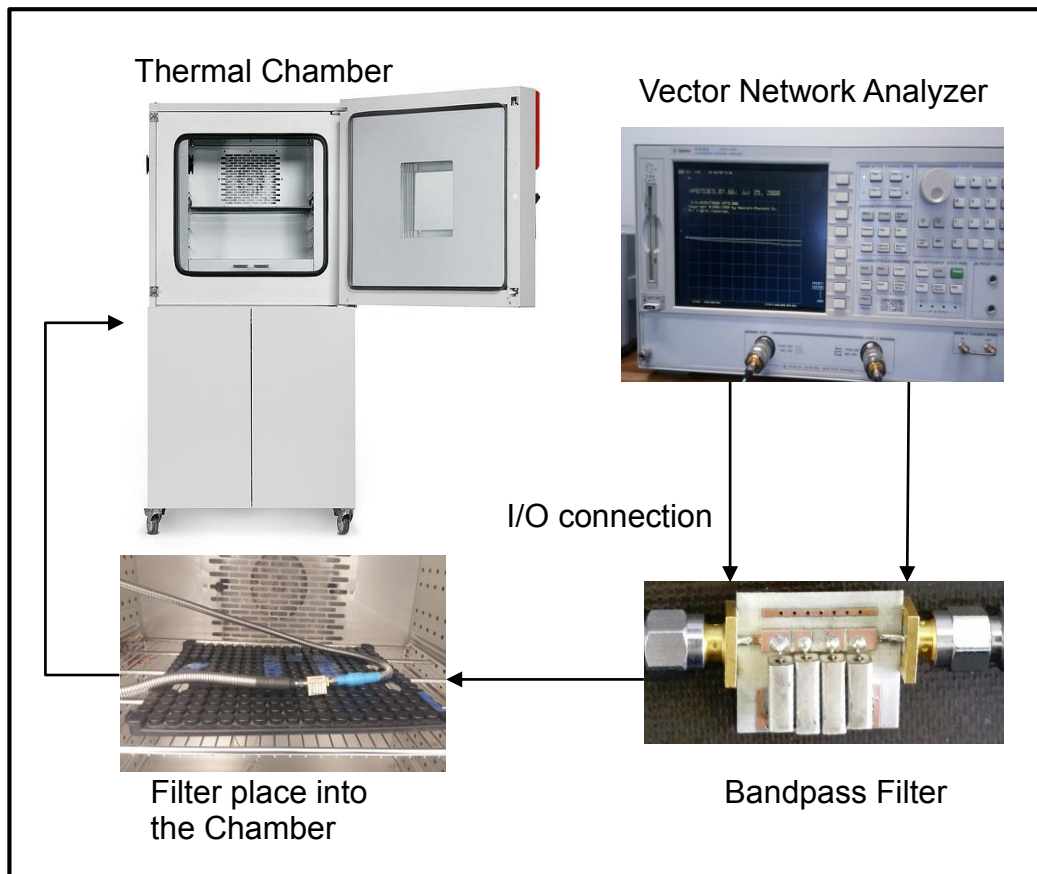


Figure 5.10: Temperature cycling test setup

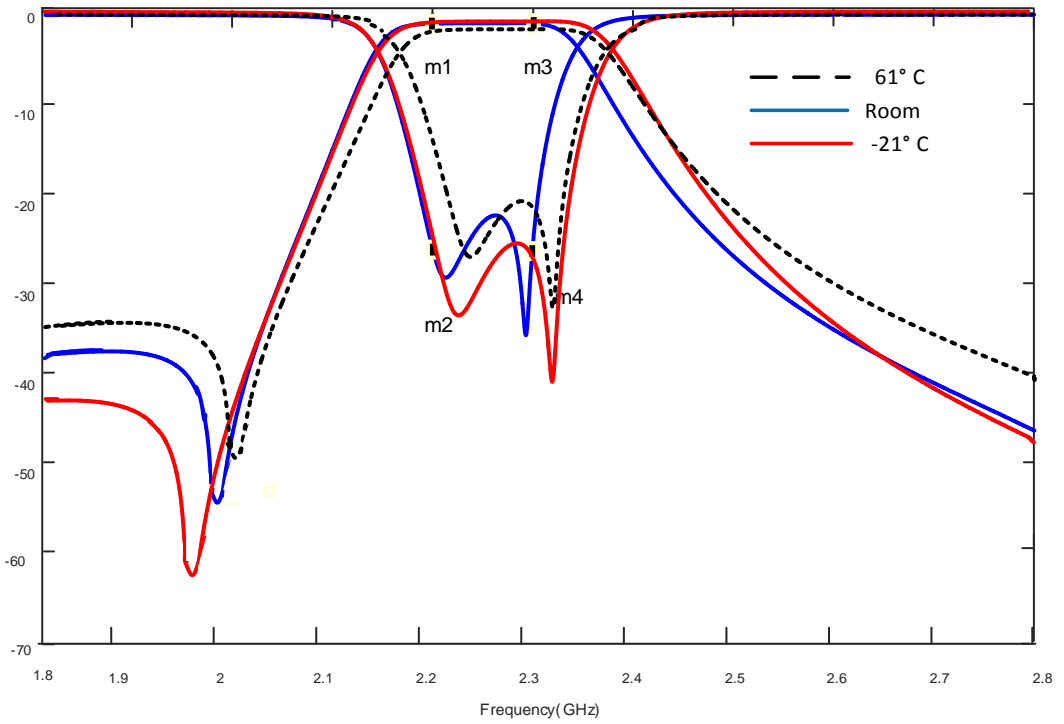


Figure 5.11: Temperature cycling at different temperature levels

5.4 Discussion of results

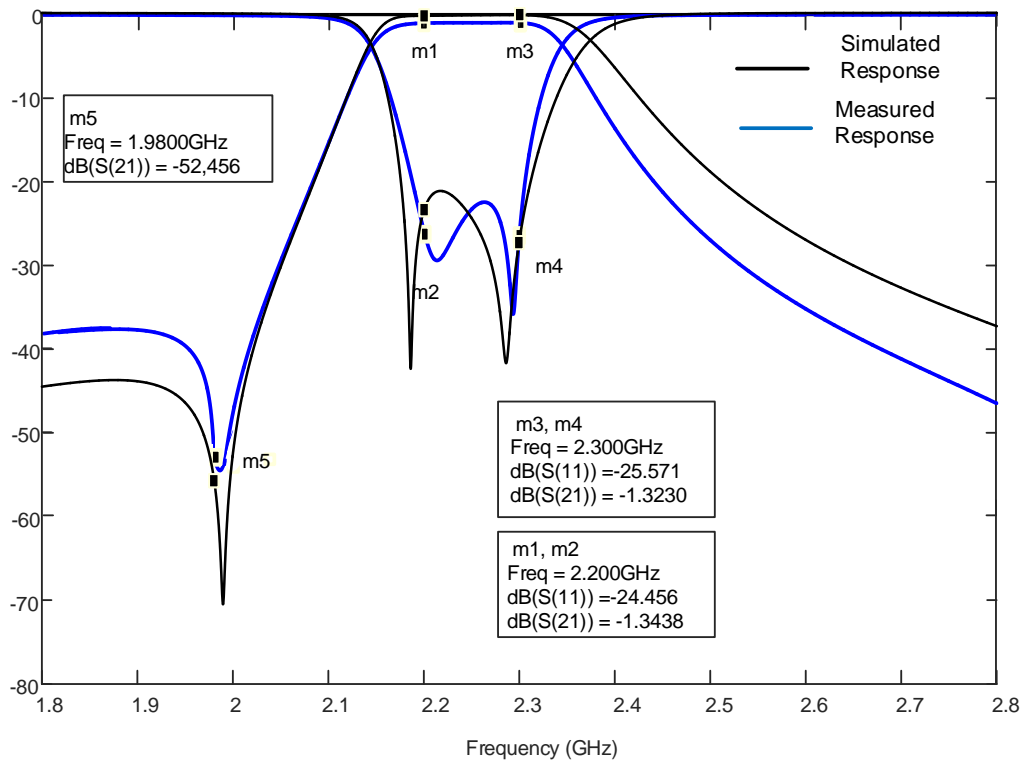


Figure 5.12: Comparison of results

The filter built on Rogers material has the dimensions of 4.73 mm x 18.24 mm x 17 mm which represent the thickness, width and length respectively. This compact filter exceeded the set dimension specifications. The allocated space on board the CubeSat communications system has always been a challenge.

The simulated filter has a return loss (S_{11}) between -20 dB and -27 dB over the specified bandpass band. The manufactured bandpass filter has a return loss between -24.456 dB and -25.571 dB over the specified bandpass band. The insertion loss (S_{21}) of the simulated bandpass filter is between -0.278 dB and -0.365 dB, while the tested bandpass filter has an insertion loss between -1.323 dB and -1.3438 dB. The delta in-band insertion loss flatness was less than -0.5 dB. More tests such as radiation level and temperature measurements were performed on the filter. These tests were performed to analyse the level of radiation of the populated board and to analyse the changes observed on the filter when operating at temperatures different from the room temperature. These tests were satisfactory, as they showed minimal changes in the performance of the filter response. The manufacturing process of the PCB at Cape Peninsula University of Technology (CPUT), the removal of the silver coating around each CCR for SRF increment, and the in-house soldering were factors that contributed to the difference in attenuation between the simulated and the measured results. Another factor that contributed to the increase of insertion loss was the inadequate soldering of the shielded housing. Table 5.1 presents a comparison of the results.

Table 5.1: Comparison table

Parameters	Designed	Simulated	Measured
Frequency Band	2.2 GHz to 2.3 GHz	2.2 GHz to 2.3 GHz	2.2 GHz to 2.3 GHz
Resonant Frequency	2.25 GHz	2.25 GHz	2.25 GHz
Insertion Loss	< 2 dB	-0.365 dB	-1.3438dB
Return Loss	\leq -15 dB	-20 dB to -27 dB	-24.456 dB to -25.571 dB
Transmission Zero (1.9 GHz–2 GHz)	\leq -30 dB	-55,418 dB	-52,456 dB

5.5 Summary

In summation, the bandpass filter presented in Figure 1.3 (printed circuit board layout) was designed using Altium Designer and printed at the CPUT on the Rogers 4003C and Rogers 3210 material. The measurement of this filter shows that the filter meets the desired specifications and has a quite stable bandwidth. The filter of Figure 5.4 has a height of 4.73 mm. It was found that the measured performance of the fabricated filter was satisfactory.

CHAPTER 6

CONCLUSION, RECOMMENDATION & FUTURE WORK

6.1 Final conclusion

The primary goal of this thesis was to describe the design of a microwave bandpass filter using a ceramic coaxial resonator for nanosatellite applications. The performance of this bandpass filter made of ceramic coaxial resonators operating over the portion of S-band frequencies used for satellite up- and downlink communication makes the filter designed and built in this research an excellent option for future nanosatellites as well as for the ground station transceiver.

Chapter 2 discussed the electrical characteristics and features of the CCR. In the intensive research done on microwave resonators, its parallel configuration looked similar to the equivalent representation of the CCR, and to the short circuited quarter wavelength transmission line resonator as presented in Figure 2.7.

In Chapter 3, intensive background research into satellite communications systems and general design issues with various filter technologies were conducted. Bandpass filters are necessary for communications systems, owing to the inter-symbol interferences between the transmitters and receivers, and the high-power harmonics. These problems in the communications block are harmful and need to be rectified. The concept of the ceramic coaxial resonator was found to be useful since compact filter design was practicable. Design formulae from the low pass prototype to the transformation to the bandpass prototype were demonstrated. The implementation method of the capacitively coupled resonator bandpass was presented by equations described in Section 3.2.2.

Chapter 4 discussed the design of the conventional bandpass filter and its representation in a 3D model. A 4th order coupled resonator bandpass filter was designed using the techniques explained in Section 3.2.2 and the physical symmetry of the filter discussed in Section 4.3.2. The lumped element result of the coupled resonator bandpass presented in Figure 4.5 was satisfactory. The shunt LC presented in Figure 4.5 was then converted into CCR using the equations presented in Section 2.3. Using CST Microwave Studio®, the 3D model of each CCR was constructed. An electromagnetic simulation of the 4 CCR coupled internally and externally to each order with lumped capacitor was simulated and the result presented a left shifting. Finally, an intensive electromagnetic study was performed on a single CCR 3D structure and on the bandpass filter 3D structure as represented in Figure 4.14, 4.15 and 4.31 to 4.36 respectively. This electromagnetic study was

performed firstly to determine the degree of accuracy of a single CCR and second to deduce the exact length of the CCR, secondly the value of the capacitance necessary for the structure to resonate at the desired frequency and finally to motivate the use of the metallic enclosure. The structure of the coupling capacitor made of parallel plate capacitors and gap capacitors in the form of array was built using the method described in Section 4.7. The structure of the coupling capacitor was then placed and connected with the ground board as shown in Figure 4.27. At first, the simulation result was acceptable, but after much turning and optimisation performed on the structure of the coupling capacitor and the CCR length, the result of simulation presented in Figure 4.30 was obtained.

Chapter 5 dealt with the fabrication, testing and discussion of results. The ceramic coaxial resonator bandpass filter presented in Figure 5.7 was manufactured at the Cape Peninsula University of Technology using the CNC machinery presented in Figure 5.3. A compact bandpass filter was designed and the overall dimensions are presented in Section 5.2. The VNA provided by CPUT was used to measure the filter, and from the measured result, a satisfactory conclusion between the measured and simulated results is drawn as presented in Table 5.1. Finally, the designed filter has met the defined specification presented in Table 4.1.

6.1.1 Addressing the investigative question

- **CCR placement on PCB**

This study was centred on designing an S-band bandpass filter using ceramic coaxial resonators technology. The large profile (LS) resonator from Trans-tech was selected for the implementation of the filter. The resonators were assembled on the PCB in such a way to create transmission zero as well as to minimise the amount of capacitance and inductance created between them. These resonators were soldered onto a ground board and to each other. Extreme care was taken with the soldering of CCRs onto the board as they can be damaged if proper soldering techniques are not observed (Trans-Tech, 2013c:10).

- **Electromagnetic radiation**

An electromagnetic test was performed first on a single CCR to analyse the effect of the solder tab on the resonators (Figure 4.14 and 4.15). It was found that the solder tab and the parasitic lumped element (LC) created by the lumped capacitor caused the reduction of the resonant frequency of the resonator. This decrease of the resonant frequency is the cause of the left shifting of the simulated result as

presented in Figure 4.12. Most of the radiation occurs at the resonator's open side; this is due to the metallic shielding around each resonator, which played a big role. The whole filter was then subjected to EM simulation, which then showed the role the metallic enclosure played in reducing considerably the amount of radiation as demonstrated in Section 4.8.

- **Enclosure implementation**

From the EM simulation performed on the filter without an enclosure, it showed that for a total suppression of radiation, the filter must be covered with an enclosure. This is due to the solder tab acting coupling between each other.

- **Transmission zeros**

The question of how to implement the transmission zero was solved during the lumped element implementation. But practically the transmission zero was inserted due to cross-coupling between resonators which then created the required lumped LC element required.

- **Coupling structure**

Diverse ways of implementing the coupling capacitor structure were assessed. The coupling capacitor structure was implemented using parallel plate capacitor techniques.

6.1.2 Simulation and modelling results

In the process of this research, simulation was conducted on the lumped element bandpass filter using ADS, which is the first stage of the design. Because of the inconvenience presented by lumped element filters at microwave frequency, the shunt LC of the circuit was converted to CCR and their 3D models were constructed using CST Microwave Studio[®]. The simulation was also conducted on the 3D model bandpass filter made of 4 CCR and the coupling to study the EM. The radiation of the filter was also studied to determine the effect of the enclosure on the filter.

6.1.3 Experimental results

The aim was to verify that the simulated and measured results agreed. The filter was constructed on the Rogers material at CPUT. The constructed filter dimension was 18.24mm x 17mm with a height of 4.73mm. The constructed filter was tested using the VNA present at F'SATI and Stellenbosch University; the measured result was satisfactory as the set specifications were met. Measurement of the radiation level was assessed to evaluate the changes it caused to the filter (Figure 5.11). When a

metallic enclosure was placed over the filter, a diminution of the radiation level was observable (Figure 5.12). Temperature cycling measurements were then performed to characterise the filter related to the level of temperature. From this measurement, minimal changes to the filter performance were apparent (Figure 5.14).

6.2 Recommendations

The bandpass filter designed and built in this thesis requires a metallic enclosure in order to contain as much as possible the radiation produced by the design. This metallic enclosure would help minimising the degradation of unwanted signal coupling to other blocks of the communications system. Having a metallic enclosure covering the entire filter is recommended. The overall size of this filter can be minimised further, thus minimising the size, weight and cost of the designed filter.

6.3 Future work

The restricted space and designated weight of the CubeSat impose the use of small circuit components, thus the need exists to reduce the size of any filter used on board a nanosatellite. The work presented in this thesis has proposed and developed a compact bandpass filter for CubeSat application, employing a ceramic coaxial resonator. Future work could include the implementation of this filter using other ceramic material from a different manufacturer. Analysis of the thermal effect on the filter related to space environment, and power handling capabilities.

REFERENCES

- Awang, Z. 2014. *Microwave systems design*. New York, NY: Springer.
- Behagi, A.A. 2015. *RF and microwave circuit design: a design approach using ADS*. Ladera Ranch, CA. Techno Search.
- Blake, R. 1997. *Comprehensive electronic communication*, West publishing company Minneapolis/St. Paul New York Los Angeles San Francisco.
- Cebrían Herrera, N. 2014. A case study on the communications subsystem for cubesat. Unpublished thesis, Universitat Politècnica de Catalunya, Fortaleza, Brazil.
- Chen, C., Huang, T., Chou, C. and Wu, R, 2006. Microstrip Diplexer Design with Common Resonator Sections for Compact Size but High Isolation. *IEEE transaction on microwave theory and techniques*, Vol. 54 No. 5, pp. 1945-1952.
- Chin, A. & Clark, C. 2012. Class F GaN power amplifiers for CUBESAT communication links. *Proceedings of the 2012 IEEE Aerospace Conference, Big Sky, MT, USA, 3–10 March*. Piscataway, NJ: IEEE: 1-6.
- Cohn, S. B. 1969. Beating a Problem to Death, *Microwave Journal*, November 1969, p. 22.
- Cohn, S.B. 1968. Microwave Bandpass filters Containing High Q Dielectric Resonators. *IEEE Transactions on microwave theory and techniques*, Vol. MTT-16 NO, 4, pp. 218-227.
- Collin, R.E. 2001. *Foundations for microwave engineering*. 2nd ed. New Delhi: Wiley India.
- Devlin, L. nd. RF filter Design Using Coupled Co-axial Resonators. Plextek Ltd, London Road, Great Chesterford, pp.1-12.
- Goyal, K., Khama, T., Geeta and Singh, H.K.2014. *KU-band Coupled-Line Banpass Filter for satellite applications*. IJETAE, vol.4, special issue 1, pp.333
- Griffiths, D.J. 2008. *Introduction to Electrodynamics*. 3rd ed. San Francisco: Pearson Education.
- Hano, K., Kohriyama, H. & Sawamoto, K.I. 1986. A direct coupled lambda/4 coaxial coaxial resonator bandpass filter for land mobile communications. *IEEE Transactions on Microwave Theory and Techniques*, 34(9):972-976.
- Hong, J.S. & Lancaster, M.J. 2001. *Microstrip filters for RF/microwave applications*. New York, NY: John Wiley.
- Hunter, I.C. 2001. *Theory and design of microwave filters*. London: Institution of Electrical Engineers.
- Hunter, I.C., Billonet, L., Jarry, B. & Guillon, P. 2002. Microwave filters – applications and technology. *IEEE Transactions on Microwave Theory and Techniques*, 50(3): 794-807.
- Kalde, J. 2015. UHF communication system for cubesatellite. Unpublished master's thesis, University of Tartu, Estonia.

- Karris, S.T. 2003. *Signals and systems with MATLAB applications*. 2nd ed. Fremont, CA: Orchard.
- Levy, R., Snyder, R.V. and Mathaei, G. 2002. *Design of Microwave Filter*. . *IEEE Transactions on microwave theory and techniques*, Vol.50, NO, 4, pp. 783-785.
- Liang, F., Wu, Z., Lu, W. & Wang, X. 2009. A microwave ceramic bandpass filter for mobile communication with new coupling structure. *Wuhan University Journal of Natural Sciences*, 14(1): 43-46.
- Lierena Castro, O.E. 2014. Study of a compact microwave ceramic coaxial resonator filter. Unpublished MSc (Electrical Engineering) thesis, University of Campinas, Brazil.
- Maloratsky, L.G. 2004. *Passive Rf & Microwave Integrated Circuits*. Burlington, USA: Elsevier.
- Matthaei, G.L., Young, L. & Jones, E. M. T. 1980. *Microwaves filters, impedance-matching networks, and coupling structures*. Dedham, MA: Artech House.
- Musonda, E and Hunter, IC. 2015. Microwave band-pass filter using re-entrant resonators. *IEEE Transaction on Microwave Theory and Techniques*, (99), pp. 8-10.
- Nalwa, H.S. 1999. *Handbook of low and high dielectric constant materials and their application, materials and processing*, vol. 2: *Phenomena, properties and applications*. San Diego, CA: Academic Press.
- Pozar, D.M. 2005. *Microwave engineering*. 3rd ed. Hoboken, NJ: John Wiley.
- Rhea, R.W. 1994. *HF filter design and computer simulation*. Atlanta, GA: Noble.
- Rhea, R.W. 2010. *Discrete oscillator design: linear, nonlinear, transient, and noise domains*. Norwood, MA: Artech House.
- Rhea, R.W. 2014. *Filter synthesis using Genesys S/Filter*. Norwood, MA: Artech House.
- Sagawa, M., Makimoto, M. and Yamashita, S. 1985. A design method of bandpass filter using dielectric-filled coaxial resonators. *IEEE Transactions on Microwave Theory and Techniques*, 33(2):152-157.
- Temex. 2015a. Ceramic coaxial resonators. http://www.exxelia.com/wp-content/uploads/pdf/Produits_hyperfrequance/Resonateurs_coaxiaux.pdf
- Temex. 2015b. Microwave products. <http://www.exxelia.com/all-products/microwave-products/resonators/coaxial-resonators/>
- Token. 2017. Dielectric filters. <http://www.token.com.tw/pdf/dielectric/dielectric-filter-df.pdf>
- Trans-Tech. 2007a. Coaxial resonator dimension and configuration. http://www.skyworksinc.com/uploads/documents/dimensions_configurations.pdf
- Trans-Tech. 2007b. Qualification summary for RoHS-compliance coaxial resonators. <http://www.skyworksinc.com/uploads/documents/QualSummaryCoax.pdf>

Trans-Tech. 2013a. Coaxial resonators and inductors (300 MHz to 6.0 GHz). http://www.trans-techinc.com/documents/Coaxial_Resonators_and_Inductors_202699A.pdf

Trans-Tech. 2013b. Coaxial resonators for VCO applications. http://www.trans-techinc.com/documents/Coaxial_Resonators_for_VCOs_202664A.pdf

Trans-Tech. 2013c. Frequency tuning of coaxial resonators. http://www.trans-techinc.com/documents/Frequency_Tuning_Coaxial_Resonators_202722A.pdf

Tung, C., Tsai, H., Shen, C. and Wu, R. 2015. Design of Compact Microwave Filter using Vertically Interdigital Resonator. IEEE.978-4799-8767-2/15/31.

Tusonix. 2008. Ceramic coaxial resonators. Table of contents. Ceramic coaxial resonators ordering information. <http://www.tusonix.com/ResonatorsCatalog2008.pdf>

Vendelin, G.D., Pavo, A.M. & Rohde, U.L. 2005. *Microwave circuit design using linear and nonlinear techniques*. 2nd ed. Hoboken, NJ: John Wiley.

Wentworth, S.M. 2007. *Applied electromagnetics. Early Transmission lines Approach*. Hoboken, NJ: John Wiley.

APPENDIX A

Coaxial Resonators and Inductors



DATA SHEET

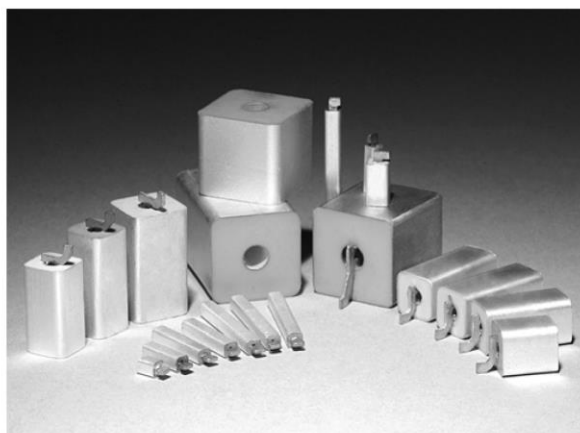
Introduction and Applications for Coaxial Resonators and Inductors (300 MHz to 6.0 GHz)

Applications

- Low phase noise VCOs
- DROs
- Narrow band filters
- Nationwide pagers
- Duplexers
- GPS
- UHF-tuned potential amplifiers
- Wireless communications
- Tuned oscillators

Features

- Frequency tuned to 0.5% and 1.0%
- High dielectric constant
- Rugged construction
- Low-loss silver
- Acts as a parallel resonant circuit or high quality inductor
- 2 mm to 20 mm designs available
- Circuit miniaturization
- Eliminates microphonics
- Repeatability of design
- Negligible aging effects
- Excellent solderability
- Improved circuit Q
- High resonant impedance
- Automation compatible



Introduction

Skyworks, through its wholly-owned subsidiary Trans Tech, offers ceramic coaxial line elements in seven sizes and four dielectric constants that span applications from 300 MHz to 6 GHz. The Very High Frequency (VHF)/Ultra High Frequency (UHF) bands are traditionally “awkward” for realizing discrete inductors and capacitors. Metallized ceramics provide an attractive alternative, as the wireless communication market now forces a continuous trade-off between performance and miniaturization.

Our ceramic solution offers advantages of a high Quality Factor (Q), reduced size, better shielding, and temperature performance that are superior to that which is obtainable from conventional L-C circuits or microstrip construction.

Two types of coaxial resonators are offered: a quarter-wave short ($\lambda/4$) and a half-wave open ($\lambda/2$). The quarter-wave has a thick-film silver applied to one end. The half-wave has both ends unmetallized.

Our four dielectric materials are shown in Figure 1, along with the recommended frequencies of use. Table 1 provides the material properties chart that can be used to determine the optimum material necessary for an application.

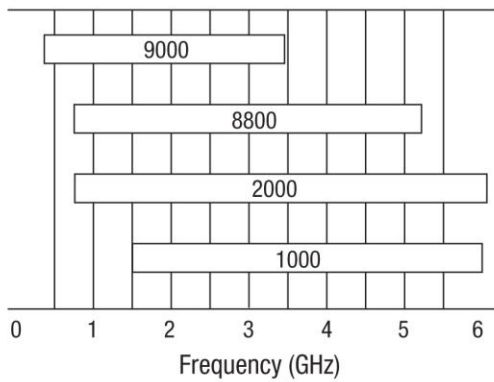


Figure 1. Material Selection Chart

Table 1. Material Properties

Item	Material Type			
	1000	2000	8800	9000
Dielectric constant	10.5 ± 0.5	20.6 ± 1.0	39.0 ± 1.5	90 ± 3
Temperature coefficient of resonant frequency τf (ppm °C)	0 ± 10	0 ± 10	4 ± 2	0 ± 10

The properties given for the ceramic materials used to produce the coaxial line elements are measured for internal quality control purposes. The electrical quality factor (Q) of the coaxial line elements is determined primarily by the metallization. Typical properties of the coaxial line elements are listed in Tables 2 through 5.

Quality Factor (Q) Specifications

1000 and 2000

Figures 2 through 5 show the quality factor charts for various resonator profiles. The resonators are grouped by:

- Wavelength type = $\lambda/4$ and $\lambda/2$
- Material = 1000 and 2000
- Profile = High Profile (HP), Enhanced Q Profile (EP), Standard Profile (SP), Large diameter (LS) profile, Miniature Profile (MP), and Sub-Miniature (SM) profile

The listed Q value on each curve is the value guaranteed for the lowest operating frequency of each component type. The Q increases approximately as the square root of increasing frequency. Typical Qs are 10% to 15% higher.

1000 Series Q Curves

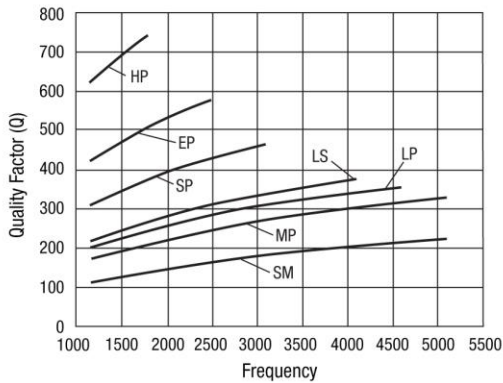


Figure 2. D1000 Quarter-Wave Q Curves

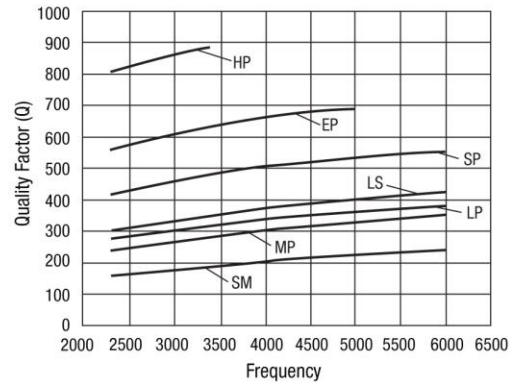


Figure 3. D1000 Half-Wave Q Curves

2000 Series Q Curves

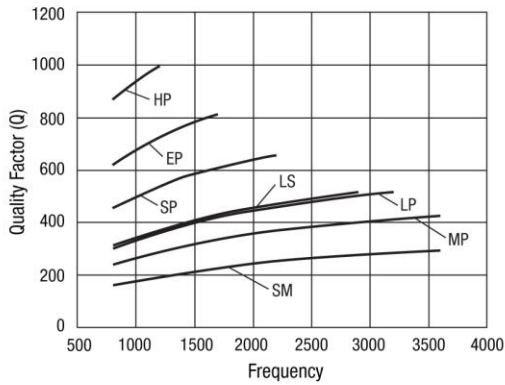


Figure 4. D2000 Quarter-Wave Q Curves

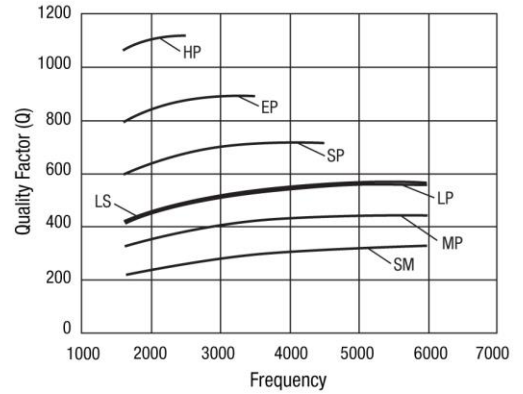


Figure 5. D2000 Half-Wave Q Curves

8800 and 9000

Figures 6 through 9 show the specified quality factor charts of the various offered resonator components. The resonators are grouped by:

- Wavelength type = $\lambda/4$ and $\lambda/2$
- Material = 8800 and 9000
- Profile = HP, EP, SP, Low Profile (LP), LS, MP, and SM

The listed Q value on each curve is the minimum value for the lowest operating frequency of each component type. The Q increases approximately as the square root of increasing frequency. Typical Qs are 10% to 15% higher.

8800 Series Q Curves

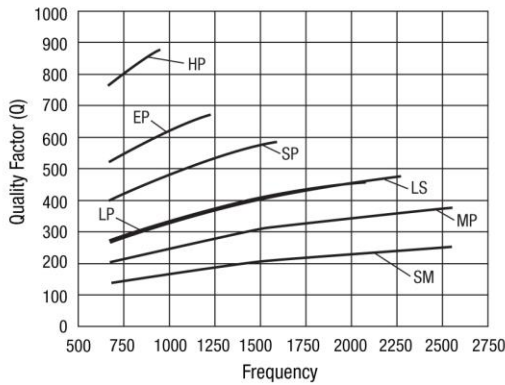


Figure 6. D8800 Quarter-Wave Q Curves

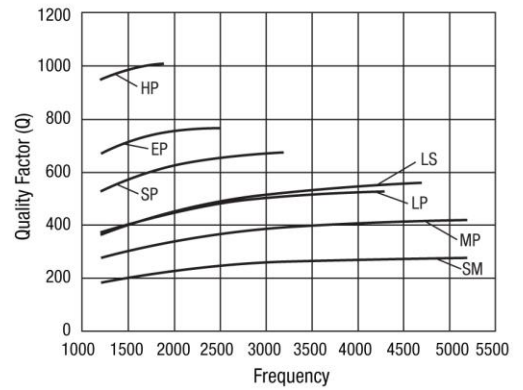


Figure 7. D8800 Half-Wave Q Curves

9000 Series Q Curves

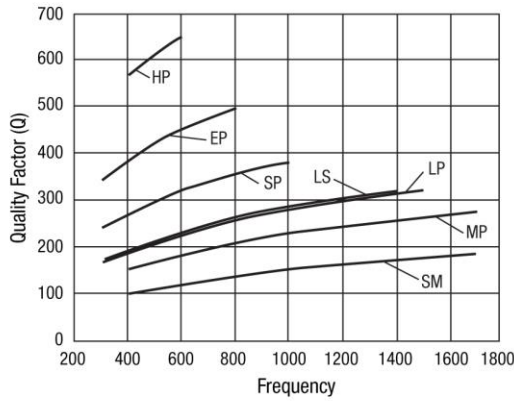


Figure 8. D9000 Quarter-Wave Q Curves

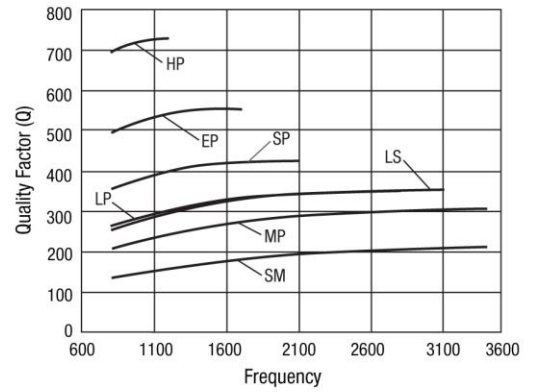


Figure 9. D9000 Half-Wave Q Curves

Dimensions and Configurations

The coaxial resonator components are available in the frequency range of 300 MHz to 6 GHz. Seven mechanical profiles are offered to give the designer the greatest flexibility in selecting the electrical quality factor (Q). There are three large profiles:

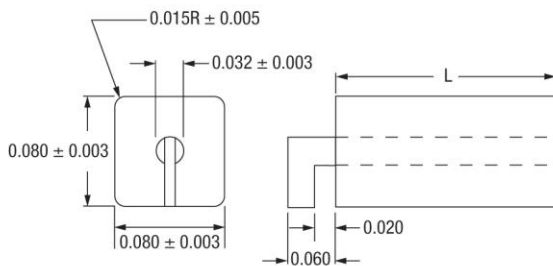
- HP = Highest Q and size
- EP = High Q and wide frequency
- SP = A compromise of electrical Q and size (should be considered the component of choice for most applications)

Four smaller profiles are available space is restricted:

- LP
- LS
- MP
- SM

The LP and LS profiles both have the same outer physical dimensions, but differ in the dimension of the inner diameter. This difference allows for different characteristic impedances, and increases the options available to designers. Overall comparisons can be determined from the given Q curves or by using our COAX program.

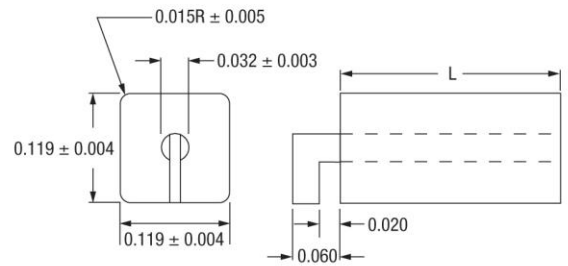
These components are available in square configurations with the dimensions shown in Figures 10 through 16.



Note: Units are measured in inches.

K088

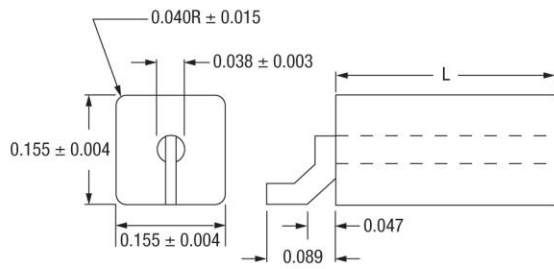
Figure 10. SM (2 mm)



Note: Units are measured in inches.

K089

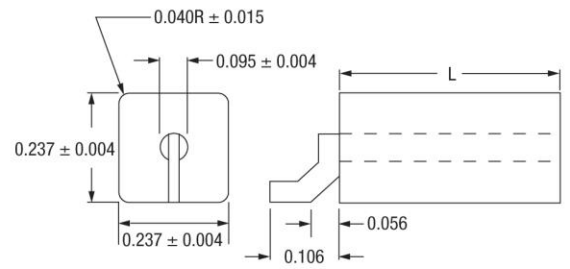
Figure 11. MP (3 mm)



Note: Units are measured in inches.

K090

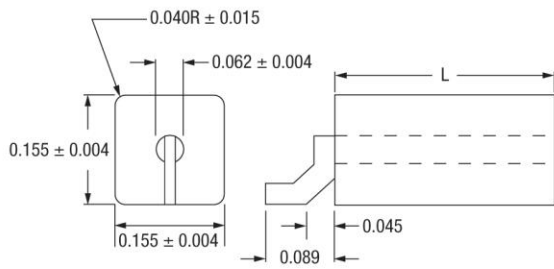
Figure 12. LP (4 mm)



Note: Units are measured in inches.

K092

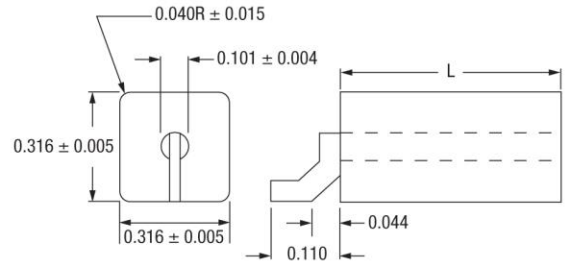
Figure 14. SP (6 mm)



Note: Units are measured in inches.

K091

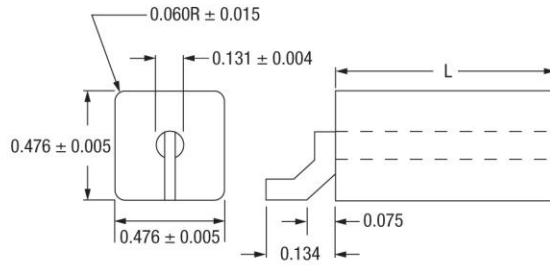
Figure 13. LS (4 mm)



Note: Units are measured in inches.

K093

Figure 15. EP (8 mm)



Note: Units are measured in inches.

K094

Figure 16. HP (12 mm)

Ceramic Coaxial Resonators

Tables 2 through 5 summarize the various profiles, materials, and types available for coaxial Transverse Electro-Magnetic (TEM) mode resonators. We provide two types, four materials, and seven profiles. This range of component variables should meet most circuit design requirements. While the component is manufactured to a frequency, a formula is given to determine the approximate length. The selected resonant frequency is available with two standard frequency tolerances of $\pm 0.5\%$ and $\pm 1.0\%$. The minimum tolerance is ± 2 MHz.

Note: The ordered value of f_0 is set according to our measurement procedure. The f_0 in your circuit may vary due to stray reactance. This offset can be corrected by changing the ordered value of f_0 .

Table 2. Recommended Frequencies for 1000 Series ($\epsilon_R = 11.5 \pm 0.5$)

Type	Profile	Recommended Range f_0 (MHz)	Nominal Length (Inches) ± 0.030 Inches	Nominal Length Range (Inches)	Characteristic Impedance (Ω)
$\lambda/4$ Quarter-Wave Length	HP	1100–1720	$L = 870/f_0$ (MHz)	0.506–0.792	24.1
	EP	1100–2390		0.364–0.792	21.5
	SP	1100–2960		0.294–0.792	17.5
	LS	1100–4400		0.198–0.792	17.5
	LP	1100–3920		0.222–0.792	26.2
	MP	1100–4860		0.179–0.792	24.5
	SM	1100–4860		0.179–0.792	17.5
$\lambda/2$ Half Wave Length	HP	2200–3240	$L = 1740/f_0$ (MHz)	0.536–0.792	24.1
	EP	2200–4780		0.364–0.792	21.5
	SP	2200–5725		0.304–0.792	17.5
	LS	2200–5725		0.304–0.792	17.5
	LP	2200–5725		0.304–0.792	26.2
	MP	2200–5725		0.304–0.792	24.5
	SM	2200–5725		0.304–0.792	24.5

Table 3. Recommended Frequencies for 2000 Series ($\epsilon_R = 21.5 \pm 1.0$)

Type	Profile	Recommended Range f_0 (MHz)	Nominal Length (Inches) ± 0.030 Inches	Nominal Length Range (Inches)	Characteristic Impedance (Ω)
$\lambda/4$ Quarter-Wave Length	HP	800–1200	$L = 635/f_0$ (MHz)	0.542–0.813	18.1
	EP	800–1700		0.382–0.813	16.1
	SP	800–2200		0.296–0.813	13.1
	LS	800–3200		0.203–0.813	13.1
	LP	800–2900		0.224–0.813	19.6
	MP	800–3600		0.181–0.813	18.4
	SM	800–3600		0.181–0.813	13.1
$\lambda/2$ Half Wave Length	HP	1600–2500	$L = 1270/f_0$ (MHz)	0.520–0.813	18.1
	EP	1600–3500		0.372–0.813	16.1
	SP	1600–4500		0.289–0.813	13.1
	LS	1600–6000		0.217–0.813	13.1
	LP	1600–6000		0.217–0.813	19.6
	MP	1600–6000		0.217–0.813	18.4
	SM	1600–6000		0.217–0.813	13.1

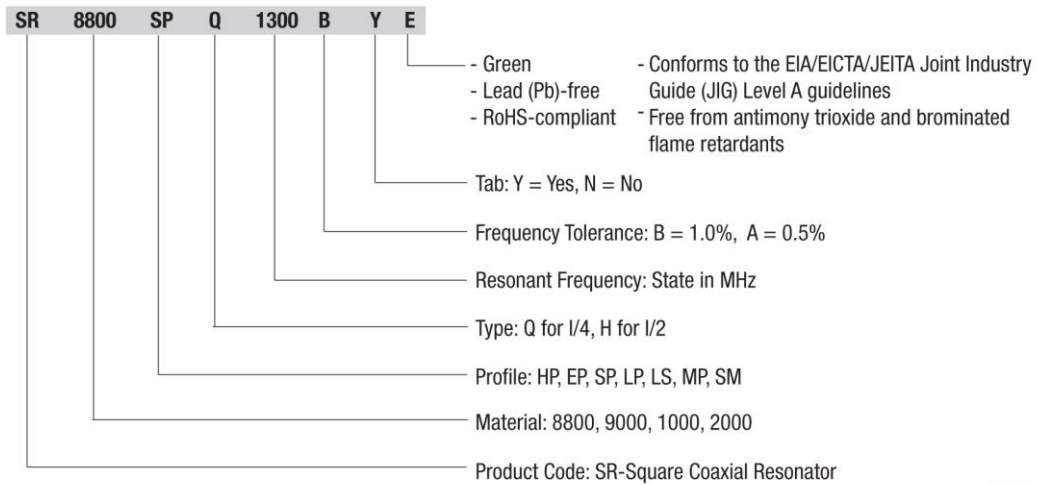
Table 4. Recommended Frequencies for 8800 Series ($\epsilon_R = 39.5 \pm 1.0$)

Type	Profile	Recommended Range f_0 (MHz)	Nominal Length (Inches) ± 0.030 Inches	Nominal Length Range (Inches)	Characteristic Impedance (Ω)
$\lambda/4$ Quarter-Wave Length	HP	600–900	$L = 469/f_0$ (MHz)	0.525–0.787	13.1
	EP	600–1200		0.394–0.787	11.7
	SP	600–1600		0.295–0.787	9.5
	LS	600–2300		0.205–0.787	9.5
	LP	600–2100		0.225–0.787	14.2
	MP	600–2600		0.182–0.787	13.3
	SM	600–2600		0.182–0.787	9.5
$\lambda/2$ Half Wave Length	HP	1200–1900	$L = 938/f_0$ (MHz)	0.497–0.787	13.1
	EP	1200–2500		0.378–0.787	11.7
	SP	1200–3200		0.295–0.787	9.5
	LS	1200–4700		0.201–0.787	9.5
	LP	1200–4300		0.220–0.787	14.2
	MP	1200–5200		0.182–0.787	13.3
	SM	1200–5200		0.182–0.787	9.5

Table 5. Recommended Frequencies for 9000 Series ($\epsilon_R = 93 \pm 2$)

Type	Profile	Recommended Range f_0 (MHz)	Nominal Length (Inches) ± 0.030 Inches	Nominal Length Range (Inches)	Characteristic Impedance (Ω)
$\lambda/4$ Quarter-Wave Length	HP	400–600	$L = 306/f_0$ (MHz)	0.518–0.778	8.5
	EP	300–800		0.389–1.037	7.6
	SP	300–1000		0.311–1.037	6.2
	LS	300–1500		0.207–1.037	6.2
	LP	300–1400		0.222–1.037	9.2
	MP	400–1700		0.183–0.778	8.6
	SM	400–1700		0.183–0.778	6.2
$\lambda/2$ Half Wave Length	HP	800–1200	$L = 612/f_0$ (MHz)	0.518–0.778	8.5
	EP	800–1700		0.366–0.778	7.6
	SP	800–2100		0.296–0.778	6.2
	LS	800–3100		0.201–0.778	6.2
	LP	800–2800		0.222–0.778	9.2
	MP	800–3400		0.183–0.778	8.6
	SM	800–3400		0.183–0.778	6.2

Coaxial Resonator Order Information



K086

Figure 17. Coaxial Resonator Order Example

Ceramic Coaxial Inductors

Our coaxial inductors are most frequently used in the resonant circuit of Voltage-Controlled Oscillators (VCOs), where a varactor provides the tuning capability. The designer is usually confronted with trade-offs between high-Q for best phase noise and component size versus circuit board real estate. An algorithm for selecting the correct part follows. In addition, our COAX program can provide valuable assistance for determining the correct part. For sample circuits, basic principles, and some helpful hints, refer to the following Application Notes:

- *Coaxial Resonators for VCO Applications* (document number 202664)
- *Computer Simulation of Coaxial Resonators* (document number 202721)

While there is no physical distinction between a coaxial resonator and a coaxial inductor, the selection of an inductor for a VCO begins by first knowing (from analysis or experiment) the equivalent inductance that the active circuit, including the varactor, must see. In general, the VCO active circuit loads the resonator, lowering the resonator's Self-Resonant Frequency (SRF). The situation is analogous to externally capacitively loading a discrete parallel resonant L-C circuit.

While there is an approximate equivalent L-C circuit for the coaxial resonator close to the resonance, this model has limited application.

The coaxial resonators and inductors are more accurately modeled as a transmission line. For more details, refer to the two Application Notes referenced above.

Values of inductance that can be achieved depend upon the separation between the VCO frequency and the SRF of the coaxial line element. Values less than 1 nH are not practical as the metal connection tab has an equivalent inductance of this order.

In our experience, equivalent inductances in the range of 3 nH through 20 nH have been popular among designers of VCOs for wireless equipment.

To order a part or check on part availability, contact us or refer to Figures 17 and 19.

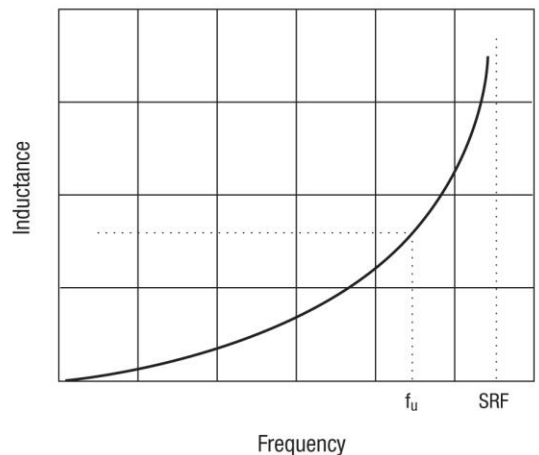
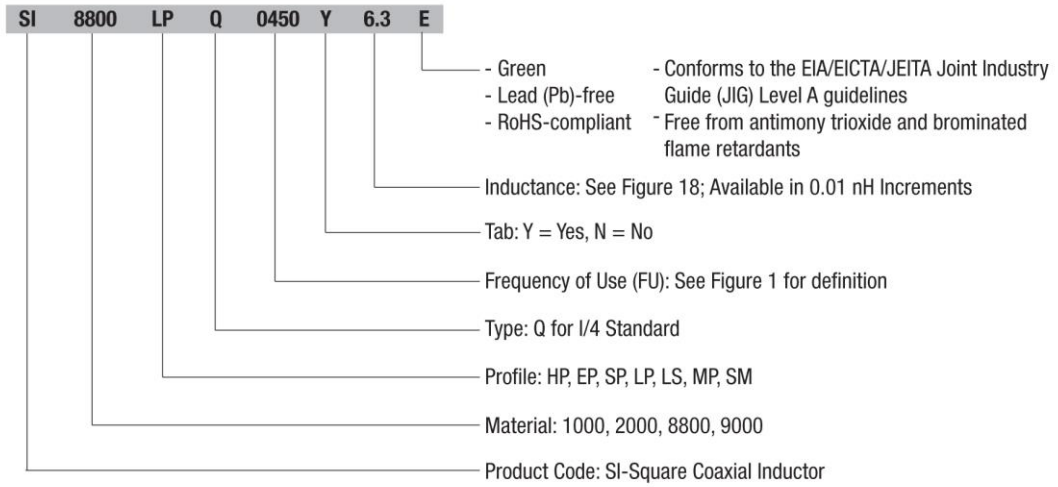


Figure 18. Frequency of Use vs Inductance

Coaxial Inductor Order Information



K087

Figure 19. Coaxial Inductor Order Example

Table 6. Coaxial Line Properties vs Profile and Material

Profile	Material Type				Tab Inductors
	1000	2000	8800	9000	
HP	24.1 Ω	18.1 Ω	13.1 Ω	8.5 Ω	1.8 nH
EP	21.5 Ω	16.1 Ω	11.7 Ω	7.6 Ω	1.0 nH
SP	17.5 Ω	13.1 Ω	9.5 Ω	6.2 Ω	1.0 nH
LS	17.5 Ω	13.1 Ω	9.5 Ω	6.2 Ω	0.9 nH
LP	26.2 Ω	19.6 Ω	14.2 Ω	9.2 Ω	1.0 nH
SP	24.5 Ω	18.4 Ω	13.3 Ω	8.6 Ω	0.6 nH
SM	17.5 Ω	13.1 Ω	9.5 Ω	6.2 Ω	0.6 nH

Table 7. Wavelength (λ_g) in Dielectric

Material	ε _R	Wavelength Formula for λ _g (Inches)
1000	11.5 ± 0.5	3480/f ₀
2000	21.5 ± 1.0	2540/f ₀
8800	39.5 ± 1.0	1876/f ₀
9000	93 ± 2	1224/f ₀

Inductor Selection Guide

1. Select one of the four dielectric materials.
2. Determine the VCOs operating frequency (f_{VCO}).
3. Determine the preferred inductance or circuit impedance (Z_{IN}). Use the following formula to convert the inductances to impedances:

$$Z_{IN} = 2 * \pi * f_{VCO} * L_{IN} \Omega$$
4. Calculate the effect of the tab. Tab inductances are given in Table 2 in the Application Note *Optimizing DROs for Low Phase Noise* (document number 202727). Use the following formula to convert the tab inductances to impedances:

$$Z_{IN} = 2 * \pi * f_{VCO} * L_{TAB} \Omega$$
5. Determine the input impedance by subtracting the effect of the tab using the following formula:

$$Z_{INPUT} = Z_{IN} - Z_{TAB}$$
6. Calculate the wavelength (λ_g) of the part in the dielectric (see Table 7 for the appropriate formula).
7. Determine the characteristic impedance (Z₀) of the part (see Table 8).
8. Calculate the physical length of the part using the following formula:

$$l = (\lambda_g / 2 * \pi) \tan^{-1} (Z_{INPUT} / Z_0) \text{ inches}$$
9. Determine the SRF of this part using the following formula:

$$SRF = (\lambda_g * f_{VCO}) / (4 * l)$$
10. Check the recommended frequency in Tables 2 through 5 for the appropriate material to ensure a valid part.

Measurement Description of Q, fo, and L

The evaluation of Q (quality factor) and fo (resonant frequency) of coaxial components is made with a one-port reflection measurement on a network analyzer. The probe is moved into the Inner Diameter (ID) of the device until the input resistance of the device matches the terminal resistance of the network analyzer. This input resistance is indicated by a 50 Ω circle on the Smith Chart display, and is known as “critical” coupling. The point on this circle where the response is purely resistive (capacitance reactance equals inductive reactance) is the point of resonance and is defined by a complex impedance of $Z = 50 + j\Omega$. The Q is computed by observing the frequency span between the Voltage Standing-Wave Ratio (VSWR) minus 2.616 ($Z = 50 \pm j50\Omega$) on either side of fo. The Q is defined as $f_0/\Delta f$.

The inductance parameter (L) is measured with an Analog Power Control (APC) 7 mm connector that is mounted flush with a conducting plane, and a full one-port calibration (open, short, broadband 50 Ω load) is performed. The inductor is then clamped into place with the tab touching the inner conductor and metallized body touching the grounding plane. The inductance (L) is measured at the frequency of use. The impedance vector on the Smith Chart of a network analyzer gives the necessary information where $Z = R + j\omega L$.

Characteristic Impedance

As shown in Table 8, the characteristic impedance (Zo) of the coaxial TEM mode components is a function of the profile dimensions and dielectric constant of the material. The Zo value is reduced over its air line value by the square root of the dielectric constant of the material. At a one-eighth wavelength, the short-circuit line exhibits an inductive reactance, while the open-circuit line exhibits a capacitive reactance equal in magnitude to Zo.

$$Z_0 = \text{character impedance} = \frac{60}{\sqrt{\epsilon_R}} \ln \left(1.079 \frac{W}{d} \right)$$

Where:

- w = width of resonator
- d = diameter of inner conductor
- ε_R = dielectric constant

Table 8. Characteristic Impedance

Profile	Material Type			
	1000	2000	8800	9000
HP	24.1 Ω	18.1 Ω	13.1 Ω	8.5 Ω
EP	21.5 Ω	16.1 Ω	11.7 Ω	7.6 Ω
SP	17.5 Ω	13.1 Ω	9.5 Ω	6.2 Ω
LS	17.5 Ω	13.1 Ω	9.5 Ω	6.2 Ω
LP	26.2 Ω	19.6 Ω	14.2 Ω	9.2 Ω
SP	24.5 Ω	18.4 Ω	13.3 Ω	8.6 Ω
SM	17.5 Ω	13.1 Ω	9.5 Ω	6.2 Ω

Ceramic Coaxial Inductor Soldering Conditions

TTI coaxial components are compatible with standard surface mount reflow and wave soldering methods. The HP components may require mechanical support mounting because of the larger size. Contact us for details.

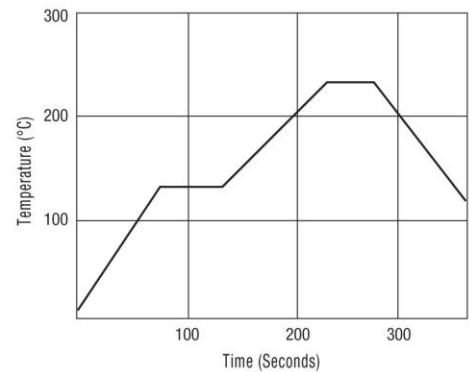
Solders *must* contain silver. Non-silver bearing solders leach silver from the resonator during reflow.

Tabs that are:

- Non-RoHS are Sn/Pb plated.
- RoHS compliant are gold-plated with a nickel underlayer or an unplated nickel silver alloy.

Additional attaching methods include a hot air gun, an infrared source, a soldering iron, a hot plate, a vapor phase, etc. The coaxial component body is ceramic and subject to thermal shock if heated or cooled too rapidly.

We recommend Figure 20 as the soldering profile. For further information, refer to the *Coax Resonators Reflow Process Compatibility for Lead (Pb)-Free and RoHS-Compliant* document on our website. Repeatable results can be best achieved with air cooling only, not quenching.



Note: The maximum temperature depends on the solder type.

Figure 20. Soldering Profile

Figure 21 indicates the maximum tolerance of the component planarity with respect to the datum plane.

Equation (1) Input Impedance f_0

$$Z_{INPUT} = fZ_0 \tan\left(\frac{2\pi f_0}{4 SRF}\right)$$

Where: f_0 = Resonant frequency

Equation (2) Resonant Frequency

$$f = \frac{c}{4 SRF \sqrt{\epsilon_R}}$$

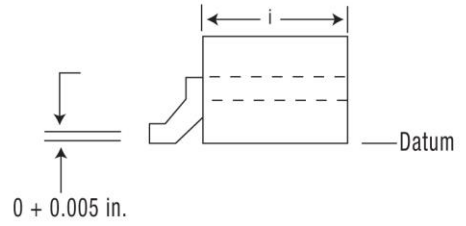
Where: c = Speed of light

$\epsilon_R = 39.5$ (8800 material)

$\epsilon_R = 93$ (9000 material)

$\epsilon_R = 11.5$ (1000 material)

$\epsilon_R = 21.5$ (2000 material)



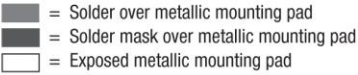
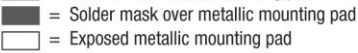

K095

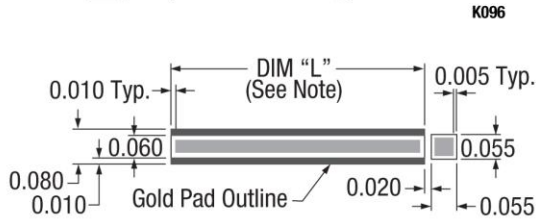
Figure 21. Surface Mount Tolerance for Components with Tabs

Packaging for Ceramic Coaxial Inductors

Tape and reel packaging is available. Contact us for details.

Notes: 1. Dimension "L" is the length, which depends on frequency.
2. Units are measure in units of inches.

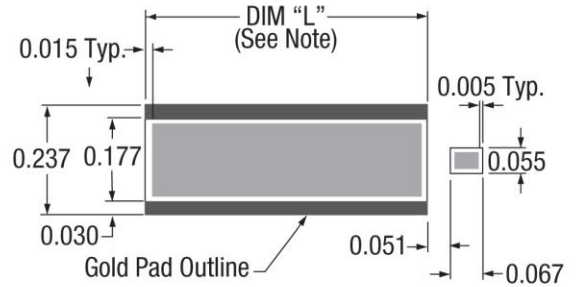
Key:  = Solder over metallic mounting pad
 = Solder mask over metallic mounting pad
 = Exposed metallic mounting pad



Note: Units are measured in inches.

K097

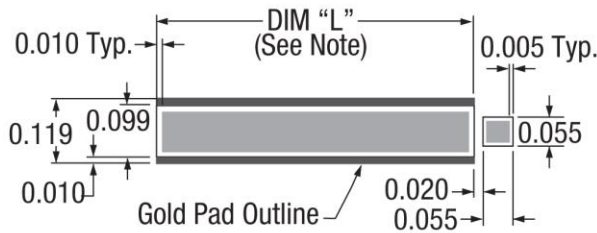
Figure 22. 2 mm (SM) Coaxial Resonator Footpad Dimensions



Note: Units are measured in inches.

K100

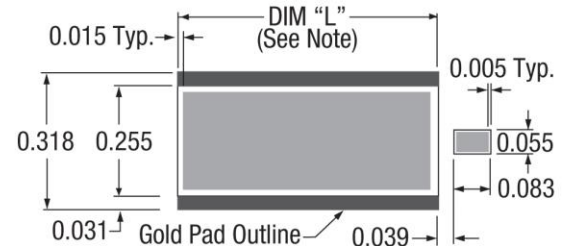
Figure 25. 6 mm (SP) Coaxial Resonator Footpad Dimensions



Note: Units are measured in inches.

K098

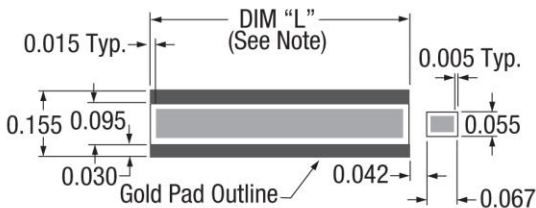
Figure 23. 3 mm (MP) Coaxial Resonator Footpad Dimensions



Note: Units are measured in inches.

K101

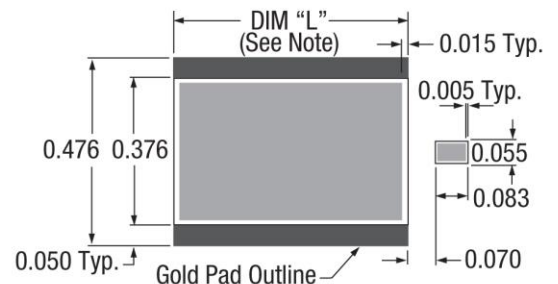
Figure 26. 8 mm (EP) Coaxial Resonator Footpad Dimensions



Note: Units are measured in inches.

K099

Figure 24. 4 mm (LP/LS) Coaxial Resonator Footpad Dimensions



Note: Units are measured in inches.

K102

Figure 27. 12 mm (HP) Coaxial Resonator Footpad Dimensions

APPENDIX B

CCR FREQUENCY TUNING



APPLICATION NOTE

Frequency Tuning of Coaxial Resonators

The space-saving design and mechanical ruggedness of Skyworks high Quality Factor (Q) coaxial resonators make them ideal for use in stable oscillators and filter applications. It is usually preferable to shift the Self Resonant Frequency (SRF) of the resonator when testing circuit prototypes. This document demonstrates three mechanical methods of tuning a coaxial resonator.

In most applications, the SRF of the coaxial resonator is loaded by stray and parallel capacitances. In an oscillator, this usually leads to a shift in the resonant frequency to a lower value.

The resonator's SRF can be increased by removing the silver metallization from the open end. Start this process by removing 10 mils to 50 mils from the top, and then continue to remove metallization from each side if necessary. Depending on the length of the part, the SRF can be increased 10 % to 20 % without degrading the unloaded Q.

The resonator's SRF can be decreased by removing the silver metallization from the shortened end of the resonator or by varying the position of the grounding plane. Removing the silver metallization from the shortened end of the resonator disturbs the current and results in a degradation of the Q.

When a designer produces a resonator that works well in a circuit, the SRF can be measured using the method described in the Skyworks *Measuring the SRF and Q of Coaxial Resonators Application Note* (document number 202724), or the part can be returned to Skyworks to characterize and provide new samples.

